UNIVERSIDADE D
COIMBRA

Mohammadamin Sadeghi

Tribological Behavior of Doped DLC Coatings in the Presence of Ionic Liquid Additive under Different Lubrication Regimes

VOLUME 1

Dissertation under the Joint European Master's Degree in Surface Tribology and Interfaces guided by Doctor Fábio Emanuel de Sousa Ferreira presented to the Department of Mechanical Engineering of the Faculty of Science and Technology of the University of Coimbra.

July 2023

1 2 9 0 FACULDADE DE CIÊNCIAS E TECNOLOGIA UNIVERSIDADE D COIMBRA

Tribological Behavior of Doped DLC Coatings in the Presence of Ionic Liquid Additive under Different Lubrication Regimes

Submitted in Partial Fulfilment of the Requirements for the Degree of European Joint European Master in Tribology of Surfaces and Interfaces.

Comportamento tribológico de revestimentos de DLC dopados na presença de aditivos à base de líquidos iônicos sob diferentes regimes de lubrificação

Author

Mohammadamin Sadeghi

Advisor

Doctor Fábio Emanuel De Sousa Ferreira
Researcher at University of Coimbra

Jury

President	Prof. Dr. Bruno Trindade Professor at University of Coimbra
Vowel	Dr. Todor Vuchkov Researcher at Instituto Pedro Nunes
Advisor	Doctor Fábio Emanuel De Sousa Ferreira Researcher at University of Coimbra

1 2 9 0 UNIVERSIDADE D COIMBRA

tribos Joint European Master in Tribology of Surfaces and Interfaces
Ljubljana • Leeds • Coimbra • Luleå

Coimbra, July 2023

Acknowledgments

I would like to begin by expressing my profound gratitude to Dr. Fabio Ferreira, for bestowing upon me this invaluable opportunity. I am sincerely thankful for their dedicated time, and the invaluable suggestions and guidance they have provided me throughout this academic year and allowing me to work independently. My deep appreciation is also extended to Dr. Amilcar Ramalho and Dr. Luis Vilhena for their insightful advice and supervision, which not only fostered my autonomy in the execution of this research endeavor.

Furthermore, I wish to convey my sincere appreciation to all those individuals who have made meaningful contributions to the progress of the work documented within this thesis. I must not overlook the resolute dedication and unwavering support offered by the entire academic and technical personnel at the Department of Mechanical Engineering, University of Coimbra, whose relentless commitment has been a driving force behind the advancement of this research.

Moreover, I am deeply grateful to the TRIBOS consortium and the Education, Audiovisual and Culture Executive Agency (EACEA) of the European Commission, as I find myself indebted to their magnanimous provision of this exceptional opportunity to partake in a high-caliber, comprehensive, and integrated master's program. In this regard, I extend my heartfelt thanks to Professor Mitjan Kalin, Professor Ardian Morina, Professor Nazanin Emami, and Professor Bruno Trindade for their discerning selection of my candidacy as a TRIBOS student. In addition, I wish to express my gratitude to my fellow classmates within the TRIBOS program for their support.

Finally, my profound appreciation goes to my beloved family, including my parents and sister, whose boundless passion, and steadfast support have served as a perpetual source of inspiration and encouragement.

Resumo

Os revestimentos de carbono tipo diamante (DLC) são amplamente utilizados em indústrias que requerem alta durabilidade, resistência ao desgaste e baixo atrito. As características únicas dos revestimentos de DLC permitem a criação de sítios de adsorção para aditivos lubrificantes por meio do processo de dopagem. Neste estudo, foi investigado o uso combinado de revestimentos de carbono tipo diamante dopados com európio (Eu-DLC) em duas concentrações diferentes do elemento dopante (1,7 at.% e 2,3 at.%), revestimentos de carbono tipo diamante dopados com gadolínio (Gd-DLC) em duas concentrações diferentes do elemento dopante (1,7 at.% e 2,4 at.%) e revestimentos de DLC puros em conjunto com dois aditivos de líquido iônico (IL), nomeadamente *trihexyltetradecylphosphonium bis* (2-ethylhexyl) *phosphate* [P_{66614}] [DEHP] (denominado IL nº 1 neste documento) e *1-Ethyl-3-methylimidazolium diethylphosphate* (denominado IL nº 2 neste documento), com uma concentração de 1 wt.% em polialfaolefina (PAO) 8 como lubrificante base. Os revestimentos de Gd-DLC apresentaram maior dureza, melhor adesão ao substrato e maior fator de resistência à deformação plástica. O revestimento de DLC puro apresentou um desempenho tribológico melhor quando combinado com PAO8. No entanto, após a introdução do IL nº 1 como aditivo no sistema tribológico, o coeficiente de atrito foi reduzido nos revestimentos de Gd-DLC com 1,7 at.% e 2,3 at.% de dopante em todos os regimes de lubrificação. Para a configuração tribológica que utiliza PAO8 + 1 wt.% de IL nº 2 como lubrificante, o Eu-DLC com 1,7 at.% apresentou o melhor desempenho no regime de lubrificação "contato corpo com corpo" de entre todos os revestimentos. O desgaste não pôde ser quantificado devido à natureza do desgaste na superfície dos revestimentos de DLC ser demasiado baixo, mas uma comparação qualitativa obtida por meio de técnicas de microscopia mostra que o uso do IL nº 2 reduz o desgaste para todos os revestimentos investigados neste estudo. A redução do atrito demonstra que a combinação de filmes finos de Gd-DLC com IL nº 1 pode ser um candidato potencial para sistemas que operam em todos os regimes de lubrificação, enquanto sistemas que operam apenas no regime de lubrificação "contato corpo com corpo" podem obter o maior benefício ao usar Eu-DLC com 1,7 at.% em conjunto com IL nº 2, pois esse par tribológico apresentou o menor coeficiente de atrito entre todos os pares tribológicos investigados. Os resultados deste estudo são bastante promissores para a implementação destes sistemas tribológicos em vários componentes que constituem os motores de combustão interna onde a redução do atrito é essencial para a melhoria da sua eficiência.

Palavras-chave: liquidos iônicos, DLC dopado, regime de lubrificação, curva de Stribeck, coeficiente de atrito

Abstract

Diamond-like carbon (DLC) coatings are widely used in industries that require high durability, wear resistance, and low friction. The unique characteristics of DLC coatings allow for the possibility of creating adsorption sites for lubricant additives through the doping process. In this study, the combined use of europium-doped diamond-like carbon (Eu-DLC) with two different concentrations of dopant element (1.7 at.% and 2.3 at.%), gadolinium-doped diamond-like carbon (Gd-DLC) with two different concentrations of dopant element (1.7 at.% and 2.4 at.%), and pure DLC (undoped) coatings paired with two ionic liquid (IL) additives, namely, trihexyltetradecylphosphonium bis (2-ethylhexyl) phosphate [P_{66614}] [DEHP] (named as IL #1 in this report) and 1-Ethyl-3-methylimidazolium diethylphosphate (named as IL #2 in this report) with a 1 wt.% concentration in polyalphaolefin (PAO) 8 as a base lubricant was investigated. Higher hardness, higher thin-film adhesion, a higher ratio of hardness to elastic modulus, and a higher plastic deformation resistance factor were achieved with the 1.7 at. % Gd-DLC coating. The pure DLC coating had a better performance when paired with PAO8 in a tribological system. However, after introducing the IL #1 as an additive to the tribological system, the CoF was decreased for the 1.7 % Gd-DLC and 2.3% Gd-DLC coatings in all lubrication regimes. For tribological configuration using PAO8 + 1 wt.% IL#2 as a lubricant, 1.7 at. % Eu-DLC had the best performance in boundary lubrication regime among all coatings. The wear could not be quantified due to the nature of the wear on the surface of the DLC coatings but qualitative comparison obtained from microscopy techniques shows that introducing IL #2 reduces wear for all coatings investigated in this study. The friction reduction demonstrates that combining Gd-DLC thin films with IL#1 can be a potential candidate for the systems that are working in all lubrication regimes, while systems that are operating in only boundary lubrication regime, can get the most benefit by using 1.7 at. % Eu-DLC paired with IL #2 since this tribological pair had the lowest CoF among all the tribological pairs investigated. The results of this study can be implemented in development efforts to reduce friction and increase the efficiency of moving parts in internal combustion engines, for instance.

Keywords: Ionic liquid, doped DLC, lubrication regime, Stribeck curve, friction

Table of Contents

List of figures

List of tables

List of Abbreviations

AFM	Atomic force microscopy
Ar	Argon
AW	Anti-wear
CoF	Coefficient of friction
BL	Boundary Lubrication
DC	Direct current
DCMS	Direct current magnetron sputtering
DLC	Diamond-like carbon
EDS	Energy dispersive X-ray spectroscopy
EL	Elastohydrodynamic lubrication
GLC	Graphite-like carbon
HIPIMS	High impulse power magnetron sputtering
HL	Hydrodynamic lubrication
IL	Ionic liquid
ML	Mixed lubrication
Mo	Molybdenum
PAO	Polyalphaolefin
PP	Phosphonium phosphate
PVD	Physical vapor deposition
RF	Radio Frequency
SEM-EDS	Scanning electron microscopy
SIAM	Synthesis, irradiation & analysis of materials
SRIM	Stopping and range of ions in matter
ZDDP	Zinc dialkyldithiophosphate

List of Symbols

E	Young's modulus
Eu	Europium
Gd	Gadolinium
H (GPa)	Hardness
H	Hydogen
h_0	Minimum film thickness
L_c	Critical load
Ne	Neon
u	Sliding speed
λ	Lambda ration

Chapter 1 – Introduction and objectives

1.1. Introduction

Energy source diversification is essential for ensuring energy security while improving industrial production and profitability. The enhancement of energy efficiency is a key component in accomplishing this. The imperative need to reduce greenhouse gas emissions calls for prompt action if we are to have a favorable impact on our planet in the foreseeable future. The proper management of friction factors directly affects systems' performance which allows it to save energy during system use, a reduction that is typically quite considerable over the unit's lifespan. Friction management also increases the longevity of the components by decreasing unwelcome wear and tear, which has a favorable effect on energy savings by lowering the demand for component renewals [1].

The development of materials that enable friction decrease while extending the lifespan of mechanical moving parts is necessary and urgently requires investigation. Noteworthy tribological investigations must offer insight into the dynamics of the moving elements under the influence of a lubricant since friction and wear are system characteristics rather than material features. Ionic liquids (ILs) and diamond-like carbon (DLC) thin coatings have been examined as friction-reducing lubricant additives and wear-resistant surface innovative solutions, correspondingly, among the materials that have received considerable interest in tribology [2].

Previous research works have proven the advantages of utilizing DLCs, ILs, or base lubricants alone or simultaneously to minimize friction or wear. Considering this fact, in this work, the combined use of DLC coatings and ILs in tribological systems is investigated for trihexyltetradecylphosphonium bis(2-ethylhexyl) phosphate [P66614] [DEHP] and 1-Ethyl-3-methylimidazolium diethylphosphate ILs. To enhance tribological interaction between the ILs and DLC film, DLC thin films are doped with Eu and Gd elements. A primary step in developing the necessary competencies for efficiently addressing tribological challenges which depend on the incorporation of DLCs and ILs to boost tribological properties is identifying the key parameters which affect the interactions between ionic liquids and DLC films under mechanical loading. The tribological tests are performed in all different lubrication regimes using a block-on-ring tribometer at room temperature which yields a comprehensive insight into the fundamental interactions among the mentioned ILs and DLCs [1].

1.2. Objectives

Through the advancement of the information needed for the coupling of innovative nanostructured alloyed-DLCs and ILs to accomplish the aimed tribological efficacy, the project's results will thus result in a paradigm shift towards a greener and more efficient tribological system. The primary research aims encompass the examination of the following objectives:

1. To investigate the potential enhancement in the tribological behavior of DLC coatings through gadolinium and europium doping and elucidate the underlying mechanisms.

2. To determine the optimal DLC coating condition that yields the most desirable coating properties among the samples prepared.
3. To assess the tribological performance of the prepared pure DLC and doped DLC coatings paired with two different ionic liquids.

1.3. Thesis Organization

This thesis includes five chapters. The first chapter serves as an introduction and outlines the objectives of the thesis. Chapter 2 offers a comprehensive literature review and state of art focusing on the tribological aspects of DLC coatings and ionic liquids. It presents the existing body of knowledge in this field, highlighting relevant studies, theories, and findings. Chapter 3 explains the experimental methodology employed in this research. It provides a detailed description of the specimens utilized, elucidating their significance in the current study. The chapter also expounds upon the various experimental techniques employed, detailing the specific conditions and parameters implemented for each experiment. Chapter 4, offers a detailed analysis of the results obtained from the experiments, allowing a deeper understanding of the study's results. Finally, Chapter 5 draws together the main findings and conclusions derived from the thesis. It presents a summary of the research, highlighting the key outcomes and their implications. Additionally, this chapter provides recommendations for future work, offering suggestions for further investigations and areas that require further exploration.

LIST OF PUBLISHED PAPERS

The outcome of this thesis resulted in a paper published in peer-reviewed journal (open access publication).

Sadeghi, M.; Omiya, T.; Fernandes, F.; Vilhena, L.; Ramalho, A.; Ferreira, F. Tribological Behavior of Doped DLC Coatings in the Presence of Ionic Liquid Additive under Different Lubrication Regimes. *Coatings* 2023, *13*, 891. https://doi.org/10.3390/coatings13050891

Chapter 2 – State of art

2.1. An overview

Modern industrial systems involve a variety of machinery and mechanical systems that have various moving components and, as a result, interacting surfaces. Such machines' ability to perform smoothly, consistently, and over an extended period depends heavily on how effectively wear and friction are managed across all their multiple interacting surfaces [3]. Focusing on this issue, there has been significant progress in our understanding of the basic mechanisms underlying tribological phenomena and the creation of a wide range of new materials, surface engineering techniques, lubricants, and other types of technical solutions. Further, reducing the usage of fossil fuels and the subsequent reduction of greenhouse gas emissions is essential for the long-term sustainability of modern civilization [3].

The application of lubricants, which are often primarily obtained from mineral or synthetic oils, in internal combustion engines or water-based solutions implemented for machining tasks, is the standard technique to decrease friction between moving surfaces and reduce mechanical degradation. Additives for these lubricants are widely employed to enhance already existing qualities or introduce extra properties. They include chemical substances that can adhere to and/or interact with solid surfaces to form protective layers (referred to as "tribofilms"), that are intended to lower wear and friction. In addition to lubrication, surface engineering has also shown significant contributions to friction reduction [3]. DLC thin films, one of the most promising categories of surface engineering solutions, have been the subject of many investigations, specifically in the automotive industry. This chapter gives some important background on issues related to this study, including lubrication, lubricants, additives (particularly ionic liquids), thin film, DLC-based films, deposition processes (particularly PVD), and HiPIMS.

2.2. Tribology

The words "tribos" and "ology" are both Greek words that imply 'rubbing' and 'the study of', respectively, so the word tribology which is the combination of these two words means the study of rubbing. The science of lubrication, wear, and friction between two surfaces in contact in motion is known as tribology [4–6]. The tribological performance is highly influenced by the surroundings and operating circumstances, including the type of interacting materials, surface roughness, mechanical structure, lubrication, atmosphere, etc. Therefore, even though the concepts of tribology are universal, the solutions must be specific to the situation. By coming up with innovative ideas or ways of disposal for used industrial oils, solvents, cutting fluids, and coolants to reduce water contamination, tribology can contribute a lot to environmental protection [7].

2.3. Friction

The coefficient of friction is a quantity that is a measure of the resistance to movement between surfaces. At least there should be a limited amount of horizontal force to move one surface over another. [7] Contact between surfaces only occurs at some asperity points. The atoms on one

surface will attract those on the other in these areas of real contact, resulting in adhesion and the formation of junctions. This is known as cold welding in the context of metals and is most noticeable in mechanical systems operating in a vacuum, such as those found in space. These adhesions must be broken when sliding takes place, which requires shearing the junctions. The main factor causing friction between clean surfaces is the force needed to shear the connections. Another reason for friction is that if one surface is much harder compared to the other opposing surface, asperities on the harder surface will cause grooves in the softer surface, which necessitates a stronger force to make relative motion possible. Although under lubrication the plowing component (which causes grooves) may make up a significant proportion of the total frictional force, for clean surfaces the adhesional friction type typically predominates [7]. The ratio of the force opposing the motion to the force pressing the surfaces together perpendicular to the motion is what is referred to as CoF [5, 6]. When a solid item moves through a liquid or gas medium, like when an airplane is in flight, fluid friction, a form of friction, occurs [6].

There are other types of friction like Static, kinetic, and rolling friction as well. Static friction is the force preventing two bodies in contact from moving relative to each other. The force that resists two interacting bodies' relative motion as they slide over one another is known as kinetic friction. When a body rolls on a surface, rolling friction shall be considered. Rolling friction is the force that counteracts the action of rolling.

2.4. Wear

Wear damages the machine's functioning surface, which results in functionality loss. The loading situation, temperature, and the type of motion between the contact points are only a few of the variables taken into account when calculating the wear rate. In many cases wear can be measured by the loss of material from a surface [6]. In general, the most important mechanisms are adhesive, abrasive, corrosive, and fatigue wear [7].

2.4.1. Adhesive wear

Adhesive wear is explained by the theory that the attraction forces between the atoms on each surface should, in theory, cause two clean surfaces with similar crystal configurations to attach strongly to one another when they are in direct contact. If the adhesion between two surfaces is strong enough, in relative motion, fracturing will happen away from the initial sliding interface and one material will transfer to the other, causing adhesive wear. The wear will typically start in the softer material and transfer materials adhesively to the surface of the harder one [7].

2.4.2. Abrasive wear

When hard surfaces slide over softer materials, asperities on the hard surface act similar to a cutting tool to scrape material off the softer surface, and abrasive wear occurs. When a loose debris particle becomes stuck between the sliding surfaces, another significant mechanism causing abrasive wear occurs: the particle cuts the softer surface and creates a wear groove. Such debris

may be of external origins, like sand particles, or it may be created on-site by the main wear, like oxide particles [7].

2.4.3. Corrosive Wear

A surface degrades through corrosion when chemicals in the environment react with it. A solid's clean surface, like the surface of a metal, will typically react with its surroundings, producing corrosion products that will eventually create a contamination layer. As the corrosion layer thickness rises, the rate of creation of such layers declines. However, the corrosion resultant film frequently adheres to the surface only weakly in many situations, such as rust on iron. Thus, rubbing may cause the top film to be scraped off, revealing the clean surface beneath. This surface then reacts with its surroundings to create fresh surface films, which are then removed through additional rubbing. As a result, in this instance, the material is repeatedly being taken off the surface. Environments that are corrosive can be advantageous for wear reduction in some cases. For example, a mechanically stable oxide film that doesn't flake off while sliding, can operate as a strong barrier layer, stop metal-to-metal contact, and slow down wear. The oxide must stick tightly to the metallic substrate, have enough thickness to be flexible, and share alike mechanical properties with the metal in order to form a mechanically stable layer [7].

2.4.4. Fatigue Wear

When a surface is loaded cyclically as a result of repetitive sliding, rolling, or collisions, fatigue wear could occur. Even when the load is lower than what is sufficient to cause other types of mechanical failure, fatigue failure might nevertheless happen after a significant number of loading cycles. The adhesive and abrasive wear mechanisms cannot occur if the surfaces are separated by a lubricant layer (assuming that abrasive particles are excluded). The lubricant film still allows the applied load to pass through to the solid surface, creating surface tensions and the potential for significant fatigue wear [7].

2.5. Thin films

The interdisciplinary field of surface engineering tries to response to the realization that a vast number of engineering systems have the chance to deteriorate or completely fail in use due to parameters associated with surfaces such as wear, corrosion, and fatigue. To manufacture a product with features not possible in either the base or surface material, surface engineering entails applying both conventional and cutting-edge surface enhancement technologies. Identifying the surface and substrate demands is the initial milestone in choosing a surface modification technique [8, 9]. One of the main surface engineering techniques is layered nanostructures that are applied on the surface with thicknesses between a few nanometers (nm) to micrometers which are called thin films or coatings [10]. The coating can be deposited from a solution of ions (like electroplating), from the liquid state (such as thermal spraying), or from vapor. Chemical vapor deposition (CVD) and physical vapor deposition (PVD) are two categories of techniques for creating films from the vapor phase. PVD refers to the thin film deposition method that uses a physical vapor. Essentially, this kind of deposition technique entails converting the source material

from a solid or liquid to a vapor phase before passing through a plasma environment, low-pressure gaseous environment, or vacuum environment to the substrate. After condensing as a thin film on the substrate, the vapor then transitions back into the solid form. With greater control over the applied chemical and physical characteristics of source materials, PVD is reported to produce coatings with high adherence to most materials. The two most used PVD techniques, evaporation and sputtering, both enable the deposition of particles from the target to the substrate using electrodes linked to a power source and a vacuum chamber. The principle behind the PVD technique known as sputtering is to bombard the target with energetic ions, frequently utilizing inert argon gas, causing the atoms of the target to eject form it and deposit on the substrate [11, 12]. A variety of materials can be coated using the adaptable technique of sputtering. Reactive sputtering, which modifies the process by including a reactive gas, is frequently applied to deposit oxides, nitrides, and carbides. Generally, sputtered films demonstrate relatively stronger adherence than evaporated films because of the increased inter-diffusion and mixing that occurs between ejected atoms and the surface atoms of the substrate in the sputtering process (due to the higher thermal energy of sputtered atoms compared to evaporated atoms) [10]. Figure 1 shows the main mechanisms involved in PVD processes.

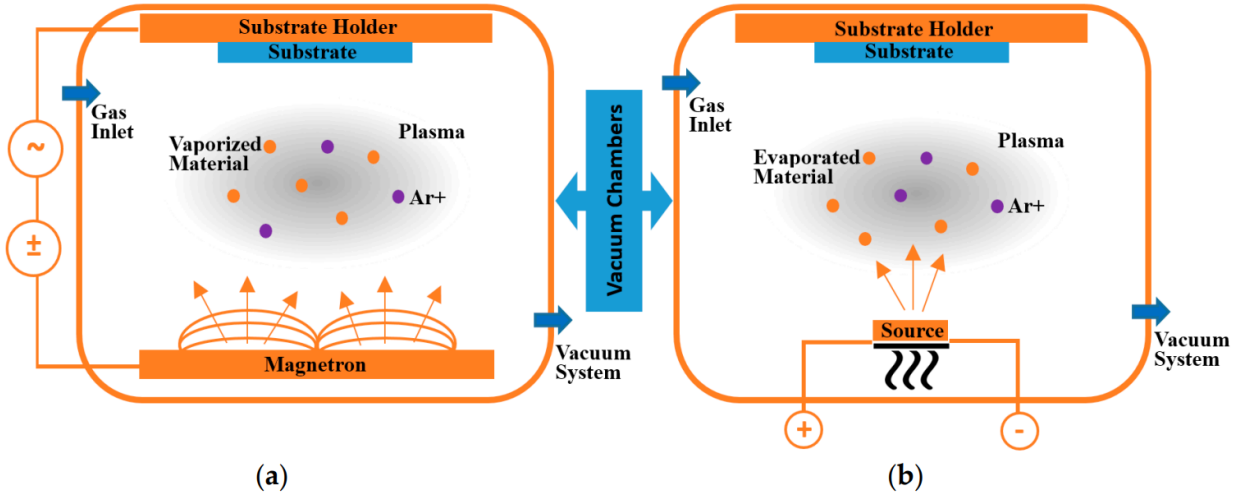

Figure 1) Schematic drawing of two conventional PVD processes: (a) sputtering and (b) evaporating (reproduced from [11]).

2.5.1. Deposition of thin films using deep oscillation magnetron sputtering process (DOMS)

Sputtering techniques that enable controlling the flux of sputtered material have been developed during the past few years in response to the requirement for coatings with increased efficiency and characteristics. If the deposition flux has a higher percentage of ionized than neutral particles, these processes are known as ionized PVD (IPVD). Controlling the ejected material, for instance, makes it possible to cover cavities' interiors with a constant thickness, which is a crucial requirement in the microelectronics sector. Nevertheless, compared to DCMS, most IPVD approaches need advanced hardware, consequently, investment in them has primarily been in the scientific environment. A novel magnetron sputtering coating technology known as HiPIMS which was descended from the traditional DCMS has made it possible in the last decades to produce

severely ionized volumes of ejected material. By raising the power linked to the target in DCMS, the plasma concentration can be raised. But the melting point and cathode cooling capacity of the target place a restriction on the amount of power that can be delivered to it. HiPIMS applies power in very brief periods, allowing for a considerable boost in the power's instantaneous amount without melting the target. The considerable decline in deposition rate when compared to DCMS, is HiPIMS technology's primary problem. However, usually, the films deposited by HiPIMS have a denser structure because of incredibly energetic metal ions [13]. Modulated Pulse Power Magnetron Sputtering (MPPMS), a novel variation of HiPIMS, splits each pulse into pieces with varying voltage and current value, resulting in longer pulses than those used in the traditional HiPIMS, with a length of up to 3 ms. When used in a reactive mode, both HiPIMS and MPPMS techniques have a substantial drawback: a large volume of arcs is produced, which has a negative impact on the features of the films. Lately, a form of MPPMS has been created in which the voltage pulses are made to prevent sudden voltage fluctuations, hence reducing the number of arcs that are generated which is named as deep oscillation magnetron sputtering process (DOMS). In this study, thin films were deposited using a power supply running in DOMS mode. The DOMS approach, like MPPMS, enables adjusting the ionization degree of the sputtered material from extremely low values (like DCMS) up to standard HiPIMS levels.

2.6. Diamond-like carbon coatings

Industrial machines often operate in conditions where sliding occurs between surfaces (i.e., boundary lubrication regimes) and contact between asperities occurs which leads to wear and degradation of components. Furthermore, in some industrial settings, there is a demand for sliding contact in the absence of liquid lubrication. To respond to this issue, self-lubricating coatings have been developed to improve durability and performance in such situations that place high demands on the contacting surfaces. Self-lubricating coatings have proven to provide decent outcomes in a wide range of technical applications. The application of these coatings modifies the microstructure, mechanical properties, and tribological performance of the contacting surfaces [14, 15].

Self-lubricating coatings have a lower friction coefficient due to possessing a surface that can self-generate lubrication under certain conditions, such as heat or pressure. These coatings can improve the wear resistance of the material and extend the life of the parts they are applied to. However, achieving low friction and longer life simultaneously can be challenging. In some cases, increasing the wear resistance of the coating can lead to an increase in friction, while reducing friction can make the coating more prone to wear. Additionally, the conditions under which the coating operates can affect its performance, such as temperature, pressure, and environmental factors [14, 16]. To overcome these challenges, researchers have been constantly developing new materials and coatings that can provide both low friction and resistance to wear. This involves a careful balance between the material properties, deposition conditions, and techniques to optimize the performance of resultant coatings [16, 17].

Diamond-like carbon (DLC) coatings are a type of self-lubricating coatings known for their exceptional mechanical and tribological properties, such as high hardness, low friction, and excellent wear resistance [14, 18]. Diamond-like carbon (DLC) coatings are differentiated from

graphite-like carbon (GLC) coatings based on the carbon fractions of sp^2 and sp^3 present in the coatings. In DLC coatings, the sp^3 carbon fraction predominates, while graphite-like carbon sp^2 fraction is the dominant one [19]. Also, a tribological response is heavily influenced by surface topology, and mechanical interlocking between surface asperities which leads to a higher coefficient of friction, particularly during the running-in stage. The roughness parameter of DLC coatings is largely determined by the topology of their substrate [20].

DLC coatings come in a variety of types with different structural and chemical properties that can affect their tribological behavior. Some common types of DLC coatings include hydrogenated amorphous carbon (a-C:H), tetrahedral amorphous carbon (ta-C), amorphous carbon (a-C), and hydrogenated tetrahedral amorphous carbon (ta-C:H) films [21]. These coatings are used on parts like tappets, pistons, piston rings, fuel injectors, and biomedical devices (orthopedic, cardiovascular, and dental equipment), to lower friction. This reduction in friction not only improves savings but also aids in meeting regulatory environmental and legislative requirements [21–23]. According to a report [24], the market size of Diamond-like Carbon (DLC) was assessed at USD 1786.04 Million in 2021 and is anticipated to reach USD 3068.78 Million by 2030. This growth is expected to occur at a Compound Annual Growth Rate (CAGR) of 6.30% during the period from 2023 to 2030. Moreover, the number of DLC publications indexed in the ScienceDirect database in the last ten years has increased from 550 publications published in 2012 to 1300 published articles only in 2022. The substantial increase in worldwide revenue and the corresponding rise in research outputs indicate the increasing significance and strong demand for DLC coatings.

Figure 2 shows ternary phase diagram of amorphous carbons and illustrates three distinct regions representing diamond, graphite, and hydrocarbons. Within these regions, the classification of DLC (diamond-like carbon) varies based on the sp^3 content (the proportion of carbon atoms bonded in a tetrahedral arrangement) and the H content (hydrogen content) [25]. Specifically, there are four classifications: ta-C (tetrahedral amorphous carbon), which lacks hydrogen and has a sp^3 content greater than 60%; PLCH (polymer-like carbon with hydrogen), which contains more than 40 atomic percent of hydrogen and has a sp^3 content up to 70%; DLCH (diamond-like carbon with hydrogen), where hydrogen content ranges from 20-40 atomic percent; and GLCH (graphite-like carbon with hydrogen), which has a hydrogen content below 20 atomic percent and a sp^3 content lower than 20%. In the case of ta-C:H (tetrahedral amorphous carbon with hydrogen), the sp^3 content can reach approximately 70% while the hydrogen content ranges from 25-35%. Furthermore, the C-C sp^3 content is significantly higher in ta-C:H compared to PLCH. DLCH, on the other hand, has a lower sp^3 content than ta-C:H for a given hydrogen content [25].

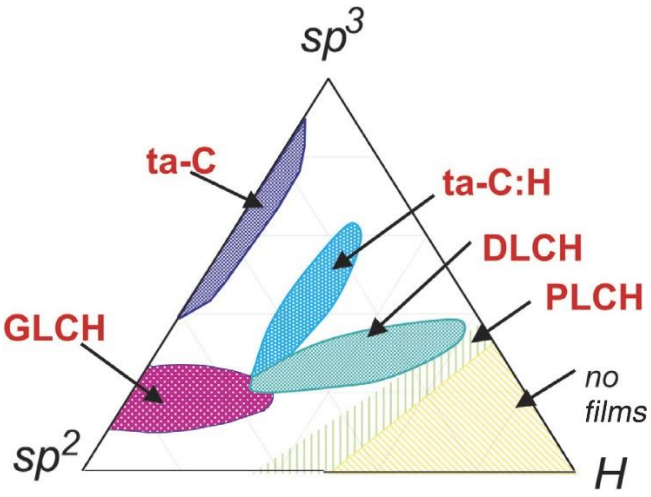

Figure 2) Ternary phase diagram of amorphous carbons [25]

2.6.1. Major research trends in the production process of DLCs

Currently, there is an intense focus on enhancing and optimizing DLC coatings through various areas of investigation, but in this review, only two of them will be reviewed. The first is operational and deposition parameters and the second is doping DLCs with other elements to improve their performance.

The first area pertains to operational parameters such as plasma potential, ion energies, and power source, which are being extensively analyzed for their impact on DLC quality. PVD and PECVD are the most common methods for the deposition of DLCs. Common technologies used for the deposition of DLC coatings are magnetron sputtering [26], Filtered Cathodic Vacuum Arc [27], Microwave plasma [28], Radio frequency glow [29], Pulsed laser depositing [30], ion beam [31], Plasma Immersion Ion Implantation and deposition [32] and combination of these techniques [33–35]. Each technology of DLC deposition has multiple variables that affect its growth and performance, such as electric power inputs [36, 37], distance factors (such as substrate to source distance) [38], and deposition temperatures [39, 40]. Various methods, including sputtering, arc deposition, ion beam deposition, and hybrid methods (such as RF + PECVD), are being utilized to increase the sp^3 ratio in DLC coatings [35]. It is worth noting that while a higher sp^3 fraction leads to higher hardness, lower friction, and higher wear resistance, such coatings also have some drawbacks, such as higher residual stresses and lower toughness[35]. The aforementioned concerns have resulted in the expansion of the field of DLC structural design, encompassing monolayers [41–43], multilayers [44, 45], and hybrid microstructures [15, 35].

Data analytics-based optimizing techniques have been used to help researchers find the optimal parameter for deposition [46]. However, the best value for one parameter, such as bias voltage, does not necessarily result in the best combination of properties. Many parameter combinations may need refinement to achieve the best properties for DLC coatings. Jean et al. implemented the Taguchi method for optimizing deposition parameters and assessed the significance of process parameters by conducting an analysis of variance (ANOVA) [47]. In another study [48], various properties of DLC coatings, including their morphology, structure, bonding states, friction

coefficient, and wear behaviors were optimized using an adaptive neuro-fuzzy inference system (ANFIS) identification technique assisted with Taguchi's algorithm to reduce the error of fuzzy estimator system for tribological properties. Additionally, the optimal process parameters for the deposition of DLC films using plasma enhanced chemical vapor process (deposition temperature, Methane-Argon flow rate, and hydrogen flow rate) were searched using the repulsive particle swarm optimization algorithm and a traditional genetic algorithm (GA) [49]. Solis-Romero et al. [50] optimized working settings for reducing wear and friction of multi-layered a-C:H coating by implementing a hybrid grey-fuzzy algorithm. However, it is crucial to consider the fact that optimization or prediction works well when the model is made properly and accurately. A higher number of input parameters leads to more sophisticated models. Custom functions that are defined by the user have an impact on the results. Furthermore, the intricacy of the model has a bearing on its ability to be trained on the available data and also diminishes its potential to generalize well to new, unseen data [46].

The second area of investigation is related to the development of DLC nanocomposite coatings by introducing other elements. This approach involves doping the DLC coating with other elements (i.e., co-deposition of DLC coatings with metal, ceramic, and gaseous elements) to produce nanocomposites with improved properties [19]. For instance, to optimize tribological properties, DLCs have been doped with Cr [51], Mo [52], and Ni [53].

High residual stress in DLC films causes improper adhesion, which can lead to the peeling of coating even during film deposition. According to several studies [19, 54–57], using metallic/non-metallic elements as dopants can reduce residual stress by controlling the microscopic structure, adhesion, sp^3/sp^2 ratio, and surface roughness of DLC coatings. As a result, a controllable carbon bond structure and low residual stress are critical factors in obtaining preferable properties in a DLC film [56]. To reduce residual stress, DLCs have been doped with Ti [58, 59], W [56, 60], Si [61], N [62], F [57], Nb [55], Au[54].

Doping also improves the performance of DLC thin films in biomedical applications. This is the case for functional coatings in ureteral stents [63] or textiles for hospital use that need to be antibacterial [64], where, for example, Ag gives this property to DLC [65].

2.6.2. Characteristics of DLC coatings

2.6.2.1. Thermal stability of DLC coatings

One of the characteristic which researchers aim to enhance in DLC coatings is improving their maximum working temperature limit. This would allow DLC coatings to be useful in industries like aerospace, automotive, and turbomachinery, as they can currently only handle temperatures up to 300°C [35, 66]. When exposed to high temperatures, DLC films can experience various changes such as oxidation, graphitization, and dehydrogenation. Therefore, they can lose their lubricating capabilities and even detach from the surface they are applied on. This can lead to the creation of a transfer layer and wear debris on the surfaces of the objects in contact [67]. The graphitization phenomenon is thought to be responsible for lowering friction within the temperature range of 0 to 150°C, in this range, heat can facilitate the transformation of some sp^3

bonded carbons to sp^2 carbons when a load is applied [68]. Similarly, the findings of Zhang et al. [69] showed that subjecting the DLC films to thermal annealing resulted in their graphitization. elevating the annealing temperature caused a decrease in the hydrogen content in hydrogenated DLC films, which facilitated the shift from sp^3 to sp^2 hybridization. But they reported that at 300°C and higher, the ultra-low friction behavior fails because the heat produced during friction might not dissipate promptly, and the system's temperature becomes too high to sustain a proper structure.

Yu et al. [70] Studied the tribological characteristics of three different DLC films with varying Si contents applied on a tungsten interlayer. At temperatures below 300 °C, the pure DLC film exhibits impressive tribological characteristics. The low friction coefficient at room temperature is primarily due to the presence of Van deer Waals bonds, while the high-temperature properties between 100 °C and 300 °C are believed to be a result of graphitization. The addition of Si content to the film allows for lubrication to be sustained at 400 °C, with the low friction coefficient obtained being a result of the enhanced thermal stability achieved through Si alloying. However, at temperatures higher than 500 °C, the film failed due to the oxidation of silicon. A composite film comprising oxidized tungsten and tungsten carbide phase is responsible for low CoF of Si-DLC with tungsten interlayer.

2.6.2.2. Chemical Resistance of DLC films

Diamond's lack of reactivity with chemicals is highly desirable for its use as a shielding layer to prevent chemical reactions of a substrate with surrounding compounds [71, 72]. To evaluate the chemical resistance of DLC films, the researchers applied DLC coatings of varying thicknesses. They found that thicker coatings offered more protection against chemical reactions than thinner ones and that using a layered approach with a silicon interlayer was the most effective at preventing permeation. However, the presence of defects in the coatings still had an impact on the permeation process [73]. In another study, Ohtake et al. conducted a concentrated nitric acid corrosion test to assess the acid resistance of the DLCs [74]. Although a high sp^3 content was believed to reduce film corrosion, the actual relationship between sp^3 content and corrosion resistance were found to be insignificant. Instead, corrosion resistance was found to be more closely linked to the presence of pinholes, micrometric growth defects, and dust particles. It was also discovered that increasing sp^3 content and density during film application did not necessarily lead to improved corrosion resistance.

Wongpanya et al. [75] focused on examining the corrosion resistance, bonding structure, and biocompatibility of diamond-like carbon (DLC) films deposited on stainless steel with an interlayer of titanium. Results indicated that ta-C:Ti/Ti exhibited the highest level of corrosion resistance and biocompatibility, thanks to the formation of TiO2 on its surface. Moreover, the presence of two barrier layers was observed in ta-C:Ti/Ti, making it a promising material for joint replacement.

Fayed et al. [76] examined the deposition of Si/DLC films on 2024-Al alloy using a plasma-enhanced chemical vapor method at different pulse voltages. Results showed that increasing the pulse voltage to 1800 V led to thicker coatings with better mechanical and corrosion resistance

properties in 3.5 wt.% NaCl solution compared with other coatings due to an increase in sp^3 hybrid in the coating, limiting electrical conductivity. However, increasing the pulse voltage to 2200 V increased the corrosion rate of the coatings.

2.6.2.3. Friction and wear of DLC coatings

Numerous research papers have explored the frictional characteristics of DLC films in various settings. In the past few years[77]. The primary method by which DLC films typically control friction involves the formation of a transfer film, which then facilitates easy-shear sliding within the interfacial material. However, the effectiveness of this mechanism is significantly influenced by the type of gas environment present in the contact area [78].

DLC coatings are highly susceptible to the effects of oxidizing agents, such as oxygen and water vapor, during friction. The presence of such agents can lead to a significant tribo-oxidation, which in turn can increase both friction and wear. While wear rates can sometimes be very low, they can also be extremely high, rendering the coating unsuitable for certain applications [79]. The sustained low friction observed in DLC films under ambient air conditions is a result of wear-induced graphitization, which entails the creation of a tribolayer with a graphitic structure that exhibits low friction [80]. The process of graphitization in their experiments was affected by two factors: the speed at which the surfaces were sliding against each other, and the amount of force being applied. This is because when the surfaces come into contact, the resulting friction causes the temperature to increase at the contact points. This rise in temperature causes hydrogen to be released from the DLC structure, which contributes to the graphitization process [81].

Films that have varying amounts of hydrogen possess distinct physical characteristics, including the way the carbon atoms are arranged, hardness, level of stress, and how they behave under controlled tribological conditions [78]. Miyake et al. conducted a study comparing the friction of two DLC coatings with different amounts of hydrogen. Both of the films had similar hardness values. The DLC film with lower hydrogen content had higher friction in a vacuum environment than the film with more hydrogen. However, in humid ambient air, the DLC film with lower hydrogen content had smaller friction compared to the film with higher hydrogen content. They speculated that hydrogen presence modifies the adsorption process of moisture and increases friction [82].

Donnet et al. reported that in PACVD systems, high-impact energy caused by bias directly controls the deposition process and leads to higher precursor dissociation. This results in a carbon network that is more crosslinked, has a lower sp^3 fraction, lower hydrogen content, and a lower fraction of hydrogen bonded to carbon. Films deposited under such conditions are harder, and exhibit very high friction (>0.5) in UHV conditions. DLC films can achieve ultralow friction and wear in UHV if they have high enough hydrogen content (around 40 at. %), a crosslinked carbon network, and a noticeable fraction of unbounded hydrogen. By increasing the absolute bias from 500 to 800 V using the deposition system in their study, the hydrogen content in films deposited could be lowered by about 6 at. % and the fraction of hydrogen bonded to carbon by about 0.16, thereby increasing friction in UHV from less than 0.01 to more than 0.5. This indicates that the structure

and composition of DLC films strongly affect their friction behavior, making it crucial to control both friction and wear by paying close attention to the deposition process[78].

Besides, hydrogen content, relative humidity also affects the tribological behavior of DLC coatings. Kokaku et al. [83] studied the impact of being exposed to a highly humid atmosphere on the wear and friction properties of hard carbon films. The exposed sample showed an increase in friction coefficients. This increase in friction coefficients occurred due to the oxidation reaction on the surface of the carbon, leading to changes in its surface properties. The creation of a carboxylic acid soap was responsible for the formation of the friction layer. This was found to occur when oxidized DLC films reacted chemically with ferrous oxide [84].

Kim et al. demonstrated how different normal loads and velocities can cause variations in CoF and wear [85]. An increase in load results in a reduction in the graphitization temperature due to the elevated contact stress. During experiments, it was observed that under constant sliding velocity, as the normal load increased, the average wear rates of both DLC coatings and AISI 52100 steel balls decreased. However, the average wear volume of the two surfaces increased. Conversely, as sliding velocity increased under constant load, both the average wear rates and wear volumes of the two surfaces increased until reaching a maximum value, after which they decreased as the sliding velocity further increased. The process of graphitization can be facilitated by friction-induced annealing on local contact areas and the strain energy induced by sliding [86]

Due to the poor compatibility with oil additives currently available, hard hydrogen-free ta-C coating usage is significantly restrained [87]. Although it has been demonstrated that DLC thin films have appealing friction and wear responses when exposed to oils that constitute distinct chemical groups, such as alcohols and fatty acids, their use in the technological field has not been extensively reviewed in the literature [88].

Lanthanides (which include Eu and Gd elements) are supposed to have a positive effect on tribolayer formation when ionic liquids are used as additives because they show high affinity to ILs [2, 89–93]. DLC thin films which are doped with Eu or Gd between 1% and 3% atomic concentration exhibit the usual traits of un-doped DLCs, including a low specific wear rate and high hardness (23 GPa) [88].

2.7. Lubrication

Introducing a lubricant between moving surfaces in contact will reduce friction and wear. According to the mechanism of friction, this is possible to reduce friction by adding a barrier film on the asperity tips, so that, first, it can inhibit contact between the two surfaces, blocking the creation of adhesive intersections, and second, this layer should have a small shear strength so that any junctions that do form can be easily broken. It is also obvious that the film must be strong enough to endure the intense pressures at the sliding surfaces [7]. Thus, lubrication extends the lifespan of machine equipment by eliminating wear-related problems while simultaneously increasing system performance by decreasing friction. Other functions of lubrication include clearing away debris from the system and cooling the contacting bodies [6].

The two lubricants most frequently used are oil and grease. A thickening agent and oil are combined to make grease. Mineral-based, synthetic, vegetable-based, and hybrid oils are all acceptable types of oils. Although synthetic oils are sometimes utilized in harsh situations, most vegetable oils are environmentally beneficial.

A representation of a liquid lubricant's frictional properties that typically includes the boundary, mixed, and hydrodynamic regimes is referred to as a "Stribeck curve." The ratio of lubricant layer thickness to surface roughness determines each regime. Stribeck curve relates COF to Hersey number (which is equal to μv/p where v is speed, μ lubricant's viscosity, and P is the contact pressure) [6]. These curves are frequently used to assess the impact of variations in the viscosity of the lubricant, the effect of additives, or the impact of surface properties on friction.

2.8. Simultaneous use of base oils and DLC thin films

Cardoso et al. [94] compared the performance of Chromium nitride (CrN) and DLC thin films produced with different compositions of Ne in plasma using SAE 10 W 40 semi-synthetic under different lubrication regimes. The DLC 25% Ne performed better than the other thin films evaluated in their research, according to their data. When compared to CrN coatings, the 25% Ne-DLC surpassed the other films for lubricated contact in mixed lubrication conditions reducing the friction coefficient from 0.127 to 0.107.

Recently, Vahidi et al. [95] reported that when compared to CrN and typical DLC films in the boundary lubrication regime, Ne-DLC films showed improved tribological performance using PAO 8 as lubricant and concluded that compared to typical DLC films, the Ne-DLCs produced with HiPIMS method enabled the development of DLC films with significantly improved tribological and mechanical qualities.

2.9. Ionic liquids

Zinc dialkyl dithiophosphate (ZDDPs) have been used as additives in engine oil compositions, for instance, since the 1940s to lessen wear [96]. Research on the ZDDP's lubricating process has been ongoing for many years. The surface response of ZDDP to produce patchy glassy phosphate coatings is the widely accepted explanation for how ZDDP prevents wear. The significant levels of phosphorus, sulfur, and zinc in this category of additives, which are believed to induce filter clogging and catalyst deterioration in exhaust after-treatment processes in internal combustion engines, have pushed the environmentally adverse effects of ZDDPs application into sharper criticism despite their exceptional efficacy under a wide variety of settings. As a result, investigations have been going on to find alternatives for ZDDPs [96–98]. It is necessary to prioritize the advancement of biodegradable lubricants that are friendly to the environment and have reduced toxicity levels. Efficient lubrication plays a vital role in reducing the energy wasted due to friction. Furthermore, the use of high-quality lubricants reduces friction and wear and contributes to their long-term durability [99].

Ionic liquids (ILs), in between several solutions recommended as an addition to or equivalent for ZDDPs, have attracted a lot of attention from tribologists during the past years. An anion and an organic cation make up ILs, which are liquid salts with melting points under 100ºC [100–102].

Large organic molecules represent the majority of the ILs' ions. The electrostatic interaction between their cation and anions is weak because of their molecular dimensions and chemical structure, making them a liquid at room temperature [103]. In an ionic liquid, the positively charged part commonly contains organic substances like ammonium or imidazolium, which are accompanied by alkyl chains and various additional groups [104, 105]. The characteristics of the ionic liquid are influenced by its cations and anions. By carefully engineering the structures of both the positively and negatively charged components, the properties of ionic liquids can be customized to meet the requirements of different applications [106]. Figure 3 shows typical ions found in ILs.

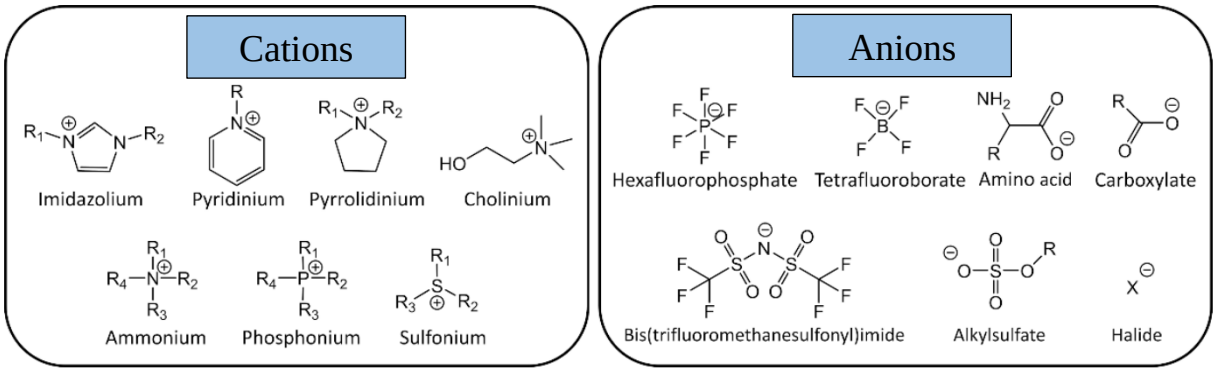

Figure 3) Common ions in ionic liquids (ILs) (reproduced from [107])

High thermal stability and low volatility [108–110] are only a few of the advantageous traits of ionic liquids, which make them suitable as both lubricants and lubricant additives [100, 101, 103]. When employed as a lubricant or lubricant additive, the ILs additionally exhibit some physical qualities that allow them to "separate" the contacting surfaces due to a sudden shift in the IL's phase towards a solid-like phase below a threshold thickness, which suggests capillary freezing in confinement [111]. The most significant property of ILs is that they are tribochemically active, and easily decompose to form a tribofilm when in touch with metal or metal oxide surfaces [103]. The charge-carrying atoms of ILs are crucial for understanding their tribochemical activity. The IL molecules that are absorbed into the metal surface disintegrate and create a tribofilm under tribological stresses. The ionic heads in the ILs can be attracted to the metal surface. When ILs are in direct touch with metal or metal oxide surfaces, they become tribochemically active, easily break down, and develop a tribofilm. The tribochemical activities on the surface of metal are shown to involve both the anions and cations of the Ionic liquids [102, 112, 113].

Oxide products of Iron and wear traces need to be involved in a regular ionic liquid's tribofilm process that contains phosphate. The formation of the tribofilm can also enclose the wear debris as it grows. This also causes the IL tribofilm to be thinner than the ZDDP's film consequently [114]. The majority of ILs don't have any metal components. Therefore, they react with metal

substrates or produced debris coming from the wear process. This results in a metal-based film that is created by ILs. Usually, tribofilm compositions are quite similar when ILs containing P get utilized to that of ZDDP tribofilm. Both have polyphosphate in them. The sole distinction is that IL tribofilm captures some wear particles while ZDDP tribofilm contains zinc traces [103].

2.9.1. Thermal Stability of ionic liquids

Thermal stability plays a vital role in preserving the integrity of lubricants within their designated temperature range [115, 116]. The utilization of air as a fundamental and pragmatic medium for evaluating the lubrication effectiveness of ionic liquids (ILs), where oxidation is an unavoidable phenomenon, holds significant importance. Generally, ILs demonstrate enhanced thermal stability in comparison to hydrocarbon oils that undergo decomposition at approximately 250°C. Earlier research findings have provided evidence suggesting that the thermal stability of phosphonium-carboxylate and ammonium-phosphate ionic liquids (ILs) is comparatively lower than that of phosphonium-phosphate ILs. In addition, ILs derived from imidazolium and pyridinium manifest exceptional thermal stability, even in the presence of cationic alkyl chains [117].

2.9.2. Corrosion behavior of ionic liquids

Before their industrial application, ionic liquids need to meet certain criteria and undergo comprehensive testing to assess their potential corrosive effects on equipment materials [118]. Uerdingen et al. [118] investigated flow-induced localized corrosion (erosion corrosion) of ILs, using the rotating cage technique, representing one of the initial comprehensive studies on this matter. The outcomes revealed the detrimental effects of tosylate and dimethyl phosphate anions. When exposed to dilution or contamination by water, various anions employed in the synthesis of ionic liquids may undergo hydrolysis, resulting in the formation of acids like sulfuric and phosphoric acid. Consequently, this acidification process creates an acidic environment that triggers corrosion.

Within a comparable investigation employing a rotating cage apparatus, an assessment was carried out to explore the corrosive characteristics of multiple ionic liquids (ILs) possessing distinct ion structures. The findings of the study elucidate a substantial reliance of the corrosion behavior on the specific chemical arrangement. Notably, it was observed that a majority of the tested ILs exhibited a minimal degree of corrosive activity when exposed to stainless steel surfaces [119].

Corrosion inhibitors are compounds introduced in minute concentrations to the working fluid, where they engage in chemical or mechanical interactions with the metal surface. This interaction serves the purpose of inhibiting additional metal deterioration and diminishing the occurrence of corrosion [120–123]. Numerous research endeavors have been conducted to explore the capacity of ionic liquids (ILs) as corrosion inhibitors [120, 124, 125]. Sometimes ionic liquids (ILs) possess the potential to function as corrosion inhibitors; however, it is crucial to note that in certain circumstances, they may also exhibit corrosion-promoting properties. The corrosive behavior of ILs is influenced by several factors, such as the chemical composition of the IL, the nature of the metal surface, and the surrounding environmental conditions. The findings of these investigations

underscore the significance of considering the specific IL and prevailing conditions when employing them in industrial settings.

2.9.3. Optimum concentration of IL as an additive

Some studies have investigated the appropriate concentration of ILs when used as additives. For instance, the dependence of the friction and wear response on the concentration of a ZDDP, a phosphonium-alkyl phosphate IL, and an IL+ZDDP combination, regarding the tribofilm structure and nature were methodically evaluated in a study by implementing a ball-on-flat reciprocating sliding device, where a hardened AISI E52100 steel ball slides on a CL35 grey cast iron. A thicker, rougher, and more fragile tribofilm was strongly observed simultaneously with an increase in friction coefficient which was generated by the ZDDP percentage increasing from 0.4 to 6.4 wt%. The fact that there were fewer phosphates but more sulfur compounds in the ZDDP tribofilm helped to clarify this observation. The IL and IL+ZDDP, on the other hand, kept their friction coefficient low and steady at 0.5 wt% or higher levels of concentrations. No sulfur was reported in the IL tribofilm, and even at significant concentrations, the sulfur compounds were kept at a low level in the tribofilm for IL+ZDDP. According to the findings, reducing the sulfur content of the tribofilm would be a useful strategy for reducing friction. Both of the IL-containing AWs clearly showed an exciting relationship between the AW concentration and the wear loss, with an optimal value at 2 wt% when IL was implemented alone and 0.46-0.92 wt% for the IL+ZDDP application together, respectively [126].

2.9.4. Explanations of the lubrication mechanism of ionic liquid

Ionic liquids based on phosphonium phosphate (PP-ILs) have been mainly investigated among ILs that have been indicated to function on solid surfaces when typical pressures and shear stresses are present because of their remarkable miscibility with hydrocarbon fluids [127, 128]. The prevailing consensus in the academic community is that the introduction of neat ionic liquids (ILs) or IL additives between contacting work pairs results in the physical and/or chemical adsorption of IL molecules onto the surfaces of the workpieces. This phenomenon leads to the formation of a well-organized boundary lubricating film, effectively shielding the moving components from direct contact and consequently reducing friction. Moreover, as the sliding friction ensues, a protective tribofilm is formed on the substrate surface through tribochemical reactions involving ILs or their decomposition products and the metal surfaces in contact [129]. Figure 4 illustrates both the mentioned mechanisms.

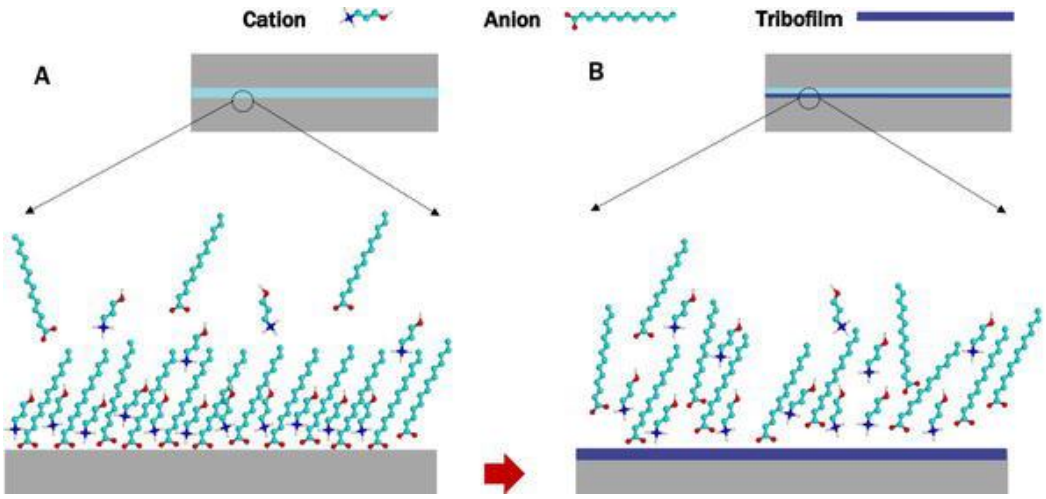

Figure 4) Visual representation illustrating (A) the formation of a boundary lubricating film by ionic liquids and (B) the creation of a tribofilm on the metal surface due to the presence of ionic liquids. ([129])

PP-ILs tribochemically react at sliding steel/cast iron contacts to create surface layers that may possess iron phosphate. For this case, it was suggested that these films serve as sacrificial layers that effectively reduce friction and wear values [127, 130–132].

2.9.5. Available Ionic liquids for this research work

Two ionic liquids will be used for this research work:

2.9.5.1. Trihexyltetradecylphosphonium bis(2-ethylhexyl) phosphate [P_{66614}] [DEHP]

trihexyltetradecylphosphonium bis(2-ethylhexyl) phosphate [P_{66614}] [DEHP] was synthesized using the method described in Ref. [133]. Trihexyltetradecylphosphonium bis (2- ethylhexyl) phosphate ([P_{66614}] [DEHP]), a prospective antiwear lubricant addition for steel-cast iron contacts, was described in 2012 as having mutually miscible features in nonpolar hydrocarbon lubricants. [134–136] Later investigations from a few different groups [137, 138] confirmed the oil miscibility and showed efficient wear mitigation in lubricating steel–aluminum and steel–steel contacts, which strengthened the idea of employing [P_{66614}][DEHP] as an antiwear additive [133].

Using a conventional four-ball tribometer, the wear reduction properties of two oils (base oil PAO and synthetic motor oil labeled as 5W-40) was studied by mixing them with metal oxide nanoparticles and phosphonium-based ionic liquids (trihexyltetradecylphosphonium bis(2-ethylhexyl) phosphate [P_{66614}] [DEHP]). The worn surface area decreased when 1% phosphonium-based ionic liquids and nanoparticles were added to pure PAO, and for the case of synthetic motor oil mixed with the same additives, the wear trace was reduced. Commercially speaking, it is significant that ionic liquid-nanoparticle additions in oils require only a minimal amount to have a significant impact on their tribological behavior [139].

When used as an oil additive for the boundary lubrication of a Ti-6Al-4V surface moving against a bearing steel ball, trihexyltetradecylphosphonium bis(2-ethylhexyl) phosphate [P_{66614}] [DEHP] exhibited enhanced friction behavior to varying degrees and exceeded the traditional ZDDP.

Trihexyltetradecylphosphonium bis(2-ethylhexyl) phosphate [P_{66614}] [DEHP] showed outstanding wear reduction, indicating superior material-chemical affinity, in contrast to ZDDP, which negatively resulted in a larger material degradation [140]. In this text, IL #1 is used for this ionic liquid.

Atomic force microscopy (AFM) has gradually come into prominence as a decent technique for assessing mechano-chemical processes in situ at sample surfaces. AFM is quite effective for studying the fundamentals of tribology and lubrication science, but it doesn't give any specific details on the components or foundations of the tribofilms. In order to obtain a proper insight into the lubrication process of a family of PP-ILs, specifically trihexyltetradecylphosphonium bis(2-ethylhexyl) phosphate ([P_{66614}][DEHP]), in situ single-asperity AFM testing was implemented simultaneously with ex-situ laterally resolved surface measurements. According to the AFM data, friction significantly decreases, and it is hypothesized that these surface adjustments are related to an effect of surface roughness and the adsorption of bis(2-ethylhexyl) phosphate anions by the creation of tightly packed, lubricious boundary films which occurs only on metallic iron [127].

2.9.5.2. 1-Ethyl-3-methylimidazolium diethylphosphate

Nanao et al. [141] investigated the tribological features of 1-Ethyl-3-methylimidazolium diethylphosphate by ball-on-disk-type reciprocating machine room temperate. Mentioned IL was found to be a more effective lubricant for reducing friction than poly-alpha-olefin. Kawada et al. [67] compared the tribological behavior of 13 sulfur, phosphorus, and cyanoanion-based halogen-free anion-based ionic liquids using a ball-on-disk sliding device for evaluating tribochemical performance. According to their results, it is crucial to choose the appropriate IL type based on the sliding condition when these ILs are used as lubricants in the field. For instance, the ILs founded on sulfur and phosphorus anion have high viscosities and can slide in the low-velocity domain. Additionally, since they create tribofilms, they are appropriate for high contact pressures. But, owing to their high viscosity indices, cyanoanion based ILs are anticipated to demonstrate efficiency for sliding components exposed to significant temperature variations. In this text, IL #2 is used for this ionic liquid.

2.10. Simultaneous use of DLC coatings and ionic liquids

The industry has long used solid lubricants to lessen wear and friction under varied circumstances. Advanced vacuum methods have been used to deposit materials like tungsten disulfide, hexagonal boron nitride, borides, and soft metals like Cu, Ag, Sn, and Au as protective coatings or as lubricant additives. These substances provide a barrier that shields friction pairs from one another, reducing friction and enhancing wear resistance [142]. While operating under boundary lubrication conditions, applying solid lubricant thin films (coatings) can improve the lubrication of moving pairs. The unpleasant effects of abrupt liquid lubrication failure can be lessened with the use of solid lubricating coatings [143, 144]. A solid-liquid composite lubricating system can have a synergistic impact by integrating the benefits of liquid and solid lubrication. Solid lubrication coating has favorable load-bearing capabilities and low volatility. By doing so, the system is able to retain the benefits of solid lubrication while simultaneously gaining the benefits of liquid

lubrication [145]. When the thin layers of fluid that separate surfaces fail, solid coatings can bear the load and serve as a secondary form of lubrication. This provides a backup mechanism to prevent direct contact between surfaces and reduce friction [146]. The combination of solid and liquid lubrication systems has become a popular choice for dynamic equipment, including space and automotive mechanisms. This composite lubricating system offers an effective solution for reducing friction and preventing surface wear. Thus, recent research has explored the potential benefits of integrating ionic liquids (ILs) with solid lubricating films. This promising approach has the potential to further improve the performance and durability of composite lubricating systems [144]. Because of its outstanding qualities, carbon has attracted the most interest in these solid lubricants. There are various forms of carbon, and each form's characteristics rely on its particular structure. Researchers have intensively investigated different carbon forms and their applications over many decades [142]. The outstanding qualities of DLC coatings, such as high hardness, excellent chemical stability, high thermal conductivity, low friction, and exceptional wear-resistance, have piqued the interest of researchers [144]. Table 1 provides brief information on the available studies performed to investigate the synergistic effects of ILs and DLCs.

Table 1) Summary of available literature focusing on the simultaneous use of DLC coatings and ionic liquids.

Name of ionic liquids	**Tribometer**	**Concentration of IL (**100 wt. % shows that IL was used as the main lubricant)	**DLC type**	**Ref.**
• 1-octyl-2,3-Dimethylimidazolium bis(trifluoromethyl)sulfonyl	Ball-on-disk (UMT-3 tribometer)	100 wt.%	Undoped-DLC	[147]
• 1-butyl-1-methylpyrrolidinium tris(pentafluoroethyl)trifluorophosphate	Ball-on-disk (UMT-3 tribometer)	1 wt.% additive to polyalphaolefin (PAO 6)	Undoped-DLC	[148]
• (lignin-[Choline][L-Proline] (L-[CH][Pro]))	Ball-on-disk configuration (Optimol SRV-III)	100 wt.%	Three different kinds of commerciall y available DLC coatings (Tribobond 40(Cr + a-C:H:W), Tribobond 43 [(Cr+) a-C:H), and Tribobond 44(a-C:Cr)]	[149]
• ethyl-dimethyl2 methoxyethylammonium tris(pentafluoroethyl)trifluorophosphate [(NEMM)MOE][FAP]	Ball-on-disk configuration (UMT-3 tribometer)	1 wt.%	Cr-DLC	[150]

• 1-butyl-1-methylpyrrolidinium tris(pentafluoroethyl)trifluorophosphate [BMP] [FAP]				
• ethyl-dimethyl-2 methoxyethylammonium tris(pentafluoroethyl)trifluorophosphate [(NEMM)MOE][FAP]	Ball-on-disk configuration (UMT-3 tribometer)	1 wt.%	Undoped-DLC	[151]
• The synthesized ionic liquids of functionalized borate esters (The specific names are not mentioned but molecular structure is explained in the article)	Ball-on-disk configuration (name of the tribometer not mentioned)	2 wt.%	Undoped-DLC	[152]
• 3-Hexyl-1-methyl-imidazolium hexafluorophosphate	Ball-on-disk configuration (name of the tribometer not mentioned)	100 wt.%	TiC/a-C:H type DLC	[153]
• tributylmethylphosphonium dimethylphosphate (PP), • 1,3-dimethylimidazolium dimethylphosphate (IM), • 1-butyl-1-methylpyrrolidinium tris(pentafluoroethyl)trifluorophosphate (BMP)	Pin-on-disk configuration (TE 38-Phoenix Tribology)	1 wt.%	Undoped-DLC, W-DLC, and Ag-DLC	[154]
• 1-butyl-3-methylimidazolium tetrafluoroborate • trihexyltetradecylphosphonium bis(trifluoromethy-lsulphonyl) amide	Ball-on-disk configuration (T-01M tribometer)	100 wt.%	a-C:H type DLC	[155]
• Tributylmethylphosphonium dimethylphosphate, • (2-hydroxyethyl) trimethylammonium dimethylphosphate • 1-butyl-1-methylpyrrolidinium tris(pentafluoroethyl) trifluorophosphate ([BMP][FAP])	Ball-on-disk configuration (UMT-2 tribometer)	1 wt.%	W-DLC	[156]
• 1-methyl-3-allyl imidazole tetra-Fluoroborate • 3-methyl-1-butylimidazolium tetra-fluoroborate	Ball-on-disk configuration (name of the tribometer not mentioned)	100 wt.%	Cr-DLC	[157]

Milewsk et al. [155] investigated the tribological response of two ionic liquids (1-butyl-3-methylimidazolium tetrafluoroborate and trihexyltetradecylphosphonium bis(trifluoromethy-lsulphonyl) amide) using ball-on-disc tribotester on a-C:H type diamond-like carbon coating in boundary lubrication conditions and reported that the smallest amount of the friction coefficient

was experienced for the a-C:H type DLC film and the ionic liquid acting as the lubricant. The largest amount of friction coefficient was observed for the DIN 100Cr6 steel sample without thin film tested under dry friction settings. The friction coefficient was smaller for the samples with DLC thin film than for the samples without thin film under dry friction conditions which shows the interesting tribological features of DLC films.

Gonzalez et al. [158] assessed the performance of a Cr-DLC film with ethyl-dimethyl2-methoxyethylammonium tris(pentafluoroethyl)trifluorophosphate [(NEMM)MOE] [FAP] and 1-butyl-1-methylpyrrolidinium tris(pentafluoroethyl)trifluorophosphate [BMP] [FAP] ionic liquids as 1 wt% additive to a polyalphaolefin as base oil. They reported that both ILs cause a friction drop, particularly at the lowest load tested (20 vs 40 N).

Arshad et al. [159] studied the tribological interactions of 3 ILs (namely Tributylmethylphosphonium dimethylphosphat, trimethylammonium dimethylphosphat, and 1-butyl-1-methylpyrrolidinium tris (pentafluoroethyl) trifluorophosphate ([BMP][FAP]) and tungsten-doped DLC thin film. W-DLC surface lubricated with the IL additives with dimethylphosphate anions exhibited acceptable performance, even better than the ZDDP under severe experimental conditions, while IL with the trifluorophosphate group had the worst properties of all the ILs against W-DLCs.

Khanmohammadi et al. [160] analyzed the two various additive-adsorption mechanisms dominating the tribological behavior of three types of DLCs (pure DLC, W—DLC, and Ag-DLC) in the presence of 3 groups of ILs (tributylmethylphosphonium dimethylphosphate (PP), 1,3-dimethylimidazolium dimethylphosphate (IM) and 1-butyl-1-methylpyrrolidinium tris(pentafluoroethyl)trifluorophosphate) and concluded that a triboelectrochemical activation process for Ag-DLC, and an electron transfer mechanism for tungsten-doped DLC lead to the efficient drop of friction in contact.

Yan et al. [161] showed that the viscosity and wettability of the ILs had a direct impact on how well they decreased the friction on Cr-doped graphite-like carbon (Cr-GLC) coatings and Cr-doped diamond-like carbon (Cr-DLC) contacts. Better antiwear and antifriction effects were displayed by ionic liquids. The Cr-DLC film outperformed the Cr-GLC film in terms of tribological behavior, which can be attributed to higher tribofilm formation under friction. The corrosive effect of the ILs also strongly influenced the performance of Cr-GLC/IL pair, whereas Cr-DLC/IL pair were barely affected by the corrosive nature of the ILs [15].

2.11. Research gap

Despite the fact that previous investigations have shown that lanthanoids (which includes Eu and Gd) have a high affinity for ILs, their potential advantage for improving the tribological interaction between lanthanoid-doped DLC thin films and ILs has not been thoroughly investigated [2, 89–93]. Therefore, in this research work, the effect of doping DLCs with Eu (Europium) and Gd (Gadolinium) (deposited using High Power Impulse Magnetron Sputtering) on their tribological response to two ILs (trihexyltetradecylphosphonium bis(2-ethylhexyl) phosphate [P_{66614}][DEHP] and 1-Ethyl-3-methylimidazolium diethyl phosphate) will be studied by mixing ILs (as additive)

with PAO 8 as base oil (1 wt.%) under all various lubrication regimes by changing the speed of rotating disk on a block-on-ring tribometer in room temperature and comparing the results with the undoped DLC samples and lubricated with base oil (without additives), in order to show the advantage of the doping process on the tribological performance of the DLC and ILs [15].

2.12. Objectives

This project aims to:

a) Assess the wear and friction reduction efficiency of a cluster of novel thin films, named europium- and gadolinium-alloyed DLC (Eu-DLC and Gd-DLC), lubricated with a group of lubricant additives, named phosphorus-based ionic liquids (ILs).

b) Provide perspective into the interactions between Eu/Gd doped DLCs and phosphorus-based ionic liquids.

To obtain a superior operating setting, the effect of coupling a novel group of wear-resistant coatings (alloyed DLCs) with a unique class of novel lubricants (i.e., ionic liquids, ILs) is studied. This strategy is distinctive in two key aspects. The goal is to gain a core knowledge of practical behavior to highlight the significance of particular material qualities. Then this data will be employed to establish the necessary design requirements and composition of DLCs and ILs. Results can improve sustainable development by minimizing friction's negative ecological and economic effects (such as lower energy prices and less contamination), while also playing an essential role in the endeavor to achieve the demanding environmental goal of decreasing emissions of greenhouse gases by opening the door for the creation of innovative, ecologically friendly, and energy-efficient products for a range of industries, such as the manufacturing and transportation ones.

Chapter 3 – Experimental Procedure

This chapter provides information about the procedures followed for preparing samples, along with an elucidation of the experimental parameters employed accompanied by an overview of the characterization methodologies utilized in this study.

3.1. Preparation of materials

The substrate for DLC coating was steel (AISI M2, 25 mm in diameter and thickness of 4 mm), while the substrate for the morphological study of the coatings was silicon [100] wafer, 20 x 20 mm. Abrasive grit papers with grit sizes of 240, 320, 400, 600, 800, and 1200 were utilized to grind steel specimens. Diamond abrasive paste with particle sizes of 6 μm and 3 μm was employed for mirror polishing. All substrates were cleaned in 100% ethanol and acetone for a total of 15 minutes with a series of ultrasonic baths, respectively. The substrates were cleaned, and then before placing the samples inside the deposition chamber, silver glue was used to adhere them to the substrate holder [2, 15, 88]. Table 2 illustrates the chemical composition of AISI M2.

Table 2) Chemical composition of AISI M2 Steel

Material	Fe	C	Cr	Mo	W	V
M2 Steel	Balance	1%	0.4%	5%	6%	2%

3.2. Deposition processes of coatings

A DOMS (Deep Oscillation Magnetron Sputtering) power supply (HiPIMS Cyprium plasma generator, Zpulser Inc.) was used to produce the coatings. The substrate holder rotated at a speed of 23.5 rev/min along the chamber's axis for all depositions, and the substrates were kept 80 mm away from the carbon and chromium targets. Targets composed of chromium (purity 99.99%) with sizes of 150 mm by 150 mm and 10 mm thick and pure graphite (purity 99.95%), respectively, were utilized to deposit the interlayers and DLC coatings. The carbon target, chromium target, and substrates were sputter etched prior to all depositions. The graphite target was machined with circular grooves of 10 mm diameter and 2 mm depth to hold the doping pellets (Gd or Eu pellets) during the deposition process [15]. For depositing pure DLC films, graphite pellets were employed to fill the round holes and standardize the target surface in the absence of doping pellets. Figure 5 shows the image of carbon target and position of dopant elements.

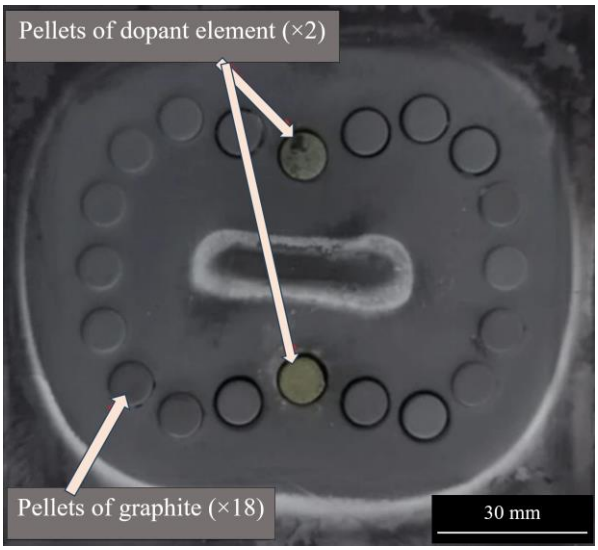

Figure 5) Configuration of Carbon target and dopant elements

To establish a base pressure of less than 3×10^{-4} Pa, two (a rotary and a turbomolecular) pump systems were used. To increase the DLC film's adherence to the substrates, two interlayers were coated prior to the final DLC thin film. A layer of Cr was applied first, followed by a layer of CrN [2, 88]. Three stages made up the deposition process: 1) etching the substrate and target, 2) depositing the interlayer, and 3) depositing the DLC-based coating. During the etching process, the carbon target was cleaned for 10 minutes utilizing Direct Current (DC) of 0.4 kV at 0.4 Pa of pressure. Then cleaning process was also performed on the chromium target applying a power of 0.25 kW and a pressure of 0.35 Pa [15]. At the same time cleaning of substrate was also performed using a pulsed power source (120 kHz, 1616 ns) for 60 minutes. Cr interlayer deposition process was performed at 0.3 Pa pressure with switched on bias at -60 V and Cr target at 1200 W for 10 minutes. Later with gradual increase of N_2 % in the deposition chamber and reducing Ar %, CrN layer was deposited (both interlayers are around 400 nm thick). Then DLC coating was deposited for 60 min with a pressure of 0.4 Pa. The micro-pulse duration lasted for a period of 6 microseconds, while the interval between successive micro-pulses was 150 microseconds. The complete pulse had a duration of 1800 microseconds. The substrate voltage bias was set at -80 volts, and the average power was maintained at 600 watts [2]. Figure 6 shows the coating machine used in this work and Figure 7 shows a summary of the deposition process.

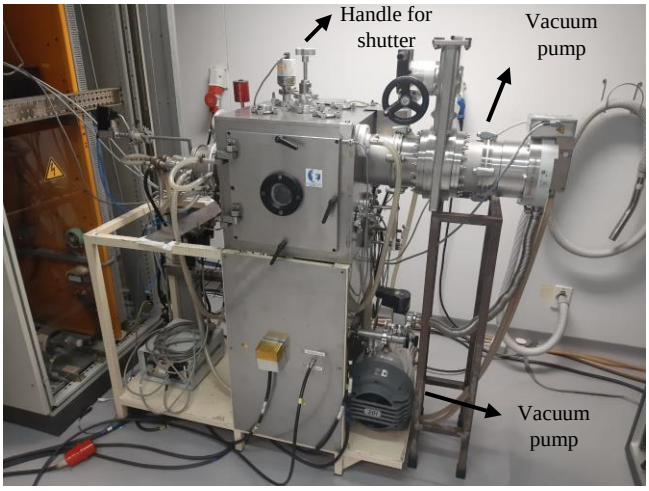

Figure 6) Physical vapor deposition instrument used in this work.

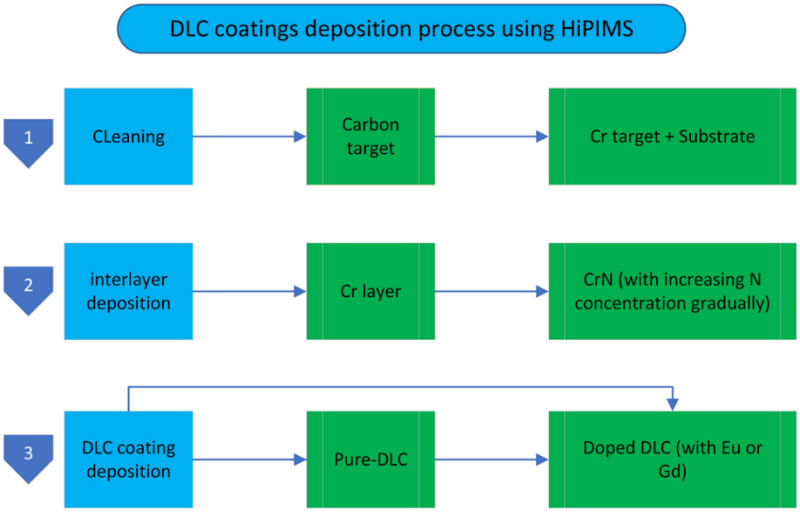

Figure 7) Schematic view of deposition process of DLC thin films.

3.3. Lubricants

In order to clarify the role of the coatings, it was necessary to employ a basic lubricating oil that was devoid of additives and later mix it with additives to investigate the tribological features of the thin films when exposed to 1 wt. % IL+ base lubricant. The hydrodynamic and mixed lubrication regimes in internal combustion engines dominate the contact between the piston ring and cylinder liner for the most part, boundary lubrication regime is frequent at the top dead center of the stroke, which necessitates the implementation of coatings. Polyalphaolefin (PAO) 8 base oil was selected as the base lubricating oil because it serves as the basis oil for various commercial engine oils [15, 162–164].

Two ionic liquids will be used for this research work:

1) Trihexyltetradecylphosphonium bis(2-ethylhexyl) phosphate [P_{66614}] [DEHP] (IL #1)
2) 1-Ethyl-3-methylimidazolium diethylphosphate (IL #2)

By combining 1 g of [P_{66614}] [DEHP] with 99 g of PAO 8 using an analytical balance, lubricant with 1 wt% of [P_{66614}] [DEHP] was created [2]. The same procedure was repeated for the second IL.

3.4. RBS-ERD

In Rutherford backscattering spectroscopy (RBS), a beam of high-energy ions, usually protons or alpha particles, impinge on a specimen, and backscattering is recorded to assess the structure and composition of objects. A projectile with high kinetic energy collides with a stationary particle inside the specimen in a hard-sphere elastic collision known as Rutherford backscattering. The severity of any element's backscattered ions is related to its concentration [165]. The chance of a discernible interaction between the incident beam and the subject material is quantified by the scattering cross section [166]. A further method, elastic recoil spectroscopy detection (ERD), is related to RBS. The detection of light atomic weight species being forward scattered, rather than backscattered particles, is what makes this method special. To distinguish between signals from several atomic species that are existent, such as hydrogen, deuterium, and tritium in a single specimen, ERD uses energy loss (ΔE) in the filter. These two techniques when used together yield better results because for a particular incident beam, RBS is sensitive to elements heavier than the incident beam while ERD is sensitive to the lighter ones. The chemical content of the thin film was assessed by the SIAM platform based on Rutherford Backscattering Spectrometry (RBS) and Elastic Recoiling Detection (ERD). The specimen was tilted at 70 degrees and exposed to an alpha beam examination at 2.3 MeV while collecting backscattered particles using a fixed detector positioned at 30 degrees from the incident beam path (homemade, Namur, Belgium). Records of the elemental depth [167] were produced by using DataFurnace to process the five spectra that were captured for each specimen [168]. SigmaCalc data were implemented for measuring cross-section functions and the SRIM documents for stopping power were used in these evaluations [15, 169].

3.5. Nano-indentation

A method for determining a material's hardness is nanoindentation. It is a quantitative technique for determining mechanical behavior from very small locations [6, 170]. Nano-indentation is implemented to determine reduced Young's modulus and hardness (NanoTest from Micromaterials). A Berkovich diamond indenter was part of the nanoindenter. To assure that the indentation depth is less than 10% of the coating thickness, a maximum load of 10 mN (typical settings in the CEMMPRE laboratory) is applied. For each sample, 16 evaluations were made to determine the mean and standard deviation of the mechanical parameters. The atomic ratio of the doping elements to the main elements is directly related to the hardness of the DLC films that HIPIMS deposits. The structural analysis and morphological type (sp^2 or sp^3 hybridization and density) in the corresponding DLC films are shown to explain the high hardness of DLCs. When sp^3 bindings are dominant, the material exhibits diamond-like behavior, which results in materials with high levels of hardness and elastic modulus [15, 88, 171–174].

3.6. Scratch Test

The adhesion and cohesion characteristics of a coating play a significant role in determining the film's performance in tribological applications. These properties, typically assessed through scratch testing, enable the evaluation of the strength of the coating's bond with the substrate and itself. They offer valuable insights into the properties of coatings by determining the critical load at which the coating begins to exhibit failure. In the scratch test, a rounded diamond stylus is employed to apply gradually increasing loads on a coated panel. As the load reaches a certain point, the coating initiates failure, resulting in torn edges and lifted coating along the scratch path [175]. The critical load, which signifies the minimum amount of load required for the occurrence of failure at the interface between the coating and substrate, serves as a pivotal parameter for assessing the characteristics of thin films. This quantitative measure can be ascertained by meticulously scrutinizing the scratch through pics obtained from a microscope.

To assess the coating adhesion, an automatic scratch tester (CSEM Revetest, Switzerland) (Figure 8) was used with a Rockwell “C” diamond-tipped indenter having a spherical tip diameter of 200 µm. The scratch test was performed with a linear increase in the normal load from 0 to 60 N, and the test speed was set to 10 mm/min with a loading rate of 10 N/mm (ISO 20502:2005 standard [176]). The samples and the indenter were cleaned with ethanol before testing. The adhesive properties of the coatings were quantified using an optical microscope (Alicona Infinite Focus, Raaba, Austria), and the test was repeated three times for each sample in order to verify the consistency of the results [15].

Figure 8) Scratch test device used in this work

3.7. Viscosity of lubricants

One of the most crucial factors in lubricated contacts is viscosity since it affects the lubricants' tribological characteristics. The SV-100 A&D viscometer (A&D Weighing, Tokyo, Japan) is used to measure the viscosity-temperature-time parameters of the lubricant based on the Tuning-fork vibration principle. An electromagnetic force is used to cause a pair of thin sensor plates with similar natural frequencies to oscillate at the specified amplitude in the tuning-fork vibration

viscometer. According to the amount of electronic current needed to operate the sensor plates and keep them at a constant amplitude, the viscidity formed between the sensor plates and the sample liquid is determined. The sensor plates' very low thermal capacity and minimal movement of the sample liquid preclude fluctuations in the sample's temperature and physical characteristics [177]. The measurements of viscosity of three different lubricants in this work are performed at room temperature. The viscometer was calibrated based on the manufacturer's instructions before performing the tests and the container was cleaned using ethanol and acetone and dried thoroughly to avoid any contamination that might affect the viscosity [15].

3.8.Tribology rig

The device used for the tribology testing was an in-house tribometer with a block-on-ring configuration, where the contact geometry was a rectangle. The laboratory setup included a power supply and controller, sample support, counter body, oil reservoir, and two force sensors (one for the normal force and another for the tangential force). The tangential force is directly proportional to the normal force, where the coefficient of proportionality (μ) is the coefficient of friction. The contact was kept lubricated by a reservoir of lubricant, fully flooded. As a counterpart, an AISI 3415 steel ring with a diameter of 115 mm and width of 12 mm was used (Table 3). The ring surface was polished with an initial root mean square roughness of around 0.046 μm [34]. Root mean square roughness of the coatings were around 0.015 μm. The applied normal load of 25 N was determined, according to Hertzian contact theory, considering the geometry of the block-on-ring contact and the internal combustion engine's working pressure range, which was assumed to be on the order of 40 MPa [178]. Figure 9 shows a simple representation of the block-on-ring setup used in this work. For calculating film thickness, Dowson equation was used for calculating minimum film thickness based on the fact that block-on-ring configuration can be assumed as a line contact [179]. Lambda ratio was calculated using equation 1. All the experiments were performed at room temperature.

$$\lambda = \frac{h_{min}}{\sqrt{\sigma_A{}^2 + \sigma_B{}^2}} \qquad \text{Equation 1}$$

where

h_0 is the minimum film thickness [m];
σ_A is the RMS surface roughness of body ' A ' [m];
σ_B is the RMS surface roughness of body ' B ' [m];
λ (lambda) is the parameter characterizing the ratio of the minimum film thickness to the composite surface roughness.

Table 3) Information about the counterpart (ring) used in this work.

Properties of the counterpart (ring)	
Material	AISI 3415 steel
Diameter	115 mm

width	12 mm
Young's modulus	205 GPa
Poisson's ratio	0.285

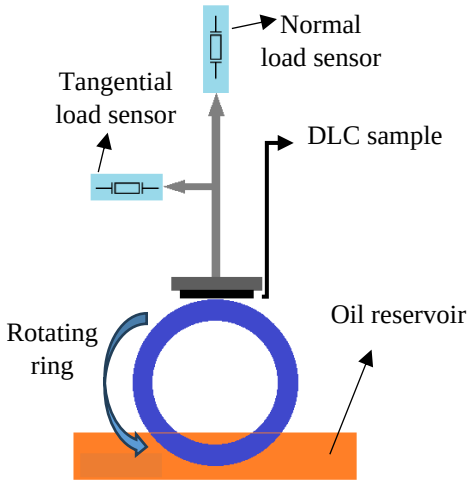

Figure 9) A simple representation of the block-on-ring setup.

3.9. Surface profilometry

In instruments of this type, the specimen's surface is physically interacting with the stylus tip. A stylus on the detector tip makes tracings on the specimen's surface. Electrical sensors collect the stylus' vertical movement. To be represented, electrical impulses are amplified and converted to digital form. Smaller stylus tips usually yield in more accurate results because it decreases contact pressure (sapphire and diamond are such hard materials, they can scratch the surface of the test object when used as styluses. Rapid feed can easily result in the stylus scratching the sample). Mitutoyo SJ profilometer was used in this work for measuring root mean square roughness based on ISO 4288-1996 [180].

3.10. Wear characterization using optical microscopy and SEM-EDS

For comparing the wear tracks after tribology test, Leica DM4000 M LED (Leica Microsystems, Wetzlar, Germany) was used. It functions using a mechanical Z-drive, equipped with motorized feature, and a mechanical stage (Figure 10 (a)).

SEM-EDS is one of the most frequently used tools for materials characterization owing to its advantages such as non-complicated sample preparation, simple data analysis, various imaging, and reasonable accuracy for chemical analysis functionalities. To examine a specific region of a sample's surface in SEM, an electron beam, emitted from the filament, is concentrated to the region. Signals released during the scanning process (due to interaction between the electron beam and the sample) are then received by several detectors simultaneously to generate visuals or conduct spectroscopic investigations [181]. The scanning electron microscopy (SEM) technique revolves around secondary electrons, backscattered electrons, and X-ray diffraction. Secondary electrons are useful for examining the shape and surface characteristics of specimens, while

backscattered electrons aid in highlighting variations in composition within samples containing multiple phases. X-ray diffraction, in conjunction with energy dispersive spectroscopy or wavelength dispersive spectroscopy, provides a means to investigate the chemical elements of the samples [6]. Hitachi High-Tech SU3800 SEM device equipped with QUANTAX Bruker EDS detector is used in this work (Figure 10 (b)) [15].

(a) (b)

Figure 10) (a) Leica DM4000 M LED, (b) Hitachi High-Tech SU3800 SEM equipped with EDS detector.

4. Results and discussion

4.1. Chemical composition

Based on the results of Rutherford Backscattering Spectrometry (RBS) and Elastic Recoiling Detection (ERD) tests (Table 4), Gd-doped DLCs contain 1.7 at. % and 2.3 at. %, respectively, of doped element. At the same time, Eu-doped DLCs contain 1.7 at. % and 2.4 at. %, respectively, of Eu element. Previous research showed that in some cases, increasing concentrations of Eu and Gd in doped DLC thin films affect the properties of the thin film in a negative trend [88]. For instance, increasing the concentration of Gd reduces the adhesion strength and hardness in the case of Gd-DLC. Therefore, in this work, thin films with a low concentration of doping elements were chosen. Hydrogen element present in the samples is due to the contamination which cannot be removed by vacuum pumps.

Table 4) Elemental composition, acquired from Rutherford Backscattering Spectrometry (RBS) - Elastic Recoil Detection (ERD), the remaining at. % is Carbon.

Sample	Chemical Composition (at. %)			
	H	Ar	Gd	Eu
Pure DLC (or DLC)	6.5 (± 0.1)	3.6 (± 0.1)	0	0
1.7% Gd-DLC	5.8 (± 0.1)	4.3 (± 0.1)	1.7 (± 0.1)	0
2.3% Gd-DLC	3.1 (± 0.1)	2.3 (± 0.1)	2.3 (± 0.1)	0
1.7% Eu-DLC	8 (± 0.1)	3.4 (± 0.1)	0	1.7 (± 0.1)
2.4% Eu-DLC	5.9 (± 0.1)	3.7 (± 0.1)	0	2.4 (± 0.1)

4.2. Hardness, reduced Young's modulus

Figure 11 demonstrates the hardness and Young's modulus obtained from nano-indentation. Measurements show that 1.7 % Gd-DLC and pure DLC have higher hardness than other coatings (considering error bars), similarly in the case of Young's modulus, 1.7 % Gd-DLC and pure DLC have the highest value for this property (considering error bars). DLC is primarily composed of two types of carbon bonds that are similar to those found in graphite (known as sp^2 hybridizations) and diamond (known as sp^3 hybridizations). DLCs are known for their exceptional hardness and high elastic modulus, although they also exhibit high internal stresses [171, 182]. These characteristics are closely attributed to the proportion of sp^3 hybridizations present in the films. It is reported that the higher the sp^3 hybridization percentage and density, the higher will be the hardness and elastic modulus [88, 183–187].

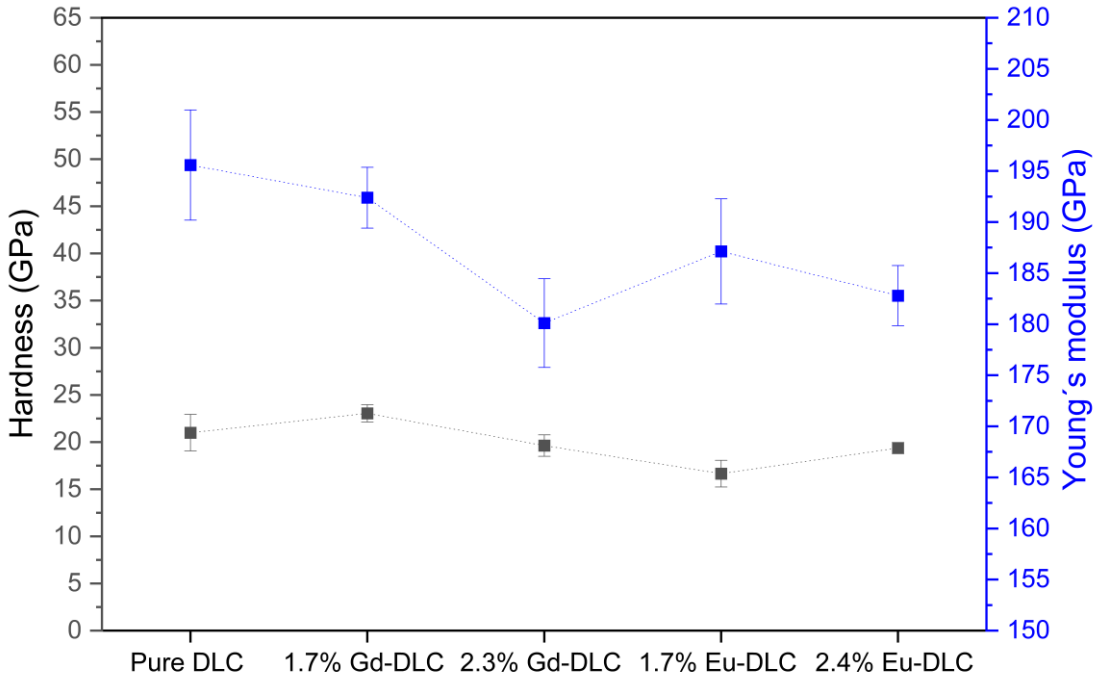

Figure 11) Hardness and Young's modulus of the DLC coatings. (The purpose of the dashed lines connecting the measured points is to provide visual guidance for the reader, without representing any specific measured values, or a continuous trend.)

Surfaces with greater hardness are more resistant to abrasive wear. Additionally, materials with lower elastic modulus experience elastic deformation with higher intensity. Therefore, the ratio of hardness to elastic modulus (H/E) and the plastic deformation resistance factor (H^3/E^2) have been discussed in the literature as a good representative for describing the mechanical characteristics of thin films [188–190].

The H/E and H^3/E^2 ratios for the thin films are presented in Table 5. There is not a big difference in H/E ratio of 1.7 % Gd-DLC, 2.3 % Gd-DLC, 2.4 % Eu-DLC, and pure DLC if the error is considered but 1.7 % Eu-DLC has the smallest H/E ratio. The 1.7 % Gd-DLC coating has the greatest H^3/E^2 ratio. From H^3/E^2 ratio it can be inferred that greater hardness overweighs elastic modulus to decrease the intensity of plastic deformation [188].

Table 5) H, E, H/E, and H^3/E^2 values for the films.

Coating	H (GPa)	E (GPa)	H/E	H^3/E^2
Pure DLC	20.9 ± 1.9	195.5 ± 5.3	0.107 ± 0.010	0.242 ± 0.050
1.7% Gd-DLC	23.0 ± 0.9	192.3 ± 2.9	0.120 ± 0.005	0.330 ± 0.024
2.3% Gd-DLC	19.6 ± 1.1	180.1 ± 4.3	0.109 ± 0.009	0.233 ± 0.052

1.7% Eu-DLC	16.6 ± 1.4	187.1 ± 5.1	0.089 ± 0.008	0.132 ± 0.020
2.4% Eu-DLC	19.3 ± 0.5	182.7 ± 2.9	0.106 ± 0.004	0.218 ± 0.027

4.3. Scratch test

Figure 12 shows the morphology of the scratches on the films designating the critical scratch load of L_{c2}. Based on the literature, the three main loads, namely L_{c1}, L_{c2}, and L_{c3}, are intricately linked to distinct stages in the scratching process. L_{c1} signifies the point at which initial cracks manifest, while L_{c2} denotes the onset of chipping along the periphery of the scratch track. Finally, L_{c3} represents the critical load magnitude that triggers complete delamination of the coatings, resulting in their complete detachment [188]. As only conformal cracking emerges, all samples exhibit proper thin film adherence [88]. Determining $L_{c1}$was very difficult because of the mechanical properties of the coating which made comparing the initial points complicated and L_{c1} could not be determined for 1.7 % Eu-DLC. L_{c3} could not also be identified since there is not visible delamination of the coating. DLC structural and morphological characterization can also assist in understanding the differences in film adherence that were observed for films that were doped with various concentrations of doping elements. Higher sp^3/sp^2 ratio and denser films have been reported to increase the adhesion of the film on the substrate [88, 191], however, the doping process has been shown to reduce the sp^3/sp^2 ratio, which affects the adhesion of the film [88, 192]. Except 1.7 at. % Gd-DLC and 1.7 at. % Eu-DLC, other coatings did not have a huge difference in L_{c1} value. The Gd-DLC film containing 1.7 at. % of Gd exhibited the greatest L_{c2} value which is a representation of better adherence of the film to the substrate followed by 2.3 at. % Gd-DLC. On the other hand, 1.7 at. % Eu-DLC and pure DLC had similar L_{c2} value in the scratch test, while 2.4 at. % Eu-DLC had better performance compared to 1.7 at. % Eu-DLC.

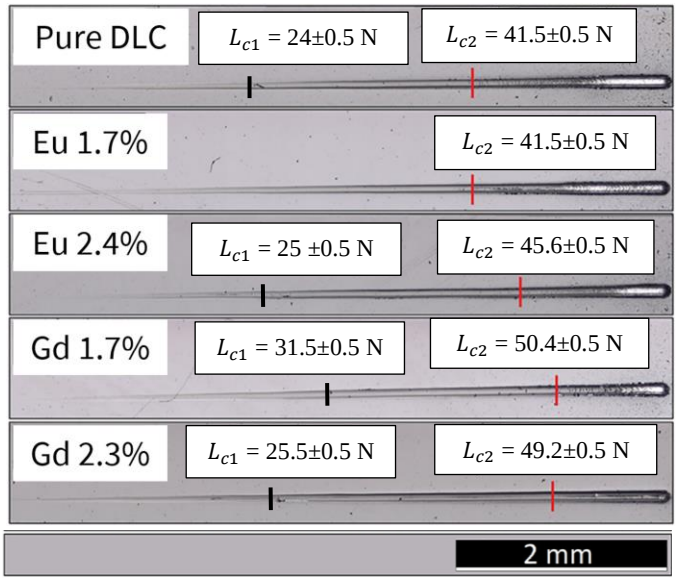

Figure 12) Scratch morphology of DLC films for increasing loads between 0 and 60 N.

4.4. Viscosity of the lubricants

Table 6 shows the measurement results for the viscosity of the used lubricant which is measured the room temperature. The results indicate that the use of these ionic liquids additives for PAO 8 did not change the viscosity significantly. The viscosity of Newtonian liquids is regarded as a transition element in the Stribeck curve. In the experiments performed in this study, when the viscosity increased, the lubrication regime shifted toward the hydrodynamic regime, and thus the film thickness was increased at the same sliding speed compared to PAO 8 without additives.

Table 6) Viscosity values for the different lubricants at room temperature.

Lubricant	Dynamic Viscosity (mPa.s)	Kinematic Viscosity (mm^2/s)
PAO 8	71.89	86.48
PAO 8 + IL #1 (1 wt.%)	75.46	90.78
PAO 8 + IL #2 (1 wt.%)	76.89	92.49

4.5. Stribeck curves

Stribeck curves are presented as the coefficient of friction vs Hersey parameter or lambda ratio (λ). The Hersey parameter is a dimensionless number equal to the dynamic viscosity of lubricant (η) times the velocity (u), divided by the normal load (P) per unit of contact length. Because velocity is the only variable in these experiments, the values of the Hersey parameter shift only through velocity in this study. The load was always approximately 25 N during experiments, although the ring was aligned with a comparator [94]. This is because of the residual misalignment of the ring, which cannot be avoided due to the dynamic nature of the rotating cylinder, but the variation was very small, therefore, the load is assumed to be constant with insignificant error.

Figure 13 represents the Stribeck curves deduced from test results at different sliding speeds for the DLC coatings. Based on these curves, three lubrication regimes can be found: boundary, mixed, and hydrodynamic lubrication (Boundary Lubrication, $\lambda < 1$; Mixed Lubrication, $1 < \lambda < 3$; Elastohydrodynamic Lubrication, $3 < \lambda < 5$ and Hydrodynamic Lubrication, $\lambda > 5$.).

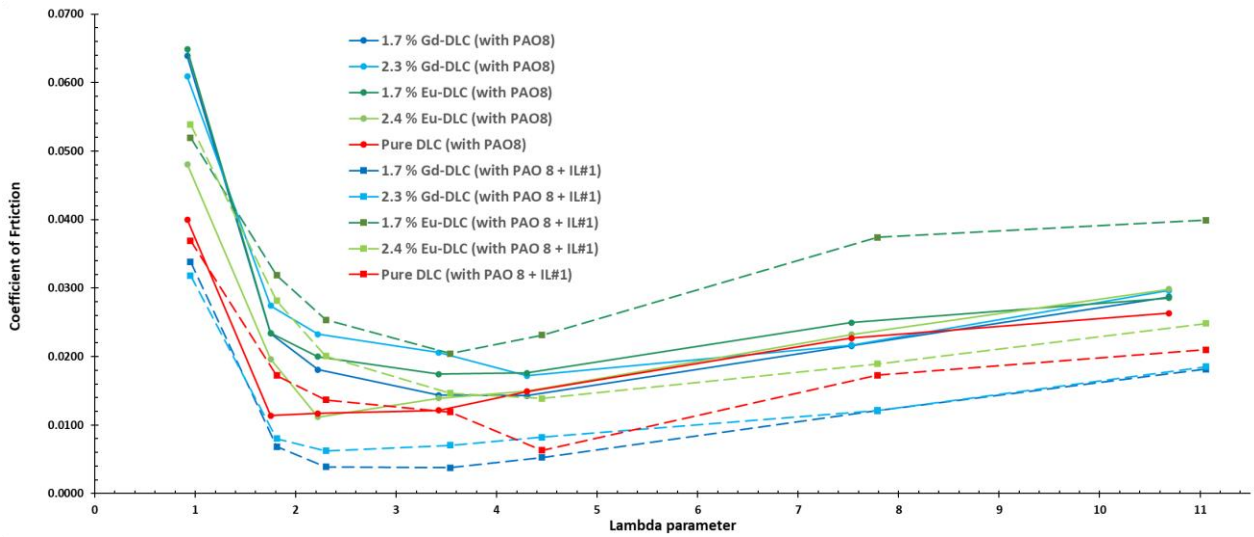

Figure 13) Stribeck curves obtained from the block-on-ring tribometer for PAO 8 and PAO 8 mixed with 1wt. % IL #1 for different lubricated coating surfaces. The purpose of lines connecting the measured points is to provide visual guidance for the reader, not representing any specific measured values. Continuous lines belong to Coatings paired with PAO 8 lubricant and dashed lines belong to coatings paired with POA 8 + 1 wt.% IL #1 lubricant.

The Stribeck curve graphically displays four regions on a horizontal axis, each with a corresponding slope that demonstrates a change in the coefficient of friction on the vertical axis. These regions are classified into four types of lubrication regimes: boundary, mixed, Elastohydrodynamic, and hydrodynamic lubrication [193, 194].

The boundary lubrication (BL) regime ($\lambda < 1$) is characterized by the support of the load through the microscopic asperities on the surface, where there is no continuous lubrication film. The sliding of asperities against each other can result in significant friction and wear, which can be detrimental to the lifespan of the system [15, 193, 195–197].

The mixed lubrication (ML) regime ($1 < \lambda < 3$) plays a significant role in internal combustion engines. It involves a combination of elastohydrodynamic lubrication and boundary lubrication characteristics. This implies that while some portions of the contact area are covered with lubricant film, in other areas, peak asperities of moving surfaces slide on each other because there is no separating liquid film. Mixed lubrication is present in many engine components, such as piston rings, cams, and engine bearings. Understanding mixed lubrication is crucial for system engineers due to the fact that it is the most challenging lubrication regime to predict friction accurately. This challenge is due to the complex interaction between surface topography and oil film thickness [15, 193, 198, 199].

The elastohydrodynamic lubrication (EHL) regime ($3 < \lambda < 5$) is an extension of hydrodynamic lubrication that considers the deformation of the surfaces in contact. The film thickness in the EHL regime is significantly smaller than in the HL regime. As a result, an uninterrupted hydrodynamic film can only be maintained through the elastic deflection of the surfaces. Therefore, it is essential to consider these deflections when studying EHL [15, 193, 194].

In the hydrodynamic lubrication (HL) regime ($5 < \lambda$), the load is supported entirely by the lubricant film, and the asperities on the sliding surfaces do not contact each other. This is generally observed when the lambda ratio exceeds 5 [15, 195, 200].

In EHL and HL regimes, as the speed increases, the lubricant film may not be able to keep up with the changes in pressure and the lubricant may not have enough time to flow into the contact area and form a thick enough fluid film, leading to increased friction [201, 202]. In addition, the viscosity of the lubricant typically decreases with increasing temperature, which can slightly occur at very high sliding speeds due to the heat generated by friction [15].

When the Stribeck curves for different films were compared (Figure 13), it was discovered that, in general, adding the ionic liquid #1 to the PAO 8 lubricant reduced the CoF at the lowest sliding speed achievable with the used tribometer, especially for the both of Gd-doped DLC films. The 1.7 % and 2.4 % Eu-DLC films did not show a better performance compared with the pure DLC film in the presence of IL #1. Before adding the IL, the doped DLC films (both Eu-DLC films and both Gd-DLC) paired with pure PAO 8 did not present a good performance compared with the pure DLC film, but after adding 1 wt.% IL to PAO 8, the performance of the 1.7% and 2.3% Gd-DLC films was even better than that of the pure DLC film in the boundary, mixed, elastohydrodynamic, and hydrodynamic lubrication regimes, which can be attributed to its better interaction with the ionic liquid additive. In the literature, two lubricating mechanisms supporting the use of ionic liquids as lubricant additives have been discussed. The formation of adsorbed layers is the first reason that has been mentioned. These layers have the ability to promote movement between two surfaces that are sliding against each other, owing to their low shear. The formation of a tribofilm on metal surfaces is the second reason that has been discussed. These protective layers are formed as a result of chemical reactions that occur between ionic liquids and the surfaces that are in contact with them during friction [188, 203].

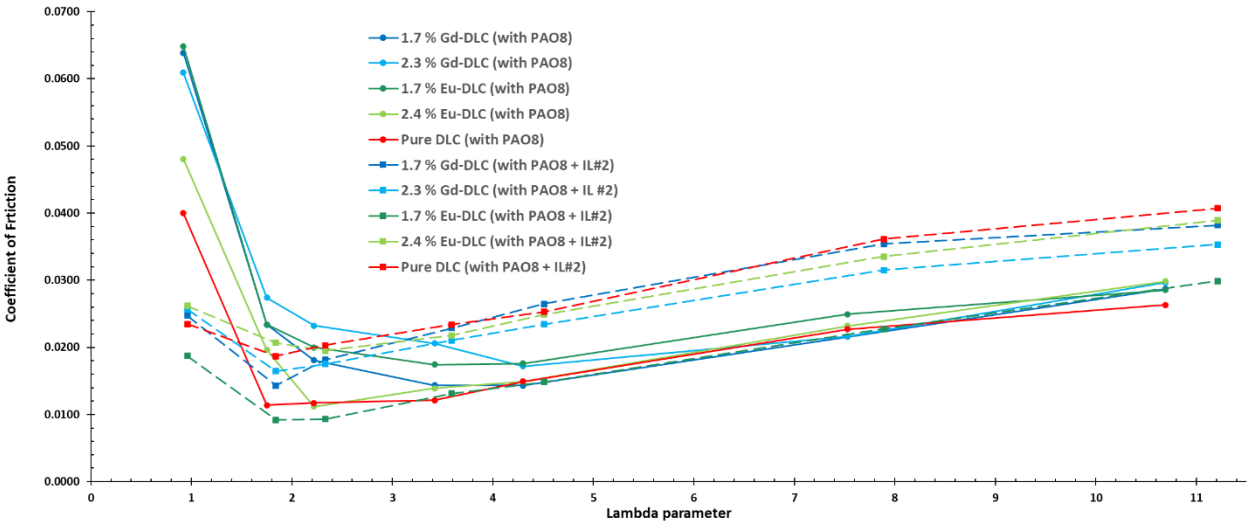

Figure 14) Stribeck curves obtained from the block-on-ring tribometer for PAO 8 and PAO 8 mixed with 1wt. % IL #2 for different lubricated coating surfaces. The purpose of lines connecting the measured points is to provide visual guidance for the reader, not representing any specific measured values. Continuous lines belong to Coatings paired with PAO 8 lubricant and dashed lines belong to coatings paired with POA 8 + 1 wt.% IL #2 lubricant.

Considering the same sliding speed for comparison, in tribological pairs which were lubricated with PAO 8 + 1 wt. % IL #2 (Figure 14), a noticeable change of CoF occurs for all pairs in the boundary lubrication regime, in which 1.7 % Eu-DLC outperforms all other coatings. In elastohydrodynamic and hydrodynamic lubrication regimes, CoF for pure DLC, 1.7 % Gd-DLC, 2.3 % Gd-DLC, and 2.4 % Eu-DLC paired with PAO 8 + IL #2 is higher when compared to same coatings paired pure PAO8. However, 1.7 % Eu-DLC paired with PAO 8 + IL #2 has performance comparable with the thin films paired with pure PAO 8 in mixed, elastohydrodynamic lubrication regimes.

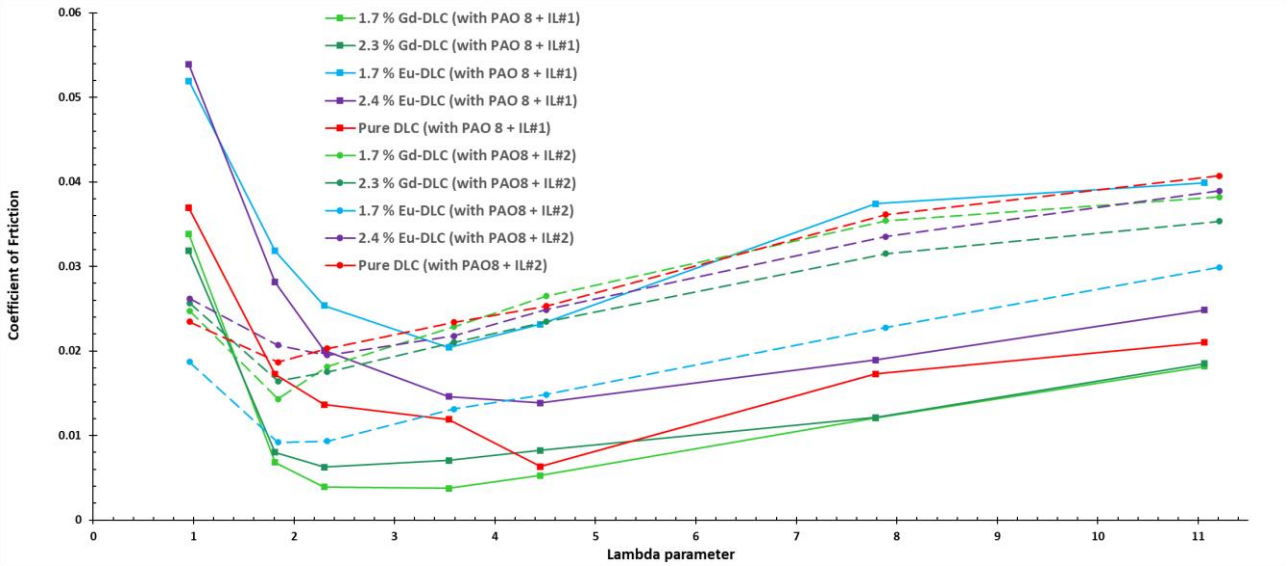

Figure 15) Stribeck curves obtained from the block-on-ring tribometer for PAO 8 mixed with 1wt. % IL #1 and PAO 8 mixed with 1wt. % IL #2 for different lubricated coating surfaces. The purpose of lines connecting the measured points is to provide visual guidance for the reader, not representing any specific measured values. Continuous lines belong to Coatings paired with PAO 8 + 1 wt.% IL #1 lubricant and dashed lines belong to coatings paired with POA 8 + 1 wt.% IL #2 lubricant.

Based on Figure 15, a comparison can be made for Coatings paired with PAO 8 + 1 wt.% IL #1 lubricant and coatings paired with POA 8 + 1 wt.% IL #2 lubricant. 1.7 % Gd-DLCs paired with PAO 8 + 1 wt.% IL #1 has better performance in ML, EL, and HL regimes (considering the same sliding speed for comparison). On the other hand, as mentioned above 1.7 % Eu-DLCs paired with PAO 8 + 1 wt.% IL #2 has better performance in the BL regime.

According to the suggested mechanism for adsorbed layers, the anionic component of Ionic liquids is drawn towards the positively charged surface of metals, leading to surface adsorption[204]. The cationic component can then be adsorbed to another anionic entity, forming single or multi-layer adsorbed structures on the surface. These structures create a film on the metal surface and have low interlayer strength, which helps to reduce friction and promote movement between the contacting surfaces [188, 203, 205, 206].

Based on the obtained data from viscosity measurements, minimum film thickness (h_0) and lambda ratio (ratio of minimum film thickness to the composite surface roughness) are calculated and presented in Table 7 (for PAO8 without additive),

Table 8 (for PAO8 with PAO8 + 1 wt. % of IL #1), and Table 9 (for PAO8 with PAO8 + 1 wt. % of IL #2) is obtained using the Dowson equation because the block-on-ring configuration resembles line contact [179]. The lambda ratio (λ) is an indicator of the lubricant regime in an operating contact. For all lubricants, the lubrication regime starts with the fully hydrodynamic regime, and as the sliding speed decreases, the lambda ratio also decreases; finally, the lubrication regime completely changes to the boundary lubrication regime, and the surfaces of the block and ring come into contact, which can cause wear on both surfaces.

Table 7) Characteristics of the lubricant film for PAO 8 based on the sliding speed of the cylinder (u is the speed of the ring). * Boundary lubrication = BL; mixed lubrication = ML; elastohydrodynamic lubrication = EL; hydrodynamic lubrication = HL.

u (m/s)	**0.02**	**0.05**	**0.07**	**0.13**	**0.18**	**0.4**	**0.66**
Duration	25 min	11 min	19 min	11 min	15 min	15 min	9 min
h_0 (m)	4.44×10^{-8}	8.44×10^{-8}	1.06×10^{-7}	1.64×10^{-7}	2.06×10^{-7}	3.61×10^{-7}	5.13×10^{-7}
λ	0.92	1.75	2.22	3.42	4.30	7.53	10.69
Lubrication regime*	BL	ML	ML	EL	EL	HL	HL
Hersey parameter	8.08×10^{-7}	1.77×10^{-6}	2.91×10^{-6}	4.50×10^{-6}	6.26×10^{-6}	1.39×10^{-5}	2.26×10^{-5}

Table 8) Characteristics of lubricant film for PAO 8 + 1 wt.% IL #1 based on the sliding speed of the cylinder (u is the speed of the ring). * Boundary lubrication = BL; mixed lubrication = ML; elastohydrodynamic lubrication = EL; hydrodynamic lubrication = HL.

u (m/s)	**0.02**	**0.05**	**0.07**	**0.13**	**0.18**	**0.4**	**0.66**
Duration	25 min	11 min	19 min	11 min	15 min	15 min	9 min
h_0 (m)	4.59×10^{-8}	8.73×10^{-8}	1.10×10^{-7}	1.70×10^{-7}	2.14×10^{-7}	3.74×10^{-7}	5.31×10^{-7}
λ	0.95	1.81	2.30	3.54	4.45	7.79	11.06
Lubrication regime*	BL	ML	ML	EL	EL	HL	HL
Hersey parameter	8.46×10^{-7}	1.86×10^{-6}	2.81×10^{-6}	4.72×10^{-6}	6.57×10^{-6}	1.46×10^{-5}	2.37×10^{-5}

Table 9) Characteristics of a lubricant film with PAO 8 + 1 wt.% IL #2 based on the sliding speed of the cylinder (u is the speed of the ring). * Boundary lubrication = BL; mixed lubrication = ML; elastohydrody-namic lubrication = EL; hydrodynamic lubrication = HL.

u (m/s)	**0.02**	**0.05**	**0.07**	**0.13**	**0.18**	**0.4**	**0.66**
Duration	25 min	11 min	19 min	11 min	15 min	15 min	9 min
h_0 (m)	4.66×10^{-8}	8.84×10^{-8}	1.11×10^{-7}	1.72×10^{-7}	2.16×10^{-7}	3.79×10^{-7}	5.38×10^{-7}
λ	0.96	1.84	2.33	3.59	4.51	7.89	11.21

Lubrication regime*	BL	ML	ML	EL	EL	HL	HL
Hersey parameter	8.64×10^{-7}	1.89×10^{-6}	2.87×10^{-6}	4.81×10^{-6}	6.70×10^{-6}	1.49×10^{-5}	2.42×10^{-5}

4.6. Wear analysis using optical microscopy and SEM-EDS

Optical microscopy (OM) was used to evaluate the wear of the coatings after tribological tests. Because quantifying the wear of DLC coatings is difficult (since it has high wear resistance), wear track pictures captured on an optical microscope were compared qualitatively [94]. The lubrication regime is the boundary or mixed regime at the lower sliding speeds, which can lead to surface–surface contact, eventually leading to wear on both surfaces. Based on the obtained results (Figure 16 and Figure 17), the introduction of IL #1 as an additive to PAO 8 decreased wear in comparison with pure PAO 8 paired with the 1.7 % Gd-DLC and pure DLC coatings. However, for other coatings, it is difficult to draw the same conclusion. In addition, comparing the five films lubricated with 1 wt.% of IL #1, it can be said that 2.4 % Eu-DLC has the worst performance. In the case of IL #2 added to the PAO8, it drastically reduces wear in all the thin films.

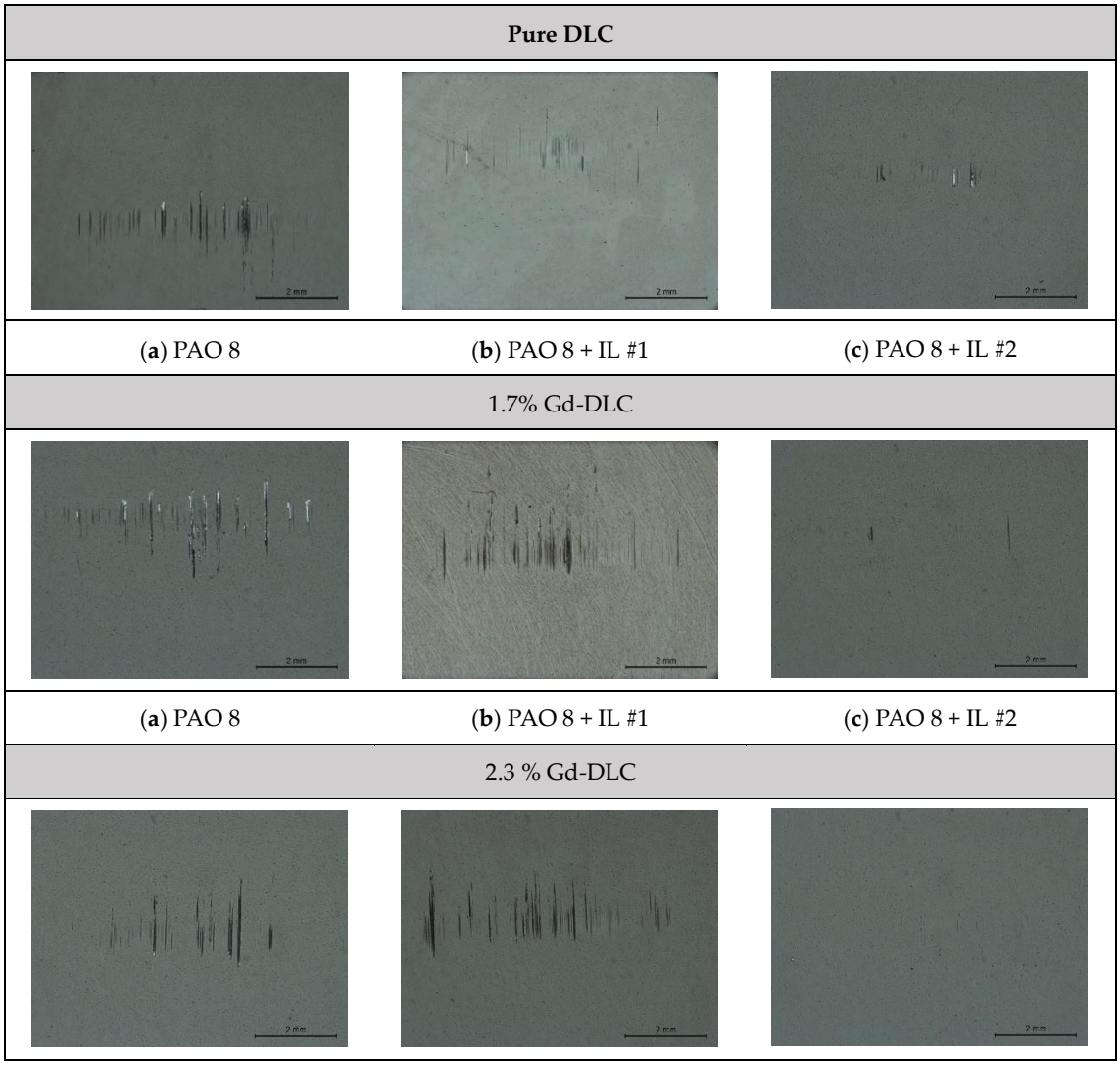

(**a**) PAO 8	(**b**) PAO 8 + IL #1	(**c**) PAO 8 + IL #2

Figure 16) Optical microscopy images of different films tested with different lubricants (pure DLC vs 1.7% Gd-DLC vs 2.3% Gd-DLC).

Pure DLC		
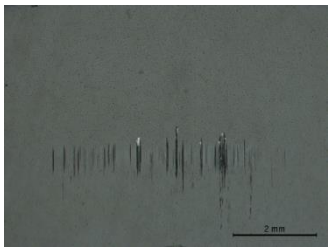	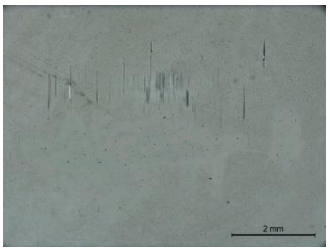	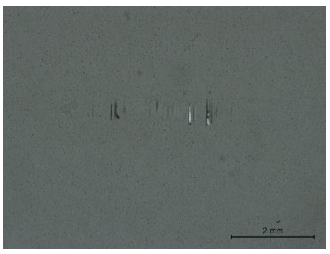
(**a**) PAO 8	(**b**) PAO 8 + IL #1	(**c**) PAO 8 + IL #2
1.7% Eu-DLC		
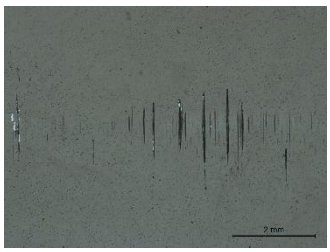	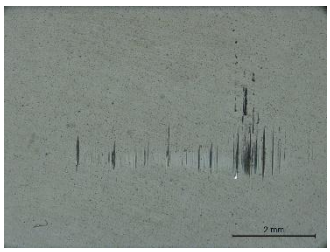	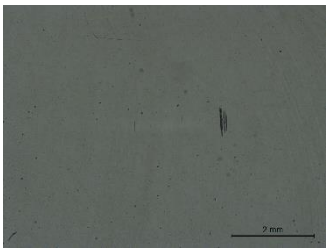
(**a**) PAO 8	(**b**) PAO 8 + IL #1	(**c**) PAO 8 + IL #2
2.4 % Eu-DLC		
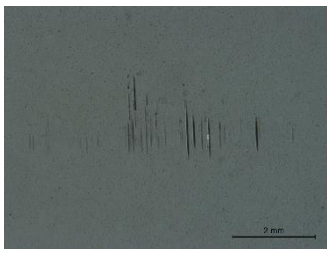	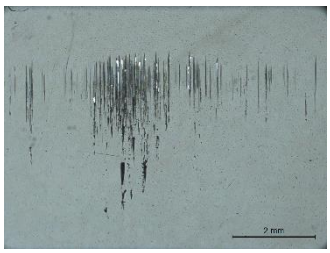	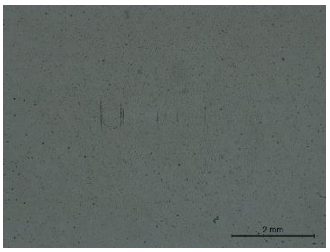
(**a**) PAO 8	(**b**) PAO 8 + IL #1	(**c**) PAO 8 + IL #2

Figure 17) Optical microscopy images of different lfilms tested with different lubricants (pure DLC vs 1.7% Eu-DLC vs 2.4% Eu-DLC).

SEM-EDS was used to evaluate the effect of using IL as an additive on coatings, but this technique cannot efficiently detect the formation of tribofilm in this case because it cannot provide information about chemical bonding, it can only provide information about elements, so it would be preferable to use more surface-sensitive characterization techniques such as time-of-flight secondary-ion mass spectrometry (ToF-SIMS) or neutron reflectometry analysis to recognize the tribofilm presence. In this section, only results for pure DLC and doped DLCs with lower atomic concentrations of dopant elements are presented. Figures 18-25 show the result obtained through SEM-EDS for the pure DLC, Gd-DLC, and Eu-DLC. As can be seen in Figures 18 and 19, for the

1.7 % Gd-DLC coating paired with PAO 8 + 1 wt.% IL #1, DLC thin film has been removed in some sections, and the chromium element of the interlayer can be detected, iron is also detected, it can be because of wear from steel ring or it can come from the substrate of the thin film because of abrasive wear. Oxygen is also present on the wear tracks which indicates the formation of oxide layers on the worn area. For the 1.7 % Eu-DLC coating paired with PAO 8 + 1 wt.% IL #1 (Figures 20 and 21), rich oxygen region is visible in the EDS result, which can indicate the formation of tribofilm. Also iron and chromium are detectable which confirms the removal of DLC film in the worn region analyzed. Figures 22 and 23 (for 1.7 % Gd-DLC coating paired with PAO 8 + 1 wt.% IL #2) and Figures 24 and 25 (for 1.7 % Eu-DLC coating paired with PAO 8 + 1 wt.% IL #2) do not show iron rich region in worn areas which indicates that there is less wear for this case, this fact is also confirmed by the results from optical microscopy.

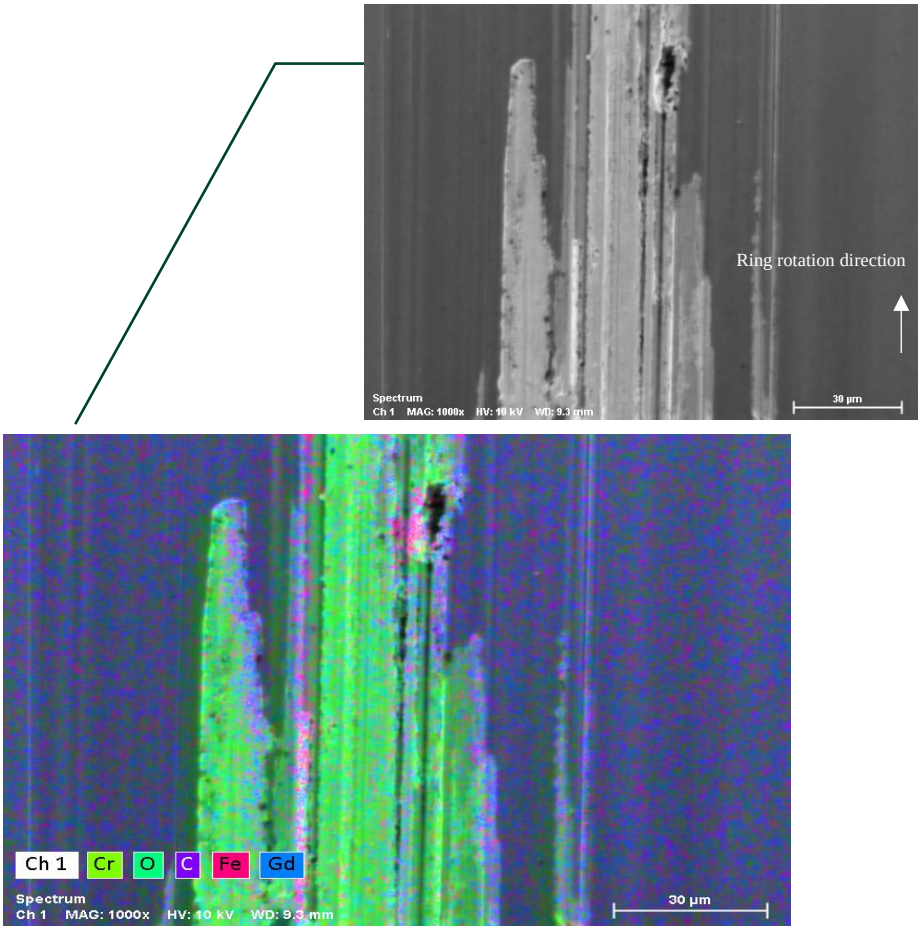

Figure 18) Upper image: shows the SEM micrograph of the 1.7 % Gd-DLC surface paired with PAO 8 + 1 wt.% IL #1 without presenting elements after the tribology test, lower image: Elemental analysis of the upper image obtained through SEM-EDS.

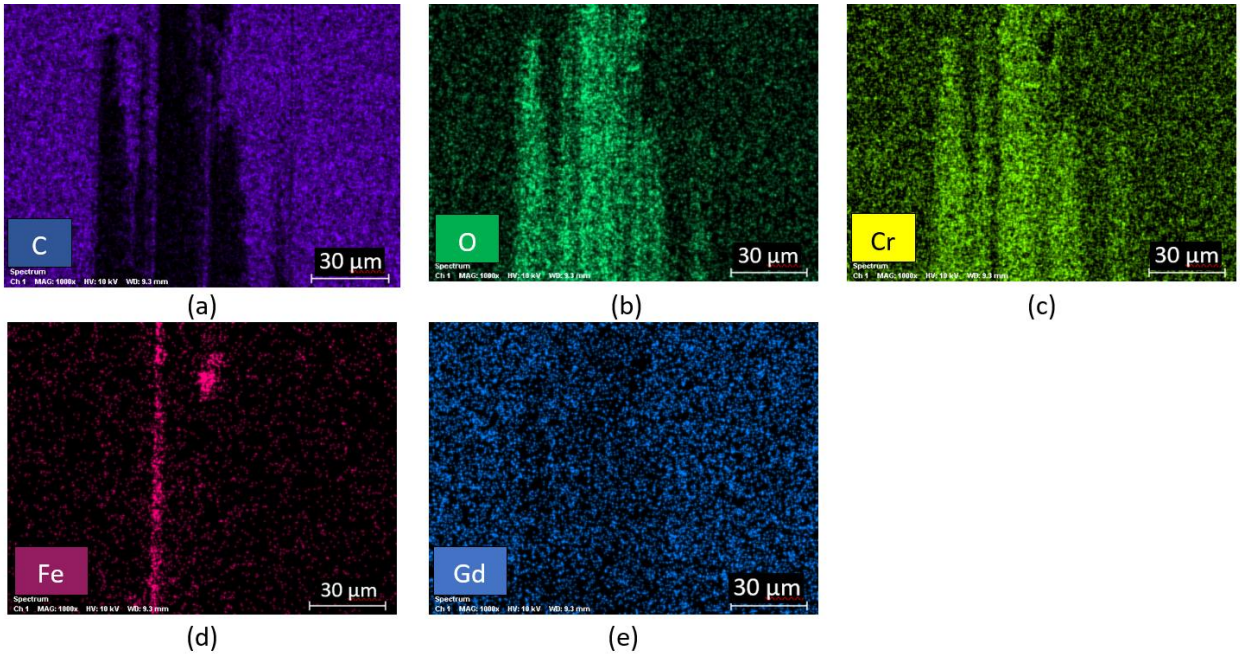

Figure 19) Element mapping of the 1.7 % DLC thin film paired with PAO 8 + 1 wt.% IL #1 after the tribology test: (a) carbon; (b) chromium; (c) iron; (d) gadolinium (obtained through SEM-EDS characterization).

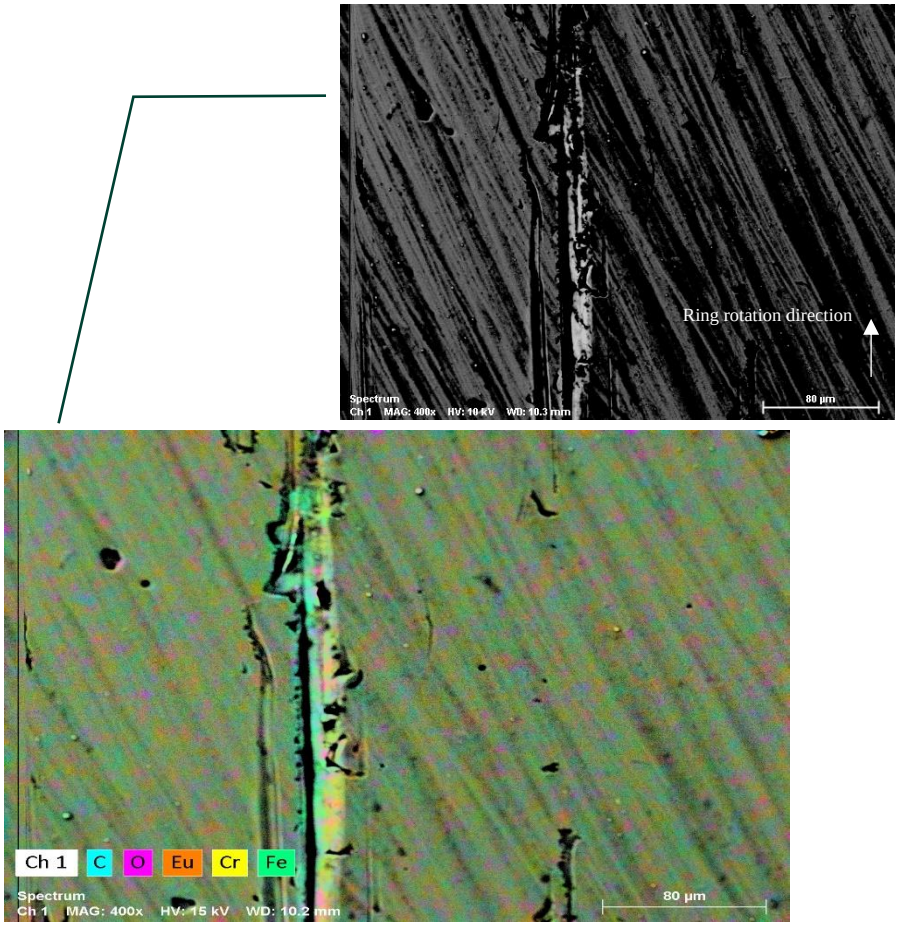

Figure 20) Upper image: shows the SEM micrograph of the 1.7 % Eu-DLC surface paired with PAO 8 + 1 wt.% IL #1 without presenting elements after the tribology test, lower image: Elemental analysis of the upper image obtained through SEM-EDS.

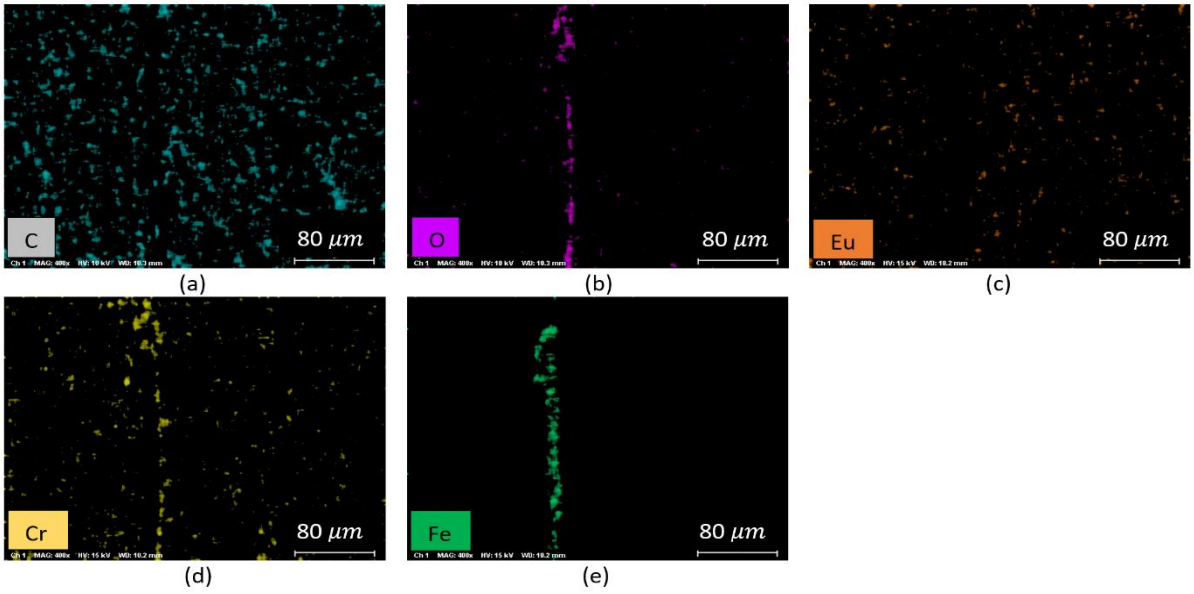

Figure 21) Element mapping of the 1.7 % Eu-DLC thin film paired with PAO 8 + 1 wt.% IL after the tribology test: (a) carbon; (b) oxygen; (c) europium; (d) chromium (e) iron (obtained through SEM-EDS characterization).

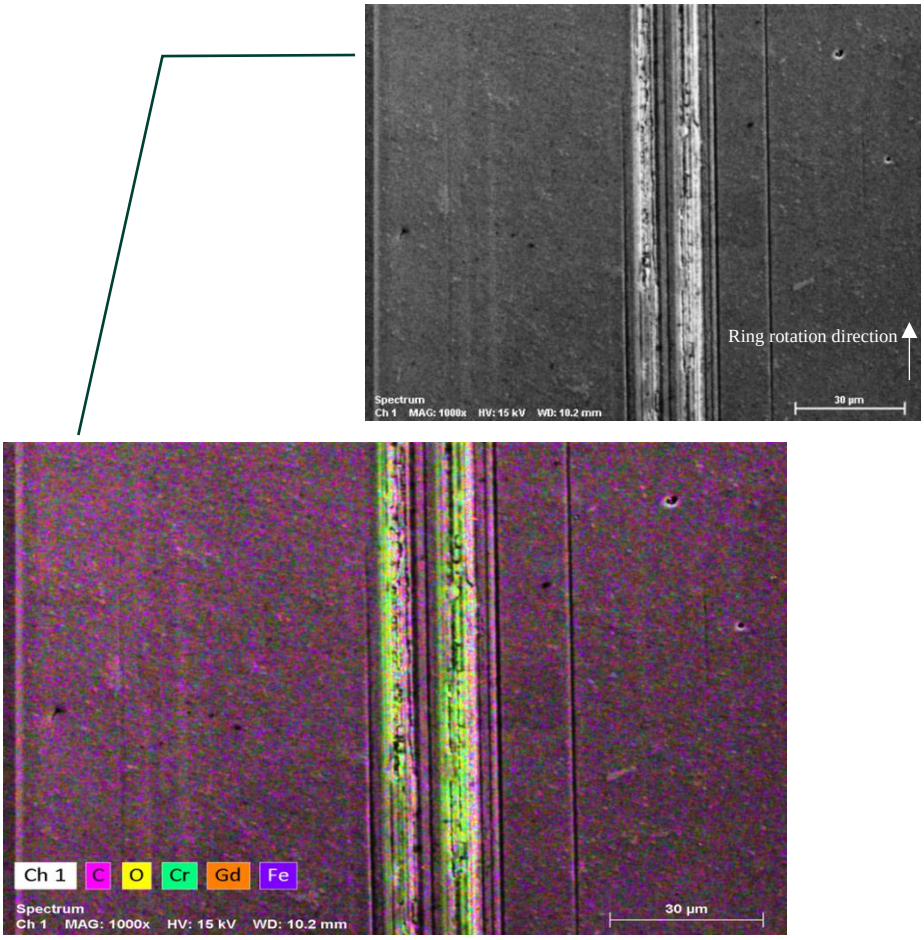

Figure 22) Upper image: shows the SEM micrograph of the 1.7 % Gd-DLC surface paired with PAO 8 + 1 wt.% IL #1 without presenting elements after the tribology test, lower image: Elemental analysis of the upper image obtained through SEM-EDS.

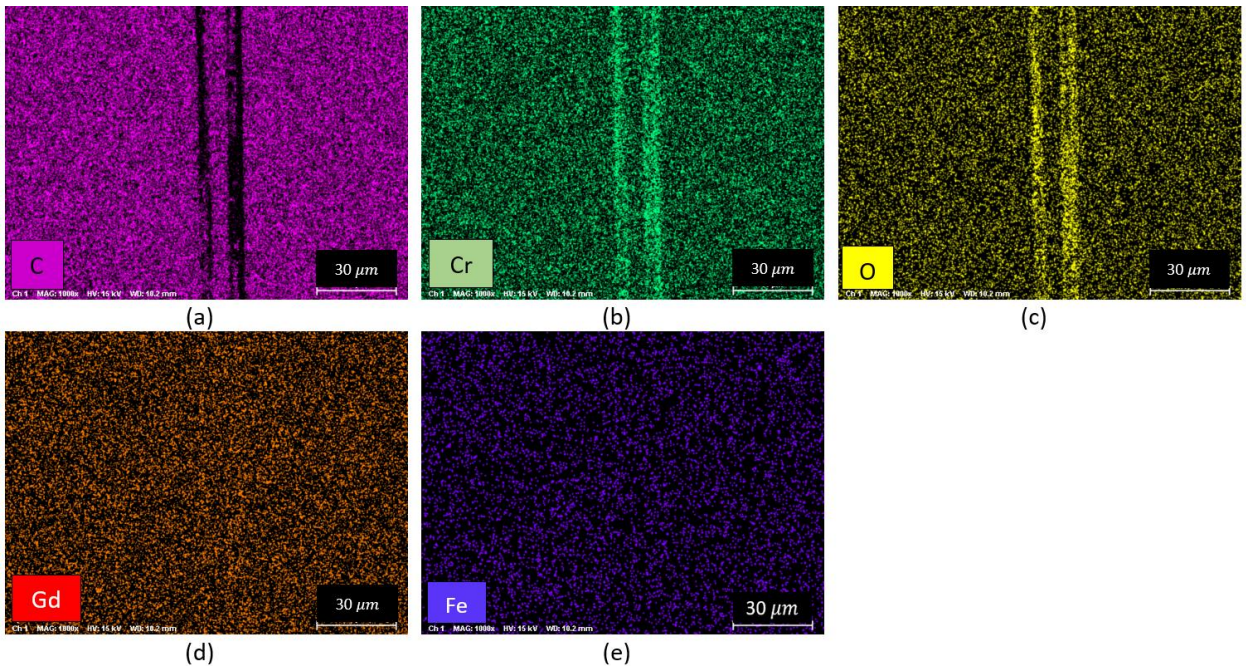

Figure 23) Element mapping of the 1.7 % Gd-DLC thin film paired with PAO 8 + 1 wt.% IL #2 after the tribology test: (a) carbon; (b) chromium; (c) oxygen; (d) gadolinium (e) iron (obtained through SEM-EDS characterization).

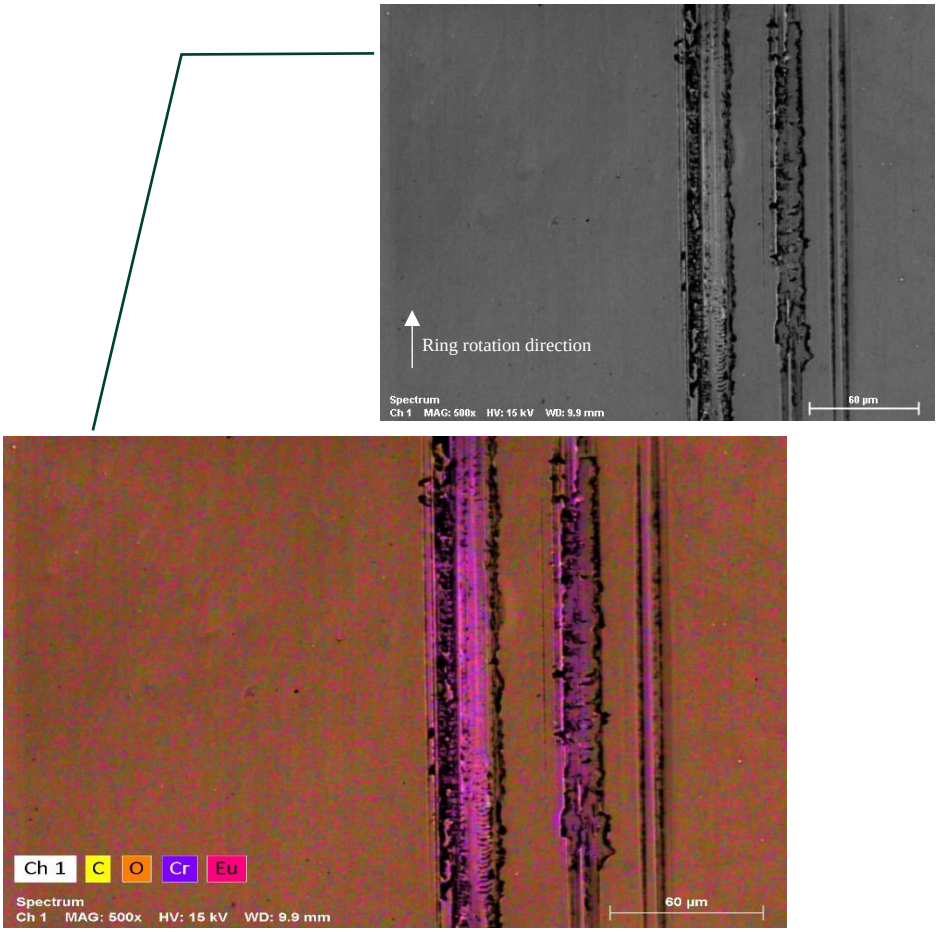

Figure 24) Upper image: shows the SEM micrograph of the 1.7 % Eu-DLC surface paired with PAO 8 + 1 wt.% IL #2 without presenting elements after the tribology test, lower image: Elemental analysis of the upper image obtained through SEM-EDS.

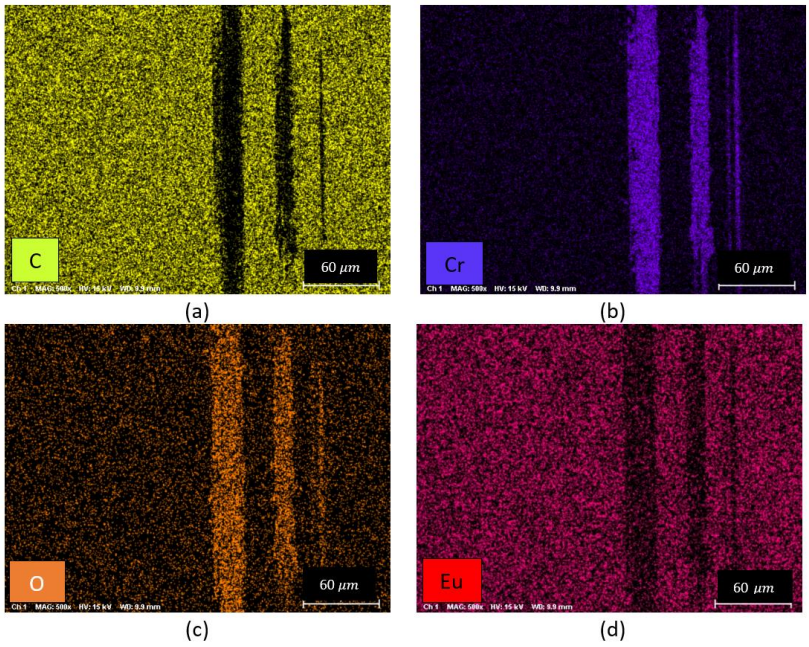

Figure 25) Element mapping of the 1.7 % Eu-DLC thin film paired with PAO 8 + 1 wt.% IL #2 after the tribology test: (a) carbon; (b) chromium; (c) oxygen; (d) europium (obtained through SEM-EDS characterization).

Chapter 5 - Conclusion and recommendations

5.1. Conclusions

In the present study, the effect of adding 1 wt.% of Trihexyltetradecylphosphonium bis(2-ethylhexyl) phosphate [P_{66614}][DEHP] (named IL #1 in this study) and 1-Ethyl-3-methylimidazolium diethylphosphate (named IL #2 in this study) ionic liquids as additives to PAO 8 for the lubricated sliding pairs of AISI 3415 steel and 5 DLC coatings (1.7% Gd-DLC, 2.3% Gd-DLC, 1.7% Eu-DLC, 2.4% Eu-DLC, and pure DLC coatings) was studied. Following conclusions can be drawn:

- The 1.7% Gd-DLC coating had the highest hardness, H/E, and H^3/E^2 ratio among all the five coatings and, according to the scratch measurements (critical load value), the highest L_{c1} value.
- When PAO8 was used as the main lubricant (before adding ionic liquids), pure DLC coating had the lowest friction against used counterpart.
- After adding 1 wt. % ionic liquid #1 to PAO8, the best interaction with the IL #1 and a significant CoF reduction in mixed, elastohydrodynamic, and hydrodynamic lubrication regimes were obtained with the 1.7 % Gd-DLC coating, however, 2.3% Gd-DLC had better performance in boundary lubrication regime.
- with the 1 wt.% IL #2 added to PAO 8, a significant CoF reduction in all lubrication regimes were obtained with the 1.7 % Eu-DLC coating.
- The wear results could not be quantitatively measured; however, the qualitative approach showed that adding an IL #1 to the lubricated contact decreased the wear on the Gd-DLC and pure DLC coatings. When a comparison of wear scars is done between PAO8 without additive and PAO8 + 1 wt.% IL #2, a significant reduction in wear was observed for all the coatings. Nevertheless, a quantitative comparison of wear among these 5 coatings in the presence of IL #2 is not feasible based on the available techniques for wear quantification. SEM-EDS results of wear scars show that the coatings are removed in contact points for presented coatings that are lubricated with POA8 + IL #1 and chromium element coming from interlayer and iron elements coming from substrate or counterpart can be detected. When lubricated with PAO8 + IL #2, chromium interlayer is detected which signifies the removal of DLC films.

5.2. Scope of future work

To facilitate a deeper investigation of the matter at hand, the implementation of the subsequent suggestions is advised, as they possess the potential to greatly assist industries in their discernment of optimal methodologies for the selection of materials utilized in piston-cylinder applications.

- Investigation of wear scars using surface-sensitive techniques like time-of-flight secondary-ion mass spectrometry (ToF-SIMS) or neutron reflectometry analysis to study the chemical composition of layers formed in this area.

- Investigation of the coatings using Raman spectroscopy to get insight about ratio of the sp^3/sp^2 in the coatings
- Measuring the thermal conductivity of the different coatings can also help to further understand the tribological interaction since full film friction reduction in DLC coatings is due to the low thermal conductivity of diamond-like carbon (DLC) coatings.

References

1. Reduce friction, save energy - ITAINNOVA, https://www.itainnova.es/blog/materiales/reduce-friction-save-energy/
2. Omiya, T., Fontes, M., Vuchkov, T., Cruz, S., Cavaleiro, A., Ferreira, F.: Tribological performance of Gd-DLC and Eu-DLC coatings in the presence of synthetic oils containing ionic liquid additives Keywords. Tribol Lett. 71, 65 (2023). https://doi.org/10.1007/s11249-023-01739-y
3. Holmberg, K., Erdemir, A.: The impact of tribology on energy use and CO2 emission globally and in combustion engine and electric cars. Tribol Int. 135, 389–396 (2019). https://doi.org/https://doi.org/10.1016/j.triboint.2019.03.024
4. Ciulli, E.: Tribology and Industry: From the Origins to 4.0. Front Mech Eng. 5, (2019). https://doi.org/https://doi.org/10.3389/fmech.2019.00055
5. Jost, H.P.: Lubrication: Tribology; Education and Research; Report on the Present Position and Industry's Needs (submitted to the Department of Education and Science by the Lubrication Engineering and Research) Working Group. HM Stationery Office (1966)
6. Sharma, S.: TRIBOLOGICAL BEHAVIOUR OF LASER TREATED C-ALLOYED TMD COATINGS IN RUBBER CONTACT, https://www.researchgate.net/publication/356785580, (2021)
7. Gawne, D.T.: Tribology: Principles and Applications in Surface Finishing. Transactions of the IMF. 70, 152–158 (1992). https://doi.org/10.1080/00202967.1992.11870964
8. Lubrication (tribology) : education and research : a report on the present position and industry's needs | WorldCat.org, https://www.worldcat.org/title/lubrication-tribology-education-and-research-a-report-on-the-present-position-and-industrys-needs/oclc/1052807084
9. Gawne, D.T.: Tribology: Principles and Applications in Surface Finishing. Transactions of the IMF. 70, 152–158 (1992). https://doi.org/10.1080/00202967.1992.11870964
10. Hutchings, I., Shipway, P.: 7 - Surface engineering. In: Hutchings, I. and Shipway, P. (eds.) Tribology (Second Edition). pp. 237–281. Butterworth-Heinemann (2017)
11. Baptista, A., Silva, F., Porteiro, J., Míguez, J., Pinto, G.: Sputtering physical vapour deposition (PVD) coatings: A critical review on process improvement andmarket trend demands, (2018)
12. Jabonero, A.M.: Deposition of Thick Nanostructured Cr-based Coatings by HiPIMS, https://eg.uc.pt/retrieve/215423/Jabonero.pdf, (2021)
13. Ferreira, F.: PROCESS-PROPERTIES RELATIONS IN DEEP OSCILLATION MAGNETRON SPUTTERING, http://hdl.handle.net/10316/79590, (2017)

14. Kumar, A., Kumar, M., Tailor, S.: Self-lubricating composite coatings: A review of deposition techniques and material advancement. Mater Today Proc. (2023). https://doi.org/https://doi.org/10.1016/j.matpr.2023.01.035

15. Sadeghi, M., Omiya, T., Fernandes, F., Vilhena, L., Ramalho, A., Ferreira, F.: Tribological Behavior of Doped DLC Coatings in the Presence of Ionic Liquid Additive under Different Lubrication Regimes. Coatings. 13, (2023). https://doi.org/10.3390/coatings13050891

16. Tasdemir, H.A., Tokoroyama, T., Kousaka, H., Umehara, N., Mabuchi, Y.: Friction and Wear Performance of Boundary-lubricated DLC/DLC Contacts in Synthetic base Oil. Procedia Eng. 68, 518–524 (2013). https://doi.org/https://doi.org/10.1016/j.proeng.2013.12.215

17. Nunthavarawong, P., Rangappa, S.M., Siengchin, S., Dohda, K.: Diamond-Like Carbon Coatings. CRC Press, Boca Raton (2022)

18. Yue, Z., Fan, X., Wang, Y., Li, H., Zhang, J., Zhu, M.: Fretting behaviors of self-mated diamond-like carbon films: The evolution of fretting regime and transfer film. Carbon N Y. 203, 695–705 (2023). https://doi.org/https://doi.org/10.1016/j.carbon.2022.12.032

19. Zia, A.W., Zhou, Z., Li, L.K.-Y.: Chapter 7 - Structural, mechanical, and tribological characteristics of diamond-like carbon coatings. In: Nguyen Tri, P., Rtimi, S., and Ouellet Plamondon, C.M. (eds.) Nanomaterials-Based Coatings. pp. 171–194. Elsevier (2019)

20. Liu, J., Yang, T., Cao, H., Deng, Q., Pan, C., Wen, F.: Diamond-like carbon films for tribological modification of rubber. Nanotechnol Rev. 11, 2839–2856 (2022). https://doi.org/10.1515/ntrev-2022-0481

21. Vieira, V.F., Shigaki, Y., Martins, P.S., Ba, E.C.T., Dias, C.A.R.: Nanoindentation test of a DLC coated high-speed steel substrate using a two-dimensional axisymmetric finite element method. Diam Relat Mater. 134, 109792 (2023). https://doi.org/https://doi.org/10.1016/j.diamond.2023.109792

22. Roy, R.K., Lee, K.R.: Biomedical applications of diamond-like carbon coatings: a review. J Biomed Mater Res B Appl Biomater. 83, 72–84 (2007). https://doi.org/10.1002/JBM.B.30768

23. Beake, B.D., Mcmaster, S.J., Liskiewicz, T.W., Neville, A.: Influence of Si-and W-doping on micro-scale reciprocating wear and impact performance of DLC coatings on hardened steel. Tribol Int. 160, 107063 (2021). https://doi.org/10.1016/j.triboint.2021.107063

24. Diamond-like Carbon (DLC) Market Size, Share, Scope, Trends & Forecast, https://www.verifiedmarketresearch.com/product/diamond-like-carbon-dlc-market/

25. Casiraghi, C., Robertson, J., Ferrari, A.C.: Diamond-like carbon for data and beer storage. Materials Today. 10, 44–53 (2007). https://doi.org/https://doi.org/10.1016/S1369-7021(06)71791-6

26. Ferreira, F., Serra, R., Cavaleiro, A., Oliveira, J.: Diamond-like carbon coatings deposited by deep oscillation magnetron sputtering in Ar-Ne discharges. Diam Relat Mater. 98, 107521 (2019). https://doi.org/https://doi.org/10.1016/j.diamond.2019.107521

27. Vetter, J.: 60years of DLC coatings: Historical highlights and technical review of cathodic arc processes to synthesize various DLC types, and their evolution for industrial applications. Surf Coat Technol. 257, 213–240 (2014). https://doi.org/https://doi.org/10.1016/j.surfcoat.2014.08.017

28. Deng, X., Kousaka, H., Tokoroyama, T., Umehara, N.: Thermal Stability and High-Temperature Tribological Properties of a-C:H and Si-DLC Deposited by Microwave Sheath Voltage Combination Plasma. Tribology Online. 8, 257–264 (2013). https://doi.org/10.2474/trol.8.257

29. Ali, A., Hirakuri, K.K., Friedbacher, G.: Roughness and deposition mechanism of DLC films prepared by r.f. plasma glow discharge. Vacuum. 51, 363–368 (1998). https://doi.org/https://doi.org/10.1016/S0042-207X(98)00115-8

30. Karuzskii, A.L., Melnik, N.N., Murzin, V.N., Nozdrin, V.S., Perestoronin, A. V, Volchkov, N.A., Zhurkin, B.G.: Pulsed-laser deposition of “diamond-like” carbon coating on YBa2Cu3O7 high-Tc superconductor films. Appl Surf Sci. 92, 457–460 (1996). https://doi.org/https://doi.org/10.1016/0169-4332(95)00276-6

31. Wang, A.-Y., Lee, K.-R., Ahn, J.-P., Han, J.H.: Structure and mechanical properties of W incorporated diamond-like carbon films prepared by a hybrid ion beam deposition technique. Carbon N Y. 44, 1826–1832 (2006). https://doi.org/10.1016/j.carbon.2005.12.045

32. de Fátima Magalhaes Mariano, S., de Dios Mitma Pillaca, E.J., Ueda, M., de Moraes Oliveira, R.: Influence of the magnetic field on DLC coatings grown by plasma immersion ion implantation and deposition in crossed fields. Surf Coat Technol. 256, 47–51 (2014). https://doi.org/10.1016/j.surfcoat.2014.01.012

33. Bulíř, J., Novotný, M., Jelínek, M., Kocourek, T., Studnička, V.: Plasma study and deposition of DLC/TiC/Ti multilayer structures using technique combining pulsed laser deposition and magnetron sputtering. Surf Coat Technol. 200, 708–711 (2005). https://doi.org/https://doi.org/10.1016/j.surfcoat.2005.01.087

34. Lin, Z., Lv, S.-B., Yu, Z.-J., Li, M., Lin, T.-Y., Ba, D.-C., Choi, C.-K., Lee, I.-S.: Effect of bias voltage on Diamond-like carbon film deposited on PMMA substrate. Surf Coat Technol. 202, 5386–5389 (2008). https://doi.org/https://doi.org/10.1016/j.surfcoat.2008.06.071

35. Zia, A.W., Birkett, M.: Deposition of diamond-like carbon coatings: Conventional to non-conventional approaches for emerging markets. Ceram Int. 47, 28075–28085 (2021). https://doi.org/https://doi.org/10.1016/j.ceramint.2021.07.005

36. Chowdhury, S., Laugier, M.T., Rahman, I.Z.: Effect of target self-bias voltage on the mechanical properties of diamond-like carbon films deposited by RF magnetron sputtering. Thin Solid Films. 468, 149–154 (2004). https://doi.org/https://doi.org/10.1016/j.tsf.2004.04.006

37. Sheeja, D., Tay, B.K., Lau, S.P., Shi, X.: Tribological properties and adhesive strength of DLC coatings prepared under different substrate bias voltages. Wear. 249, 433–439 (2001). https://doi.org/https://doi.org/10.1016/S0043-1648(01)00541-5

38. WU, K.-Y., ZHAO, G.-R., LI, Z., GONG, Z.-B.: EFFECTS OF ELECTRODE DISTANCE ON MECHANICAL AND TRIBOLOGICAL PROPERTIES OF HYDROGENATED DLC FILMS DEPOSITED BY DC-PULSE PECVD. Surface Review and Letters. 28, 2050045 (2021). https://doi.org/10.1142/S0218625X20500456

39. Lux, H., Edling, M., Lucci, M., Kitzmann, J., Villringer, C., Siemroth, P., De Matteis, F., Schrader, S.: The role of substrate temperature and magnetic filtering for DLC by cathodic arc evaporation. Coatings. 9, (2019). https://doi.org/10.3390/COATINGS9050345

40. Zavaleyev, V., Walkowicz, J., Greczynski, G., Hultman, L.: Effect of substrate temperature on properties of diamond-like films deposited by combined DC impulse vacuum-arc method. Surf Coat Technol. 236, 444–449 (2013). https://doi.org/https://doi.org/10.1016/j.surfcoat.2013.10.023

41. Kang, Y., Li, B., Zhao, J., Ge, B., Weng, M., Shi, Z., Zhao, Y.: Effect of structure on the secondary electron emission of tetrahedral amorphous carbon films. Vacuum. 172, 109043 (2020). https://doi.org/10.1016/j.vacuum.2019.109043

42. Yadav, V.S., Sahu, D.K., Singh, M., Kumar, K., Dhubkarya, D.C., Singh, Y., Ao, S.-I.: Characterization of Nano-Crystalline Diamond like Carbon (DLC) Films with Substrate Temperature Using Dense Plasma Focusing Method. In: AIP Conference Proceedings. pp. 363–373. American Institute of Physics (2010)

43. Lei, Y., Jiang, J., Wang, Y., Bi, T., Zhang, L.: Structure evolution and stress transition in diamond-like carbon films by glancing angle deposition. Appl Surf Sci. 479, 12–19 (2019). https://doi.org/10.1016/j.apsusc.2019.02.063

44. Kinoshita, H., Ippei, I., Sakai, H., Ohmae, N.: Synthesis and mechanical properties of carbon nanotube/diamond-like carbon composite films. Diam Relat Mater. 16, 1940–1944 (2007). https://doi.org/10.1016/j.diamond.2007.08.004

45. Guo, C.Q., Pei, Z.L., Fan, D., Gong, J., Sun, C.: Microstructure and tribomechanical properties of (Cr, N)-DLC/DLC multilayer films deposited by a combination of filtered and direct cathodic vacuum arcs. Diam Relat Mater. 60, 66–74 (2015). https://doi.org/https://doi.org/10.1016/j.diamond.2015.10.019

46. Zia, A.W., Hussain, S.A., Baig, M.M.F.A.: Optimizing diamond-like carbon coatings - From experimental era to artificial intelligence. Ceram Int. 48, 36000–36011 (2022). https://doi.org/https://doi.org/10.1016/j.ceramint.2022.10.149

47. Jean, M. Der, Liu, C. Du, Wang, S.F., Li, C.H., Kao, K.H.: Design and Optimization of Surface Properties for Diamond-Like Carbon Films by Sputtering Depositions. Applied Mechanics and Materials. 401–403, 762–766 (2013). https://doi.org/10.4028/www.scientific.net/AMM.401-403.762

48. Fang, J., Sheen, M.T., Jean, M. Der: Analysis of Surface Properties of Diamond-Like Carbon Films by a Sputtering Deposition. Adv Mat Res. 662, 505–510 (2013). https://doi.org/10.4028/www.scientific.net/AMR.662.505

49. Kalita, K., Ghadai, R.K.: Optimization of Plasma Enhanced Chemical Vapor Deposition Process Parameters for Hardness improvement of Diamond Like Carbon Coatings. Scientia Iranica. 0, 0–0 (2022). https://doi.org/10.24200/sci.2022.56869.4952

50. Solis-Romero, J., Rodríguez-Molina, A., Solis-Cordova, J.J., Neville, A.: Parametric optimisation of friction and wear of a multi-layered a-C:H coating on AISI 52100 steel. Mater Lett. 318, 132166 (2022). https://doi.org/https://doi.org/10.1016/j.matlet.2022.132166

51. Chang, Y.-Y., Wang, D.-Y.: Structural and electrical properties of Cr doped a-C:H films synthesized by a cathodic-arc activated deposition process. Surf Coat Technol. 200, 3170–3174 (2006). https://doi.org/https://doi.org/10.1016/j.surfcoat.2005.07.037

52. Tang, X.S., Wang, H.J., Feng, L., Shao, L.X., Zou, C.W.: Mo doped DLC nanocomposite coatings with improved mechanical and blood compatibility properties. Appl Surf Sci. 311, 758–762 (2014). https://doi.org/https://doi.org/10.1016/j.apsusc.2014.05.155

53. Khun, N.W., Lee, P.M., Toh, W.Q., Liu, E.: Tribological Behavior of Nickel-Doped Diamond-Like Carbon Thin Films Prepared on Silicon Substrates via Magnetron Sputtering Deposition. Tribology Transactions. 59, 845–855 (2016). https://doi.org/10.1080/10402004.2015.1110864

54. Majeed, S., Siraj, K., Naseem, S., Khan, M.F., Irshad, M., Faiz, H., Mahmood, A.: Structural and optical properties of gold-incorporated diamond-like carbon thin films deposited by RF magnetron sputtering. Mater Res Express. 4, 076403 (2017). https://doi.org/10.1088/2053-1591/aa7430

55. Liu, N., Zhu, H., Wei, Q., Long, H., Deng, Z., Yu, Z., Xie, Y., Wang, J., Ma, L., Zhou, K.: A Niobium and Nitrogen Co-Doped DLC Film Electrode and Its Electrochemical Properties. J Electrochem Soc. 164, H1091–H1098 (2017). https://doi.org/10.1149/2.1001714jes

56. Wang, L., Jin, J., Zhu, C., Li, G., Kuang, X., Huang, K.: Effects of HiPIMS pulse-length on plasma discharge and on the properties of WC-DLC coatings. Appl Surf Sci. 487, 526–538 (2019). https://doi.org/10.1016/j.apsusc.2019.05.046

57. Zhang, R., Wang, L.: Synergistic improving of tribological properties of amorphous carbon film enhanced by F–Si-doped multilayer structure under corrosive environment. Surf Coat Technol. 276, 626–635 (2015). https://doi.org/10.1016/j.surfcoat.2015.06.006

58. Zhang, S., Yan, M., Yang, Y., Zhang, Y., Yan, F., Li, H.: Excellent mechanical, tribological and anti-corrosive performance of novel Ti-DLC nanocomposite thin films prepared via magnetron sputtering method. Carbon N Y. 151, 136–147 (2019). https://doi.org/10.1016/j.carbon.2019.05.031

59. Jo, Y.J., Zhang, T.F., Son, M.J., Kim, K.H.: Synthesis and electrochemical properties of Ti-doped DLC films by a hybrid PVD/PECVD process. Appl Surf Sci. 433, 1184–1191 (2018). https://doi.org/10.1016/j.apsusc.2017.10.151

60. Rana, R., Walia, R.S., Murtaza, Q.: Characterization and Parametric Optimization of Performance Parameters of DLC-Coated Tungsten Carbide (WC) Tool Using TOPSIS. Coatings. 11, 760 (2021). https://doi.org/10.3390/coatings11070760

61. Liu, L., Huang, J., He, X., Wang, T., He, Z., Du, K., Diao, X.: Preparation and characterization of high quality diamond like carbon films on Si microspheres. Mater Lett. 220, 309–312 (2018). https://doi.org/10.1016/j.matlet.2018.03.057

62. Sharifahmadian, O., Mahboubi, F., Yazdani, S.: Comparison between corrosion behaviour of DLC and N-DLC coatings deposited by DC-pulsed PACVD technique. Diam Relat Mater. 95, 60–70 (2019). https://doi.org/10.1016/j.diamond.2019.04.007

63. Carvalho, I., Dias, N., Henriques, M., Calderon V, S., Ferreira, P., Cavaleiro, A., Carvalho, S.: Antibacterial Effects of Bimetallic Clusters Incorporated in Amorphous Carbon for Stent Application. ACS Appl Mater Interfaces. 12, 24555–24563 (2020). https://doi.org/10.1021/acsami.0c02821

64. Antunes, J., Matos, K., Carvalho, I., Carvalho, S., Ferreira, F., Cruz, S.M.A.: Physical Vapor Deposition Technology in Personal Protective Equipment Production: Improved Antibacterial and Hydrophobic Character of Textiles. Coatings. 12, (2022). https://doi.org/10.3390/coatings12101399

65. Bociaga, D., Komorowski, P., Batory, D., Szymanski, W., Olejnik, A., Jastrzebski, K., Jakubowski, W.: Silver-doped nanocomposite carbon coatings (Ag-DLC) for biomedical applications – Physiochemical and biological evaluation. Appl Surf Sci. 355, 388–397 (2015). https://doi.org/https://doi.org/10.1016/j.apsusc.2015.07.117

66. Tallant, D.R., Parmeter, J.E., Siegal, M.P., Simpson, R.L.: The thermal stability of diamond-like carbon. Diam Relat Mater. 4, 191–199 (1995). https://doi.org/10.1016/0925-9635(94)00243-6

67. Zeng, Q., Ning, Z.: High-temperature tribological properties of diamond-like carbon films: A review. REVIEWS ON ADVANCED MATERIALS SCIENCE. 60, 276–292 (2021). https://doi.org/10.1515/rams-2021-0028

68. Salah, N., Alshahrie, A., Iqbal, J., Hasan, P.M.Z., Abdel-wahab, M.Sh.: Tribological behavior of diamond-like carbon thin films deposited by the pulse laser technique at different substrate temperatures. Tribol Int. 103, 274–280 (2016). https://doi.org/10.1016/j.triboint.2016.07.013

69. Zhang, T.F., Wan, Z.X., Ding, J.C., Zhang, S., Wang, Q.M., Kim, K.H.: Microstructure and high-temperature tribological properties of Si-doped hydrogenated diamond-like carbon films. Appl Surf Sci. 435, 963–973 (2018). https://doi.org/https://doi.org/10.1016/j.apsusc.2017.11.194

70. Yu, W., Wang, J., Huang, W., Cui, L., Wang, L.: Improving high temperature tribological performances of Si doped diamond-like carbon by using W interlayer. Tribol Int. 146, 106241 (2020). https://doi.org/https://doi.org/10.1016/j.triboint.2020.106241

71. Bundy, F.P.: Diamonds: *The Properties of Diamond* . J. E. Field, Ed. Academic Press, New York, 1979. xvi, 674 pp. Science (1979). 207, 974–974 (1980). https://doi.org/10.1126/science.207.4434.974.a

72. Rajak, D.K., Kumar, A., Behera, A., Menezes, P.L.: Diamond-Like Carbon (DLC) Coatings: Classification, Properties, and Applications. Applied Sciences 2021, Vol. 11, Page 4445. 11, 4445 (2021). https://doi.org/10.3390/APP11104445

73. Outka, D.A., Hsu, W.L., Phillips, K., Boehme, D.R., Yang, N.Y.C., Ottesen, D.K., Johnsen, H.A., Clift, W.M., Headley, T.J.: Compilation of diamond-like carbon properties for barriers and hard coatings. , Albuquerque, NM, and Livermore, CA (United States) (1994)

74. Ohtake, N., Hiratsuka, M., Kanda, K., Akasaka, H., Tsujioka, M., Hirakuri, K., Hirata, A., Ohana, T., Inaba, H., Kano, M., Saitoh, H.: Properties and Classification of Diamond-Like Carbon Films. Materials 2021, Vol. 14, Page 315. 14, 315 (2021). https://doi.org/10.3390/MA14020315

75. Wongpanya, P., Pintitraratibodee, N., Thumanu, K., Euaruksakul, C.: Improvement of corrosion resistance and biocompatibility of 316L stainless steel for joint replacement application by Ti-doped and Ti-interlayered DLC films. Surf Coat Technol. 425, 127734 (2021). https://doi.org/10.1016/j.surfcoat.2021.127734

76. Fayed, S.M., Wu, H., Chen, D., Li, S., Zhou, Y., Wang, H., Sadawy, M.M.: Influence of positive pulse voltages on structure, mechanical, and corrosion inhibition characteristics of Si/DLC coatings. Surf Coat Technol. 445, 128749 (2022). https://doi.org/https://doi.org/10.1016/j.surfcoat.2022.128749

77. Talha Hanif, M., Zahid, R., Mufti, R., Waqas, M., Naveed, T.: A Review on Tribological Study of DLC Coatings in Combination with Bio Based Lubricants. http://www.sciencepublishinggroup.com. 10, 61 (2021). https://doi.org/10.11648/J.IJMSA.20211003.13

78. Donnet, C., Grill, A.: Friction control of diamond-like carbon coatings. Surf Coat Technol. 94–95, 456–462 (1997). https://doi.org/10.1016/S0257-8972(97)00275-2

79. Enke, K., Dimigen, H., Hübsch, H.: Frictional properties of diamondlike carbon layers. Appl Phys Lett. 36, 291–292 (1980). https://doi.org/10.1063/1.91465

80. Liu, Y., Erdemir, A., Meletis, E.I.: A study of the wear mechanism of diamond-like carbon films. Surf Coat Technol. 82, 48–56 (1996). https://doi.org/10.1016/0257-8972(95)02623-1

81. Liu, Y., Erdemir, A., Meletis, E.I.: An investigation of the relationship between graphitization and frictional behavior of DLC coatings. Surf Coat Technol. 86–87, 564–568 (1996). https://doi.org/10.1016/S0257-8972(96)03057-5

82. Miyake, S., Takahashi, S., Watanabe, I., Yoshihara, H.: Friction and Wear Behavior of Hard Carbon Films. http://dx.doi.org/10.1080/05698198708981739. 30, 121–127 (2008). https://doi.org/10.1080/05698198708981739

83. Kokaku, Y., Kitoh, M.: Influence of exposure to an atmosphere of high relative humidity on tribological properties of diamondlike carbon films. Journal of Vacuum Science & Technology A: Vacuum, Surfaces, and Films. 7, 2311–2314 (1989). https://doi.org/10.1116/1.575934

84. Yoon, E.-S., Kong, H., Lee, K.-R.: Tribological behavior of sliding diamond-like carbon films under various environments. Wear. 217, 262–270 (1998). https://doi.org/https://doi.org/10.1016/S0043-1648(98)00163-X

85. Kim, D.-W., Kim, K.-W.: Effects of sliding velocity and normal load on friction and wear characteristics of multi-layered diamond-like carbon (DLC) coating prepared by reactive sputtering. Wear. 297, 722–730 (2013). https://doi.org/https://doi.org/10.1016/j.wear.2012.10.009

86. Al Mahmud, K.A.H., Kalam, M.A., Masjuki, H.H., Mobarak, H.M., Zulkifli, N.W.M.: An updated overview of diamond-like carbon coating in tribology. http://dx.doi.org/10.1080/10408436.2014.940441. 40, 90–118 (2014). https://doi.org/10.1080/10408436.2014.940441

87. Rübig, B., Heim, D., Forsich, C., Dipolt, C., Mueller, T., Gebeshuber, A., Kullmer, R., Holecek, R., Lugmair, C., Krawinkler, M., Strobl, V.: Tribological behavior of thick DLC coatings under lubricated conditions. Surf Coat Technol. 314, 13–17 (2017). https://doi.org/10.1016/j.surfcoat.2016.09.055

88. Fontes, M.A., Serra, R.G.H., Fernandes, F.D., Cavaleiro Rodrigues de Carvalho, A.A., Ferreira, F.E. de S.: Comparison of mechanical and tribological properties of diamond-like carbon coatings doped with Europium and Gadolinium produced by HiPIMS. Proc Inst Mech Eng B J Eng Manuf. 09544054221136528 (2022). https://doi.org/10.1177/09544054221136528

89. Rout, A., Kumar, S., Ramanathan, N.: Probing the coordination of europium(III) in a functionalized ionic liquid using luminescence spectroscopy. J Mol Liq. 323, (2021). https://doi.org/10.1016/j.molliq.2020.115109

90. Stoy, L., Xu, J., Kulkarni, Y., Huang, C.-H.: Ionic Liquid Recovery of Rare-Earth Elements from Coal fly Ash: Process Efficiency and Sustainability Evaluations. ACS

Sustain Chem Eng. 10, 11824–11834 (2022). https://doi.org/10.1021/acssuschemeng.2c02459

91. MISHRA, B.B., DEVI, N.: Application of bifunctional ionic liquids for extraction and separation of Eu3+ from chloride medium. Transactions of Nonferrous Metals Society of China (English Edition). 32, 2061–2070 (2022). https://doi.org/10.1016/S1003-6326(22)65930-2

92. Turanov, A.N., Karandashev, V.K., Boltoeva, M.: Solvent extraction of intra-lanthanides using a mixture of TBP and TODGA in ionic liquid. Hydrometallurgy. 195, (2020). https://doi.org/10.1016/j.hydromet.2020.105367

93. Valente, A.J.M., Burrows, H.D., Cruz, S.M.A., Pereira, R.F.P., Ribeiro, A.C.F., Lobo, V.M.M.: Aggregation and micellization of sodium dodecyl sulfate in the presence of Ce(III) at different temperatures: A conductometric study. J Colloid Interface Sci. 323, 141–145 (2008). https://doi.org/10.1016/j.jcis.2008.03.046

94. Cardoso, F., Ferreira, F., Cavaleiro, A., Ramalho, A.: Performance of diamond-like carbon coatings (produced by the innovative Ne-HiPIMS technology) under different lubrication regimes. Wear. 477, (2021). https://doi.org/10.1016/j.wear.2021.203775

95. Vahidi, A., Fonseca, D., Oliveira, J., Cavaleiro, A., Ramalho, A., Ferreira, F.: Advanced tribological characterization of dlc coatings produced by ne-hipims for the application on the piston rings of internal combustion engines. Applied Sciences (Switzerland). 11, (2021). https://doi.org/10.3390/app112110498

96. Spikes, H.: The History and Mechanisms of ZDDP. Tribol Lett. 17, 469–489 (2004). https://doi.org/10.1023/B:TRIL.0000044495.26882.b5

97. Ren, S., Zheng, S., Pu, J., Lu, Z., Zhang, G.: Study of tribological mechanisms of carbon-based coatings in antiwear additive containing lubricants under high temperature. RSC Adv. 5, 66426–66437 (2015). https://doi.org/10.1039/C5RA08879H

98. Ratoi, M., Niste, V.B., Zekonyte, J.: WS2 nanoparticles – potential replacement for ZDDP and friction modifier additives. RSC Adv. 4, 21238–21245 (2014). https://doi.org/10.1039/C4RA01795A

99. Verma, D.K., Dewangan, Y., Singh, A.K., Mishra, R., Susan, M.A.B.H., Salim, R., Taleb, M., El Hajjaji, F., Berdimurodov, E.: Ionic liquids as green and smart lubricant application: an overview. Ionics (Kiel). 28, 4923–4932 (2022). https://doi.org/10.1007/s11581-022-04699-w

100. Zhou, F., Liang, Y., Liu, W.: Ionic liquid lubricants: designed chemistry for engineering applications. Chem Soc Rev. 38, 2590–2599 (2009). https://doi.org/10.1039/B817899M

101. Ye, C., Liu, W., Chen, Y., Yu, L.: Room-temperature ionic liquids: a novel versatile lubricant. Chemical Communications. 2244–2245 (2001). https://doi.org/10.1039/B106935G

102. Lu, R., Mori, S., Kobayashi, K., Nanao, H.: Study of tribochemical decomposition of ionic liquids on a nascent steel surface. Appl Surf Sci. 255, 8965–8971 (2009). https://doi.org/https://doi.org/10.1016/j.apsusc.2009.03.063

103. Chen, Y., Renner, P., Liang, H.: A review of current understanding in tribochemical reactions involving lubricant additives. Friction. 11, 489–512 (2022). https://doi.org/10.1007/s40544-022-0637-2

104. Banerjee, C., Mandal, S., Ghosh, S., Kuchlyan, J., Kundu, N., Sarkar, N.: Unique Characteristics of Ionic Liquids Comprised of Long-Chain Cations and Anions: A New Physical Insight. J Phys Chem B. 117, 3927–3934 (2013). https://doi.org/10.1021/jp4015405

105. Barnhill, W.C., Qu, J., Luo, H., Meyer, H.M.I.I.I., Ma, C., Chi, M., Papke, B.L.: Phosphonium-Organophosphate Ionic Liquids as Lubricant Additives: Effects of Cation Structure on Physicochemical and Tribological Characteristics. ACS Appl Mater Interfaces. 6, 22585–22593 (2014). https://doi.org/10.1021/am506702u

106. Fernandes, A.M., Rocha, M.A.A., Freire, M.G., Marrucho, I.M., Coutinho, J.A.P., Santos, L.M.N.B.F.: Evaluation of Cation−Anion Interaction Strength in Ionic Liquids. J Phys Chem B. 115, 4033–4041 (2011). https://doi.org/10.1021/jp201084x

107. Silva, W., Zanatta, M., Ferreira, A., Corvo, M., Cabrita, E.: Revisiting Ionic Liquid Structure-Property Relationship: A Critical Analysis. Int J Mol Sci. 21, 7745 (2020). https://doi.org/10.3390/ijms21207745

108. Huang, G., Yu, Q., Cai, M., Zhou, F., Liu, W.: Investigation of the lubricity and antiwear behavior of guanidinium ionic liquids at high temperature. Tribol Int. 114, 65–76 (2017). https://doi.org/https://doi.org/10.1016/j.triboint.2017.04.010

109. Wu, X., Zhao, G., Wang, X., Liu, W., Liu, W.: In situ formed ionic liquids in lard oil as high-performance lubricants for steel/steel contacts at elevated temperature. Lubrication Science. 30, 65–72 (2018). https://doi.org/https://doi.org/10.1002/ls.1404

110. Fu, X., Sun, L., Zhou, X., Li, Z., Ren, T.: Tribological Study of Oil-Miscible Quaternary Ammonium Phosphites Ionic Liquids as Lubricant Additives in PAO. Tribol Lett. 60, 23 (2015). https://doi.org/10.1007/s11249-015-0596-0

111. Comtet, J., Niguès, A., Kaiser, V., Coasne, B., Bocquet, L., Siria, A.: Nanoscale capillary freezing of ionic liquids confined between metallic interfaces and the role of electronic screening. Nat Mater. 16, 634–639 (2017). https://doi.org/10.1038/nmat4880

112. Song, Z., Liang, Y., Fan, M., Zhou, F., Liu, W.: Ionic liquids from amino acids: fully green fluid lubricants for various surface contacts. RSC Adv. 4, 19396–19402 (2014). https://doi.org/10.1039/C3RA47644H

113. Huang, G., Yu, Q., Ma, Z., Cai, M., liu, W.: Probing the lubricating mechanism of oil-soluble ionic liquids additives. Tribol Int. 107, 152–162 (2017). https://doi.org/https://doi.org/10.1016/j.triboint.2016.08.027

114. Zhou, Y., Leonard, D.N., Guo, W., Qu, J.: Understanding Tribofilm Formation Mechanisms in Ionic Liquid Lubrication. Sci Rep. 7, 8426 (2017). https://doi.org/10.1038/s41598-017-09029-z

115. Yu, B., Bansal, D.G., Qu, J., Sun, X., Luo, H., Dai, S., Blau, P.J., Bunting, B.G., Mordukhovich, G., Smolenski, D.J.: Oil-miscible and non-corrosive phosphonium-based ionic liquids as candidate lubricant additives. Wear. 289, 58–64 (2012)

116. Liaw, H.-J., Chen, C.-C., Chen, Y.-C., Chen, J.-R., Huang, S.-K., Liu, S.-N.: Relationship between flash point of ionic liquids and their thermal decomposition. Green Chemistry. 14, 2001–2008 (2012)

117. Cao, Y., Mu, T.: Comprehensive investigation on the thermal stability of 66 ionic liquids by thermogravimetric analysis. Ind Eng Chem Res. 53, 8651–8664 (2014)

118. Uerdingen, M., Treber, C., Balser, M., Schmitt, G., Werner, C.: Corrosion behaviour of ionic liquids. Green Chemistry. 7, 321–325 (2005). https://doi.org/10.1039/B419320M

119. Predel, T., Pohrer, B., Schlücker, E.: Ionic Liquids as Alternative Lubricants for Special Applications. Chem Eng Technol. 33, 132–136 (2010). https://doi.org/https://doi.org/10.1002/ceat.200900325

120. Zunita, M., Kevin, Y.J.: Ionic liquids as corrosion inhibitor: From research and development to commercialization. Results in Engineering. 15, 100562 (2022). https://doi.org/https://doi.org/10.1016/j.rineng.2022.100562

121. Akintola, S.A., Oki, M., Aleem, A.A., Adediran, A.A., Akpor, O.B., Oluba, O.M., Ogunsemi, B.T., Ikubanni, P.P.: Valorized chicken feather as corrosion inhibitor for mild steel in drilling mud. Results in Engineering. 4, 100026 (2019). https://doi.org/https://doi.org/10.1016/j.rineng.2019.100026

122. Ayoola, A.A., Babalola, R., Durodola, B.M., Alagbe, E.E., Agboola, O., Adegbile, E.O.: Corrosion inhibition of A36 mild steel in 0.5 M acid medium using waste citrus limonum peels. Results in Engineering. 15, 100490 (2022). https://doi.org/https://doi.org/10.1016/j.rineng.2022.100490

123. Hossain, N., Chowdhury, M.A., Rana, M., Hassan, M., Islam, S.: Terminalia arjuna leaves extract as green corrosion inhibitor for mild steel in HCl solution. Results in Engineering. 14, 100438 (2022). https://doi.org/https://doi.org/10.1016/j.rineng.2022.100438

124. Díaz-Jiménez, V., Arellanes-Lozada, P., Likhanova, N. V, Olivares-Xometl, O., Chigo-Anota, E., Lijanova, I. V, Gómez-Sánchez, G., Verpoort, F.: Investigation of Sulfonium-Iodide-Based Ionic Liquids to Inhibit Corrosion of API 5L X52 Steel in Different Flow

Regimes in Acid Medium. ACS Omega. 7, 42975–42993 (2022). https://doi.org/10.1021/acsomega.2c05192

125. Moustafa, A.A., Abdelbasir, S.M., Ashmawy, A.M., Ghayad, I.M., El-Zomrawy, A.A.: A novel ionic liquid for improvement of lead-acid battery performance and protection of its electrodes against corrosion. Mater Chem Phys. 292, 126764 (2022). https://doi.org/https://doi.org/10.1016/j.matchemphys.2022.126764

126. Zhou, Y., Weber, J., Viola, M.B., Qu, J.: Is more always better? Tribofilm evolution and tribological behavior impacted by the concentration of ZDDP, ionic liquid, and ZDDP-Ionic liquid combination. Wear. 432–433, 202951 (2019). https://doi.org/10.1016/j.wear.2019.202951

127. Li, Z., Dolocan, A., Morales-Collazo, O., Sadowski, J.T., Celio, H., Chrostowski, R., Brennecke, J.F., Mangolini, F.: Lubrication Mechanism of Phosphonium Phosphate Ionic Liquid in Nanoscale Single-Asperity Sliding Contacts. Adv Mater Interfaces. 7, 2000426 (2020). https://doi.org/10.1002/admi.202000426

128. Yu, B., Bansal, D.G., Qu, J., Sun, X., Luo, H., Dai, S., Blau, P.J., Bunting, B.G., Mordukhovich, G., Smolenski, D.J.: Oil-miscible and non-corrosive phosphonium-based ionic liquids as candidate lubricant additives. Wear. 289, 58–64 (2012). https://doi.org/10.1016/j.wear.2012.04.015

129. Guo, H., Victoria, P.I.: Ionic Liquids as High-Performance Lubricants and Lubricant Additives. In: Murshed, S.M.S. (ed.) Ionic Liquids. p. Ch. 4. IntechOpen, Rijeka (2021)

130. Zhou, Y., Dyck, J., Graham, T.W., Luo, H., Leonard, D.N., Qu, J.: Ionic liquids composed of phosphonium cations and organophosphate, carboxylate, and sulfonate anions as lubricant antiwear additives. Langmuir. 30, 13301–13311 (2014). https://doi.org/10.1021/la5032366

131. Qu, J., Bansal, D.G., Yu, B., Howe, J.Y., Luo, H., Dai, S., Li, H., Blau, P.J., Bunting, B.G., Mordukhovich, G., Smolenski, D.J.: Antiwear performance and mechanism of an oil-miscible ionic liquid as a lubricant additive. ACS Appl Mater Interfaces. 4, 997–1002 (2012). https://doi.org/10.1021/am201646k

132. Qu, J., Luo, H., Chi, M., Ma, C., Blau, P.J., Dai, S., Viola, M.B.: Comparison of an oil-miscible ionic liquid and ZDDP as a lubricant anti-wear additive. Tribol Int. 71, 88–97 (2014). https://doi.org/10.1016/j.triboint.2013.11.010

133. Barnhill, W.C., Qu, J., Luo, H., Meyer, H.M., Ma, C., Chi, M., Papke, B.L.: Phosphonium-organophosphate ionic liquids as lubricant additives: Effects of cation structure on physicochemical and tribological characteristics. ACS Appl Mater Interfaces. 6, 22585–22593 (2014). https://doi.org/10.1021/am506702u

134. Qu, J., Luo, H., Chi, M., Ma, C., Blau, P.J., Dai, S., Viola, M.B.: Comparison of an oil-miscible ionic liquid and ZDDP as a lubricant anti-wear additive. Tribol Int. 71, 88–97 (2014). https://doi.org/https://doi.org/10.1016/j.triboint.2013.11.010

135. Yu, B., Bansal, D.G., Qu, J., Sun, X., Luo, H., Dai, S., Blau, P.J., Bunting, B.G., Mordukhovich, G., Smolenski, D.J.: Oil-miscible and non-corrosive phosphonium-based ionic liquids as candidate lubricant additives. Wear. 289, 58–64 (2012). https://doi.org/10.1016/j.wear.2012.04.015

136. Qu, J., Bansal, D.G., Yu, B., Howe, J.Y., Luo, H., Dai, S., Li, H., Blau, P.J., Bunting, B.G., Mordukhovich, G., Smolenski, D.J.: Antiwear Performance and Mechanism of an Oil-Miscible Ionic Liquid as a Lubricant Additive. ACS Appl Mater Interfaces. 4, 997–1002 (2012). https://doi.org/10.1021/am201646k

137. Otero, I., López, E.R., Reichelt, M., Villanueva, M., Salgado, J., Fernández, J.: Ionic Liquids Based on Phosphonium Cations As Neat Lubricants or Lubricant Additives for a Steel/Steel Contact. ACS Appl Mater Interfaces. 6, 13115–13128 (2014). https://doi.org/10.1021/am502980m

138. Somers, A.E., Khemchandani, B., Howlett, P.C., Sun, J., MacFarlane, D.R., Forsyth, M.: Ionic Liquids as Antiwear Additives in Base Oils: Influence of Structure on Miscibility and Antiwear Performance for Steel on Aluminum. ACS Appl Mater Interfaces. 5, 11544–11553 (2013). https://doi.org/10.1021/am4037614

139. Välbe, R., Tarkanovskaja, M., Mäeorg, U., Reedo, V., Lõhmus, A., Taaber, T., Vlassov, S., Lõhmus, R.: Phosphonium-based ionic liquids mixed with stabilized oxide nanoparticles as highly promising lubricating oil additives. Proceedings of the Estonian Academy of Sciences. 66, 174–183 (2017). https://doi.org/10.3176/proc.2017.2.05

140. Duan, H., Li, W., Kumara, C., Jin, Y., Meyer, H.M., Luo, H., Qu, J.: Ionic liquids as oil additives for lubricating oxygen-diffusion case-hardened titanium. Tribol Int. 136, 342–348 (2019). https://doi.org/https://doi.org/10.1016/j.triboint.2019.03.069

141. Nanao, H., Takahashi, K., Shirai, M.: Lubricity improvement of imidazolium cation-based ionic liquids treated with carbon dioxide. Journal of the Japan Petroleum Institute. 60, 329–332 (2017). https://doi.org/10.1627/jpi.60.329

142. Fan, X., Xue, Q., Wang, L.: Carbon-based solid-liquid lubricating coatings for space applications-A review. Friction. 3, 191–207 (2015). https://doi.org/10.1007/s40544-015-0079-1

143. Cai, M., Guo, R., Zhou, F., Liu, W.: Lubricating a bright future: Lubrication contribution to energy saving and low carbon emission. Sci China Technol Sci. 56, 2888–2913 (2013). https://doi.org/10.1007/s11431-013-5403-2

144. Cai, M., Yu, Q., Liu, W., Zhou, F.: Ionic liquid lubricants: when chemistry meets tribology. Chem Soc Rev. 49, 7753–7818 (2020). https://doi.org/10.1039/D0CS00126K

145. Liu, X., Wang, L., Xue, Q.: High vacuum tribological performance of DLC-based solid–liquid lubricating coatings: Influence of atomic oxygen and ultraviolet irradiation. Tribol Int. 60, 36–44 (2013). https://doi.org/https://doi.org/10.1016/j.triboint.2012.10.016

146. Erdemir, A.: Review of engineered tribological interfaces for improved boundary lubrication. Tribol Int. 38, 249–256 (2005). https://doi.org/10.1016/j.triboint.2004.08.008

147. Zhao, W., Pu, J., Yu, Q., Zeng, Z., Wu, X., Xue, Q.: A Novel strategy to enhance micro/nano-tribological properties of DLC film by combining micro-pattern and thin ionic liquids film. Colloids Surf A Physicochem Eng Asp. 428, 70–78 (2013). https://doi.org/https://doi.org/10.1016/j.colsurfa.2013.03.047

148. González, R., Hernández Battez, A., Blanco, D., Viesca, J.L., Fernández-González, A.: Lubrication of TiN, CrN and DLC PVD Coatings with 1-Butyl-1-Methylpyrrolidinium tris(pentafluoroethyl)trifluorophosphate. Tribol Lett. 40, 269–277 (2010). https://doi.org/10.1007/s11249-010-9674-5

149. Hua, J., Shi, Y.: Non-corrosive Green Lubricant With Dissolved Lignin in Ionic Liquids Behave as Ideal Lubricants for Steel-DLC Applications. Front Chem. 7, 857 (2019). https://doi.org/10.3389/fchem.2019.00857

150. González, R., Battez, A.H., Viesca, J.L., Higuera-Garrido, A., Fernández-González, A.: Lubrication of DLC Coatings with Two Tris(pentafluoroethyl)trifluorophosphate Anion-Based Ionic Liquids. Tribology Transactions. 56, 887–895 (2013). https://doi.org/10.1080/10402004.2013.810319

151. Hernández Battez, A., González, R., Viesca, J.L., Fernández-González, A., Hadfield, M.: Lubrication of PVD coatings with ethyl-dimethyl-2-methoxyethylammonium tris(pentafluoroethyl)trifluorophosphate. Tribol Int. 58, 71–78 (2013). https://doi.org/https://doi.org/10.1016/j.triboint.2012.10.001

152. Jia, Z., Xia, Y., Li, J., Pang, X., Shao, X.: Friction and wear behavior of diamond-like carbon coating on plasma nitrided mild steel under boundary lubrication. Tribol Int. 43, 474–482 (2010). https://doi.org/https://doi.org/10.1016/j.triboint.2009.07.012

153. Liu, X., Wang, L., Xue, Q.: DLC-based solid–liquid synergetic lubricating coatings for improving tribological behavior of boundary lubricated surfaces under high vacuum condition. Wear. 271, 889–898 (2011). https://doi.org/https://doi.org/10.1016/j.wear.2011.03.021

154. Khanmohammadi, H., Wijanarko, W., Cruz, S., Evaristo, M., Espallargas, N.: Triboelectrochemical friction control of W- and Ag-doped DLC coatings in water-glycol with ionic liquids as lubricant additives. RSC Adv. 12, 3573–3583 (2022). https://doi.org/10.1039/d1ra08814a

155. Milewski, K., Kudliński, J., Madej, M., Ozimina, D.: The interaction between diamond like carbon (DLC) coatings and ionic liquids under boundary lubrication conditions. Anali Zavoda za Povijesne Znanosti Hrvatske Akademije Znanosti i Umjetnosti u Dubrovniku. 56, 55–58 (2017)

156. Arshad, M.S., Kovač, J., Cruz, S., Kalin, M.: Physicochemical and tribological characterizations of WDLC coatings and ionic-liquid lubricant additives: Potential

candidates for low friction under boundary-lubrication conditions. Tribol Int. 151, (2020). https://doi.org/10.1016/j.triboint.2020.106482

157. Yan, M., Wang, X., Zhang, S., Zhang, S., Sui, X., Li, W., Hao, J., Liu, W.: Friction and wear properties of GLC and DLC coatings under ionic liquid lubrication. Tribol Int. 143, 106067 (2020). https://doi.org/https://doi.org/10.1016/j.triboint.2019.106067

158. González, R., Battez, A.H., Viesca, J.L., Higuera-Garrido, A., Fernández-González, A.: Lubrication of DLC Coatings with Two Tris(pentafluoroethyl)trifluorophosphate Anion-Based Ionic Liquids. Tribology Transactions. 56, 887–895 (2013). https://doi.org/10.1080/10402004.2013.810319

159. Arshad, M.S., Kovač, J., Cruz, S., Kalin, M.: Physicochemical and tribological characterizations of WDLC coatings and ionic-liquid lubricant additives: Potential candidates for low friction under boundary-lubrication conditions. Tribol Int. 151, (2020). https://doi.org/10.1016/j.triboint.2020.106482

160. Khanmohammadi, H., Wijanarko, W., Cruz, S., Evaristo, M., Espallargas, N.: Triboelectrochemical friction control of W- and Ag-doped DLC coatings in water-glycol with ionic liquids as lubricant additives. RSC Adv. 12, 3573–3583 (2022). https://doi.org/10.1039/d1ra08814a

161. Yan, M., Wang, X., Zhang, S., Zhang, S., Sui, X., Li, W., Hao, J., Liu, W.: Friction and wear properties of GLC and DLC coatings under ionic liquid lubrication. Tribol Int. 143, (2020). https://doi.org/10.1016/j.triboint.2019.106067

162. Bolander, N.W., Steenwyk, B.D., Sadeghi, F., Gerber, G.R.: Lubrication regime transitions at the piston ring-cylinder liner interface. Proceedings of the Institution of Mechanical Engineers, Part J: Journal of Engineering Tribology. 219, 19–31 (2005). https://doi.org/10.1243/135065005X9664

163. Vahidi, A., Fonseca, D., Oliveira, J., Cavaleiro, A., Ramalho, A., Ferreira, F.: Advanced tribological characterization of dlc coatings produced by ne-hipims for the application on the piston rings of internal combustion engines. Applied Sciences (Switzerland). 11, (2021). https://doi.org/10.3390/app112110498

164. Pusterhofer, M., Summer, F., Wuketich, D., Grün, F.: Development of a model test system for a piston ring/cylinder liner-contact with focus on near-to-application seizure behaviour. Lubricants. 7, (2019). https://doi.org/10.3390/LUBRICANTS7120104

165. Jose Chirayil, C., Abraham, J., Kumar Mishra, R., George, S.C., Thomas, S.: Instrumental Techniques for the Characterization of Nanoparticles. In: Thermal and Rheological Measurement Techniques for Nanomaterials Characterization. pp. 1–36. Elsevier (2017)

166. Alford, T.L., Adams, D., Mayer, J.W.: Ion Beam Analysis. In: Bassani, F., Liedl, G.L., and Wyder, P. (eds.) Encyclopedia of Condensed Matter Physics. pp. 423–434. Elsevier, Oxford (2005)

167. Zhou, X., Tunmee, S., Suzuki, T., Phothongkam, P., Kanda, K., Komatsu, K., Kawahara, S., Ito, H., Saitoh, H.: Quantitative NEXAFS and solid-state NMR studies of sp3/(sp2+sp3) ratio in the hydrogenated DLC films. Diam Relat Mater. 73, 232–240 (2017). https://doi.org/https://doi.org/10.1016/j.diamond.2016.09.026

168. Barradas, N.P., Jeynes, C., Webb, R.P.: Simulated annealing analysis of Rutherford backscattering data. Appl Phys Lett. 71, 291 (1998). https://doi.org/10.1063/1.119524

169. Gurbich, A.F.: SigmaCalc recent development and present status of the evaluated cross-sections for IBA. Nucl Instrum Methods Phys Res B. 371, 27–32 (2016). https://doi.org/https://doi.org/10.1016/j.nimb.2015.09.035

170. Hu, Z.: Characterization of Materials, Nanomaterials, and Thin Films by Nanoindentation. In: Thomas, S., Thomas, R., Zachariah, A.K., and Mishra, R.K. (eds.) Microscopy Methods in Nanomaterials Characterization. pp. 165–239. Elsevier (2017)

171. Liu, Y., Erdemir, A., Meletis, E.I.: A study of the wear mechanism of diamond-like carbon films. Surf Coat Technol. 82, 48–56 (1996). https://doi.org/10.1016/0257-8972(95)02623-1

172. Ding, J.C., Mei, H., Jeong, S., Zheng, J., Wang, Q.M., Kim, K.H.: Effect of bias voltage on the microstructure and properties of Nb-DLC films prepared by a hybrid sputtering system. J Alloys Compd. 861, 158505 (2021). https://doi.org/10.1016/j.jallcom.2020.158505

173. Ding, J.C., Chen, M., Mei, H., Jeong, S., Zheng, J., Yang, Y., Wang, Q., Kim, K.H.: Microstructure, mechanical, and wettability properties of Al-doped diamond-like films deposited using a hybrid deposition technique: Bias voltage effects. Diam Relat Mater. 123, 108861 (2022). https://doi.org/10.1016/j.diamond.2022.108861

174. Vetter, J.: 60years of DLC coatings: Historical highlights and technical review of cathodic arc processes to synthesize various DLC types, and their evolution for industrial applications. Surf Coat Technol. 257, 213–240 (2014). https://doi.org/10.1016/j.surfcoat.2014.08.017

175. Mittal, K.L.: Adhesion Measurement of Films and Coatings. CRC Press (2014)

176. ISO 20502:2005 - Fine ceramics (advanced ceramics, advanced technical ceramics) — Determination of adhesion of ceramic coatings by scratch testing, https://www.iso.org/standard/34189.html

177. SV-100 Vibro Viscometer Instruction Manual, https://www.aandd.jp/products/manual/balances/sv.pdf

178. Budynas, R., Nisbett, K.: Shigley's Mechanical Engineering Design. McGraw-Hill Higher Education - VST E+p (2014)

179. Lubrecht, A.A., Venner, C.H., Colin, F.: Film thickness calculation in elasto-hydrodynamic lubricated line and elliptical contacts: The Dowson, Higginson, Hamrock

contribution. Proceedings of the Institution of Mechanical Engineers, Part J: Journal of Engineering Tribology. 223, 511–515 (2009). https://doi.org/10.1243/13506501JET508

180. ISO 4288:1996 - Geometrical Product Specifications (GPS) — Surface texture: Profile method — Rules and procedures for the assessment of surface texture, https://www.iso.org/standard/2096.html

181. Luo, Q.: Electron Microscopy and Spectroscopy in the Analysis of Friction and Wear Mechanisms. Lubricants. 6, 58 (2018). https://doi.org/10.3390/lubricants6030058

182. Vetter, J.: 60years of DLC coatings: Historical highlights and technical review of cathodic arc processes to synthesize various DLC types, and their evolution for industrial applications. Surf Coat Technol. 257, 213–240 (2014). https://doi.org/https://doi.org/10.1016/j.surfcoat.2014.08.017

183. Robertson, J.: Diamond-like amorphous carbon. Materials Science and Engineering: R: Reports. 37, 129–281 (2002). https://doi.org/10.1016/S0927-796X(02)00005-0

184. Grill, A.: Diamond-like carbon: state of the art. Diam Relat Mater. 8, 428–434 (1999). https://doi.org/10.1016/S0925-9635(98)00262-3

185. Evaristo, M., Fernandes, F., Cavaleiro, A.: Room and High Temperature Tribological Behaviour of W-DLC Coatings Produced by DCMS and Hybrid DCMS-HiPIMS Configuration. Coatings. 10, 319 (2020). https://doi.org/10.3390/coatings10040319

186. Ding, J.C., Mei, H., Jeong, S., Zheng, J., Wang, Q.M., Kim, K.H.: Effect of bias voltage on the microstructure and properties of Nb-DLC films prepared by a hybrid sputtering system. J Alloys Compd. 861, 158505 (2021). https://doi.org/https://doi.org/10.1016/j.jallcom.2020.158505

187. Ding, J.C., Chen, M., Mei, H., Jeong, S., Zheng, J., Yang, Y., Wang, Q., Kim, K.H.: Microstructure, mechanical, and wettability properties of Al-doped diamond-like films deposited using a hybrid deposition technique: Bias voltage effects. Diam Relat Mater. 123, 108861 (2022). https://doi.org/https://doi.org/10.1016/j.diamond.2022.108861

188. Khanmohammadi, H., Wijanarko, W., Cruz, S., Evaristo, M., Espallargas, N.: Triboelectrochemical friction control of W- and Ag-doped DLC coatings in water-glycol with ionic liquids as lubricant additives. RSC Adv. 12, 3573–3583 (2022). https://doi.org/10.1039/d1ra08814a

189. Matthews, A., Franklin, S., Holmberg, K.: Tribological coatings: Contact mechanisms and selection. J Phys D Appl Phys. 40, 5463–5475 (2007). https://doi.org/10.1088/0022-3727/40/18/S07

190. Cao, L., Liu, J., Wan, Y., Pu, J.: Corrosion and tribocorrosion behavior of W doped DLC coating in artificial seawater. Diam Relat Mater. 109, 108019 (2020). https://doi.org/https://doi.org/10.1016/j.diamond.2020.108019

191. Kashyap, A., Harsha, A.P., Kondaiah, P., Barshilia, H.C.: Study on galling behaviour of HiPIMS deposited Mo/DLC multilayer coatings at ambient and elevated temperature. Wear. 498–499, 204327 (2022). https://doi.org/https://doi.org/10.1016/j.wear.2022.204327

192. Konkhunthot, N., Photongkam, P., Wongpanya, P.: Improvement of thermal stability, adhesion strength and corrosion performance of diamond-like carbon films with titanium doping. Appl Surf Sci. 469, 471–486 (2019). https://doi.org/10.1016/j.apsusc.2018.11.028

193. Wang, Y., Wang, Q.J.: Stribeck Curves. In: Wang, Q.J. and Chung, Y.-W. (eds.) Encyclopedia of Tribology. pp. 3365–3370. Springer US, Boston, MA (2013)

194. Marinescu, I.D., Rowe, W.B., Dimitrov, B., Inasaki, I.: Process Fluids for Abrasive Machining. In: Marinescu, I.D., Rowe, W.B., Dimitrov, B., and Inasaki, I. (eds.) Tribology of Abrasive Machining Processes. pp. 531–585. William Andrew Publishing, Norwich, NY (2004)

195. Kalin, M., Velkavrh, I., Vižintin, J.: The Stribeck curve and lubrication design for non-fully wetted surfaces. Wear. 267, 1232–1240 (2009). https://doi.org/https://doi.org/10.1016/j.wear.2008.12.072

196. Wang, Y., Wang, Q.J., Lin, C., Shi, F.: Development of a Set of Stribeck Curves for Conformal Contacts of Rough Surfaces. Tribology Transactions. 49, 526–535 (2006). https://doi.org/10.1080/10402000600846110

197. Lu, X., Khonsari, M.M., Gelinck, E.R.M.: The Stribeck Curve: Experimental Results and Theoretical Prediction. J Tribol. 128, 789–794 (2006). https://doi.org/10.1115/1.2345406

198. Martini, A., Zhu, D., Wang, Q.: Friction reduction in mixed lubrication. Tribol Lett. 28, 139–147 (2007). https://doi.org/https://doi.org/10.1007/s11249-007-9258-1

199. Xin, Q.: Friction and lubrication in diesel engine system design. In: Xin, Q. (ed.) Diesel Engine System Design. pp. 651–758. Elsevier (2013)

200. Li, P., Zhang, F., Zhang, H., Wang, T., Wang, Q., Qiao, W.: Lubrication performance of kite-shaped microtexture under hydrodynamic lubrication. Tribol Int. 179, 108144 (2023). https://doi.org/https://doi.org/10.1016/j.triboint.2022.108144

201. Linjamaa, A., Lehtovaara, A., Kallio, M., Léger, A.: Running-in effects on friction of journal bearings under slow sliding speeds. Proceedings of the Institution of Mechanical Engineers, Part J: Journal of Engineering Tribology. 234, 362–372 (2019). https://doi.org/10.1177/1350650119864758

202. Kalin, M., Velkavrh, I.: Non-conventional inverse-Stribeck-curve behaviour and other characteristics of DLC coatings in all lubrication regimes. Wear. 297, 911–918 (2013). https://doi.org/https://doi.org/10.1016/j.wear.2012.11.010

203. Xiao, H.: Ionic Liquid Lubricants: Basics and Applications. Tribology Transactions. 60, 20–30 (2017). https://doi.org/10.1080/10402004.2016.1142629

204. Kajdas, C.: Importance of anionic reactive intermediates for lubricant component reactions with friction surfaces. Lubrication Science. 6, 203–228 (1994). https://doi.org/10.1002/LS.3010060302

205. Atkin, R., el Abedin, S.Z., Hayes, R., Gasparotto, L.H.S., Borisenko, N., Endres, F.: AFM and STM Studies on the Surface Interaction of [BMP]TFSA and [EMIm]TFSA Ionic Liquids with Au(111). The Journal of Physical Chemistry C. 113, 13266–13272 (2009). https://doi.org/10.1021/jp9026755

206. Perkin, S., Albrecht, T., Klein, J.: Layering and shear properties of an ionic liquid, 1-ethyl-3-methylimidazolium ethylsulfate, confined to nano-films between mica surfaces. Physical Chemistry Chemical Physics. 12, 1243–1247 (2010). https://doi.org/10.1039/B920571C